4.4. Results and Discussion

Monomials were used as basis functions ($\phi_i(x)$) in the expansion of $1/D_e(x)$ in order to obtain the results that we present and discuss in this section, that is, $1/D_e(x)$ was expressed as

$$1/D_e(x) = \sum_{i=0}^{N} A_i x^i \tag{4.22}$$

Preliminary calculations showed that for $N \geq 2$ the obtained estimates of $D_e(x)$ were close to each other, and thus, it was decided to employ $N = 2$ (in other words, use a quadratic approximation for $1/D_e(x)$) in all cases. Of the three singular values obtained for each case, the term corresponding to the smallest singular value in Eq. (4.21) was set equal to zero to get the solution. Typically, the smallest singular value was from 6 times to an order smaller than the middle singular value. For example, the three singular values used for Greer limestone at $850°C$ and 1500 mL/m^3 using the results for the larger two size ranges were 9.89×10^{-2}, 1.45×10^{-2}, and 1.64×10^{-3}. On the other hand, Iceland spar reacted at $850°C$ and 6000 mL/m^3 had singular values of 4.11×10^{-3}, 1.33×10^{-3}, and 2.61×10^{-4}. The solution obtained by omitting the contribution of the smallest singular value proved to be smoother and better, from a physical standpoint, than that resulting from SVD with all three singular values since it exhibited neither irregular (nonmonotonic) variation of $D_e(x)$ with depth nor negative values of effective diffusivity. It should be pointed out that both effective diffusivity functions (that is, obtained with three or two singular values) gave, both qualitatively and quantitatively, similar conversion vs. time curves when they were used in the mathematical model, indicating that our decision to work only with two singular values was justified. Unless mentioned otherwise, the effective diffusivity results and functions we will present and discuss hereafter were obtained using conversion vs. time data for three particle size ranges (53-62, 88-105, and 297-350 μm) and with the right-hand side of each equation in Eq. (4.19) normalized to 1.

Diffusivity Results

Figs. 4.5 and 4.6 show the variation of effective diffusivity of SO_2 along the distance from the external surface for Greer limestone, Georgia marble, and Iceland spar for the two

temperatures used in the experiments (750 and 850°C) for a bulk concentration of 1500 and 6000 mL/m^3 of SO_2, respectively. The variation of $D_e(x)$ is terminated at the largest product thickness obtained for each case experimentally. For example, after sulfation for 150 min at 750°C, the Iceland spar samples had a product layer thickness of only 1 μm, and thus, $D_e(x)$ values are shown only within this window of product layer thickness. On the other hand, Greer limestone particles reacted at 850°C and 1500 mL/m^3 developed a product layer thickness of approximately 6 μm during 150 min sulfation.

The results of Figs. 4.5 and 4.6 show that the effective diffusivity decreases very fast with the distance from the external surface of the particles, but its rate of decrease varies widely among the three stones. The value of effective diffusivity at the maximum depth (6 μm) for Greer limestone at 850 °C and 1500 mL/m^3 is about an order in magnitude lower than the value at the external surface of the particles. A similar drop in the value of effective diffusivity is seen for Iceland spar reacted at 750°C and 1500 mL/m^3 along a product layer only 1 μm thick. For most cases shown in Figs. 4.5 and 4.6, the effective diffusivity at the maximum depth was 3 to 5 times smaller than the value at the external surface. The fall in the value of effective diffusivity toward the unreacted core leads to increasing resistance for diffusion in the product shell with increasing conversion, and this in turn makes possible to obtain an agreement between theory and experiment.

Despite the sharp decrease that the effective diffusivity experiences with the distance from the surface, the value seen at the maximum depth for each case is generally two to three orders of magnitude higher than the value of effective diffusivity through the product layer for the reaction of the calcines of the same solids (Sotirchos and Zarkanitis, 1992), which had a value of $10^{-12} m^2/s$ on the average. The higher diffusivity of SO_2 through the product layer formed during direct sulfation must obviously be the reason for which this reaction proceeds with rate comparable to that of the reaction of calcined limestones with SO_2 even though it involves essentially nonporous solids.

Our experimental results (Krishnan and Sotirchos, 1993) showed that calcium utilization was the highest for Greer limestone, followed by Georgia marble and Iceland spar. Pore structure characterization and petrographic examination of the three solids revealed that their porosity decreased and their average grain size increased in the same order.

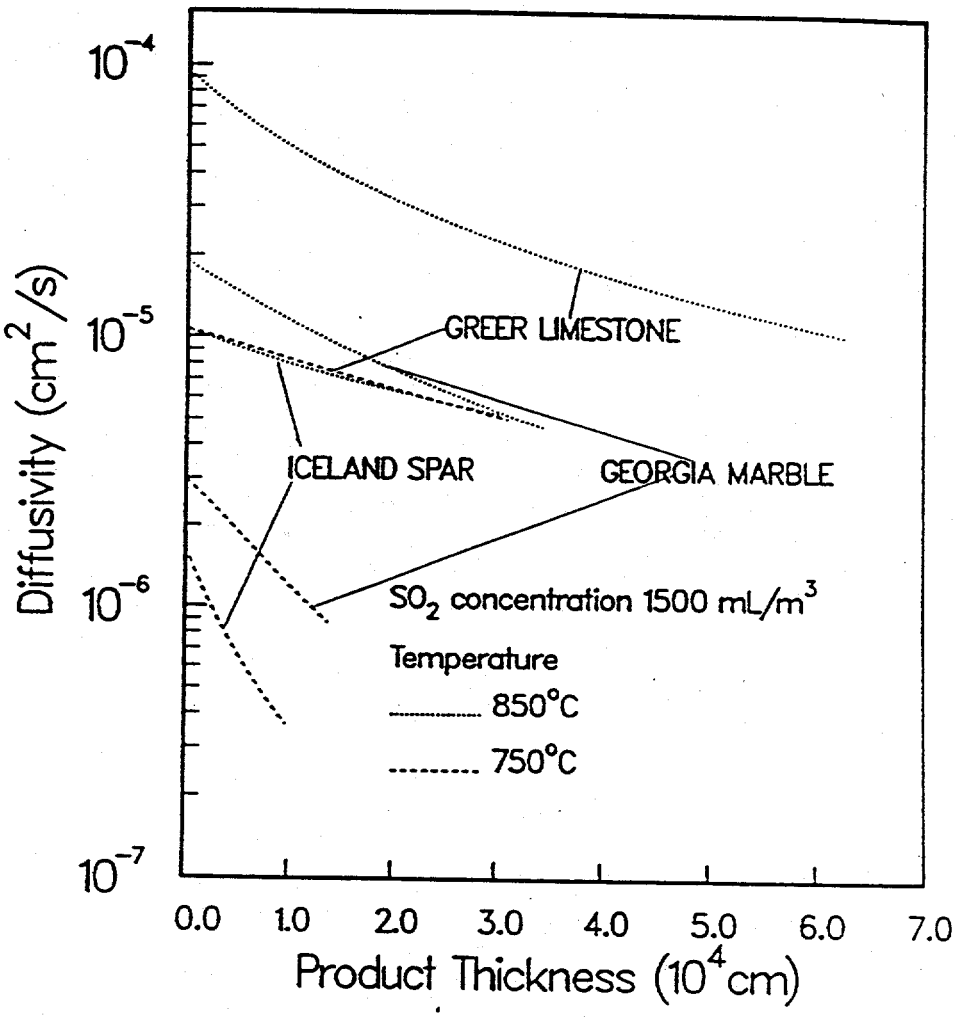

Figure 4.5: Form of effective diffusivity obtained for the three stones reacted under 1500 mL/m^3 of SO_2 in an atmosphere of 70% CO_2 ($mol\%$) and the two temperatures of 750 and 850^oC from the parameter estimation procedure.

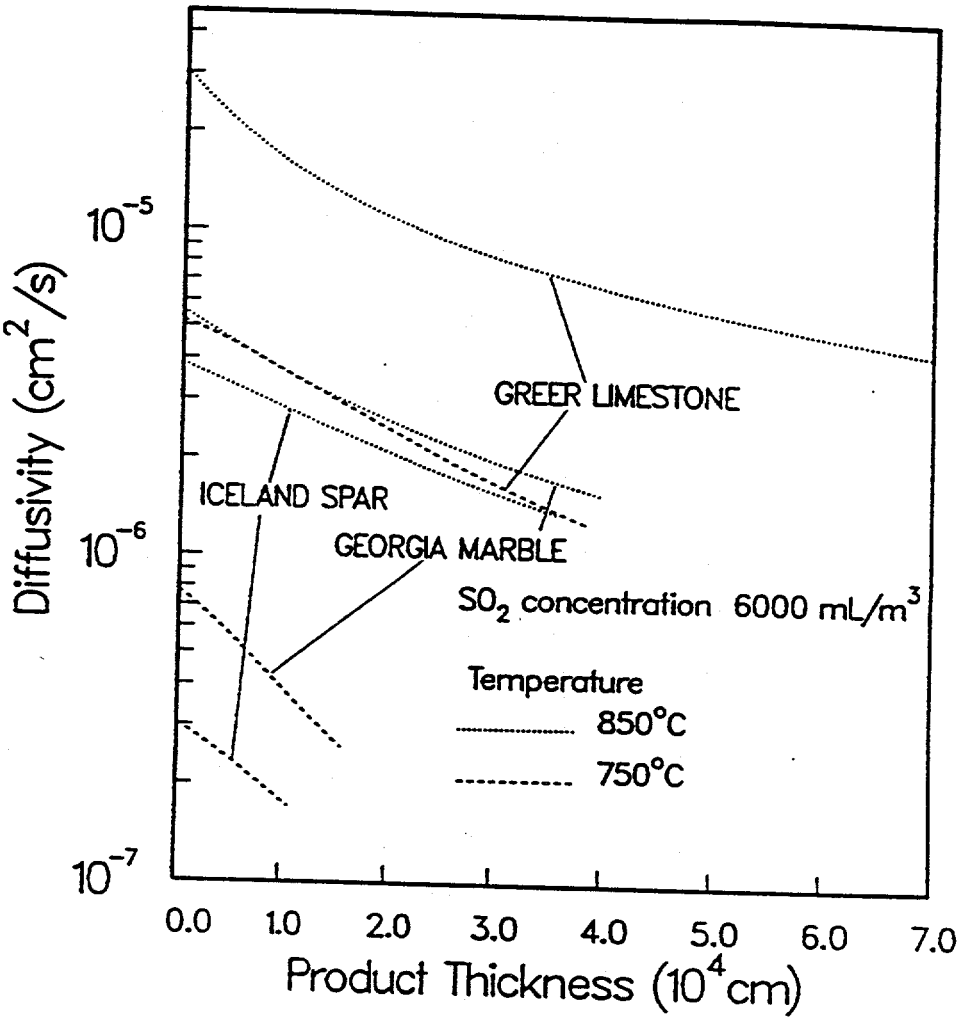

Figure 4.6: Form of effective diffusivity obtained for the three stones reacted under 6000 mL/m^3 of SO_2 in an atmosphere of 70% CO_2 $(mol\%)$ and the two temperatures of 750 and 850°C from the parameter estimation procedure.

It was thus postulated that the structure of the precursor influences the structure of the product layer that is formed during direct sulfation, yielding a more open structure and, hence, lower diffusional resistance in the direction Iceland spar → Georgia marble → Greer limestone. The relative values of effective diffusivities that were extracted from our parameter estimation scheme corroborate this hypothesis. It is seen in Figs. 4.5 and 4.6 that under identical reaction conditions, Greer limestone always has the highest value of effective diffusivity at a given depth from the surface. The diffusivity values for Georgia marble and Iceland spar are much lower than that of Greer limestone with the product layer of Georgia marble offering lesser mass transport resistance than Iceland spar at a certain thickness. It is interesting to point out that the very same order was found to be generally followed by the solid product diffusivities that were extracted from the analysis of reactivity data for the sulfation of the calcines of the same solids by Sotirchos and Zarkanitis (1992).

Model predictions obtained using the estimated form of $D_e(x)$ in Fig. 4.5 are shown in Fig. 4.7 for Iceland spar particles directly sulfated at 850^oC under 1500 mL/m^3 of SO_2. Very good agreement between the model and experimental results is seen for the two larger size ranges over the entire time period and also for the smallest size range up to a conversion level of about 10%. At higher conversion levels, the model tends to overpredict the conversion for the smallest size range, and therefore, the value of effective diffusivity that would be obtained from our parametric estimation procedure using the conversion vs. time results for the 53-62 μm particles only would be smaller than that obtained for all three size ranges, i.e., the one shown in Fig. 4.5 and used to get the results of Fig. 4.7. This point will be discussed in more detail in the following figures.

Fig. 4.8 shows the comparison between model predictions and experimental results for Georgia marble particles reacted at 750^oC and 6000 mL/m^3 of SO_2. It is seen from Fig. 4.8 that model and experiment agree very well at lower conversion levels, where presumably the reaction is under kinetic control. At higher conversion levels, though, where diffusion through the product layer starts to dominate, the model results tend to underpredict the conversion profile for the larger two size ranges but overpredict it for the 53-62 μm size range. The reason for this behavior can be seen in Fig. 4.9 which gives the estimated form

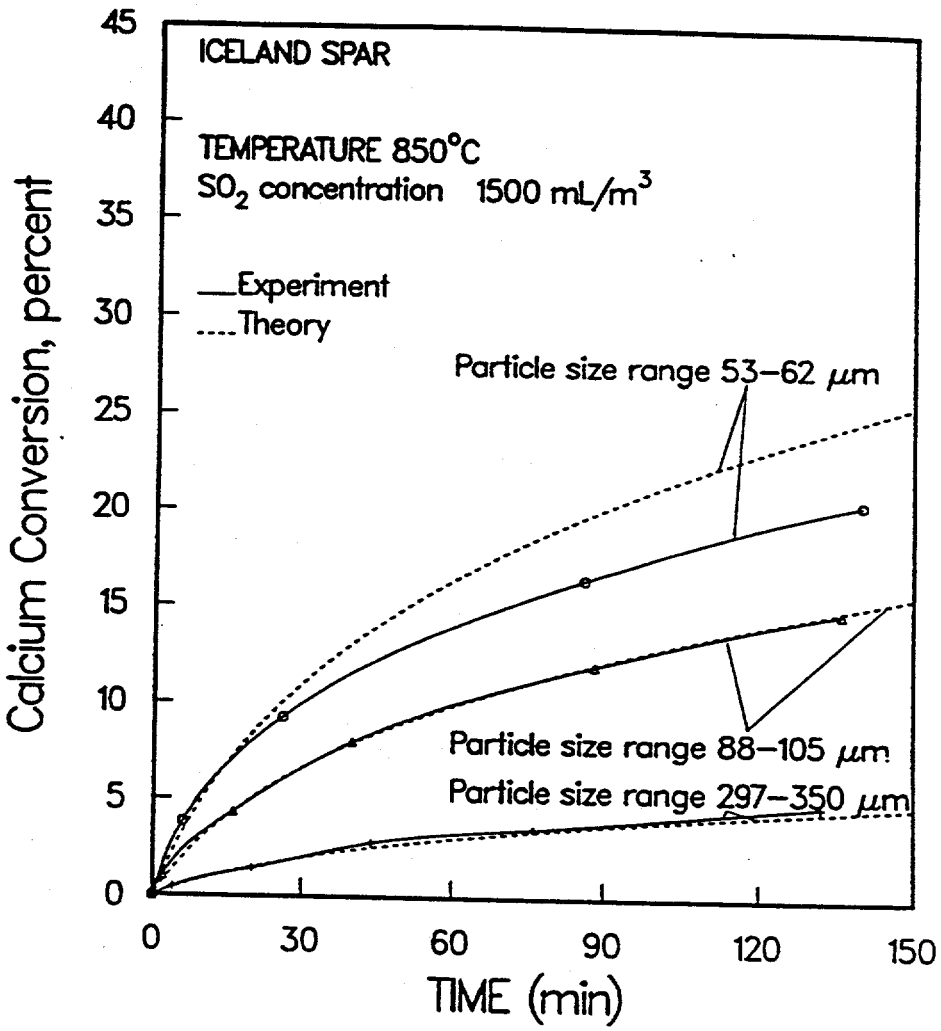

Figure 4.7: Comparison of model predictions with experimental results for Iceland spar directly sulfated at $850°C$ and 1500 mL/m^3 of SO_2 in an atmosphere of 70% $CO_2(mol\%)$.

of $D_e(x)$ when all three particle size ranges are employed and when each size is treated individually. We see in Fig. 4.9 that the value of $D_e(x)$ obtained for all three particle size ranges (solid line) is always higher at a given depth than the value obtained by employing only the 53-62 μm size range. Thus, using the functional form of effective diffusivity based on all three size ranges leads to higher mass transport rates for the smallest size range and causes the model to overpredict the conversion-time profile. Similarly, the underprediction of the conversion for the 88-105 and the 297-350 μm sized particles can be explained on the basis of the difference between the diffusivity for all sizes and the diffusivities for each of the larger sizes individually.

Since we had observed that the 53-62 μm size range for the Greer limestone sample behaved differently from the other size ranges under a given set of reaction conditions (temperature and concentration), the experimental conversion vs. time data for the smallest size range were excluded in obtaining the functional form of effective diffusivity; that is, only the larger two size ranges were employed in our parameter estimation procedure for Greer limestone samples. Figs. 4.10 and 4.11 show the comparison between model predictions and experimental results for Greer limestone reacted at $850°C$ and under a concentration of SO_2 of 1500 and 6000 mL/m^3, respectively. Very good agreement is obtained between theory and experiment for the larger two particle size ranges, but the model underpredicts badly the results for the smallest size range. This behavior lends further support to our conclusion that the smallest Greer limestone particles form a more open product layer structure, reacting almost as unconsolidated structures, than the larger two size ranges.

The results shown in Figs. 4.10 and 4.11 can be better understood and explained with the aid of Fig. 4.12, which shows the comparison between the form of effective diffusivity obtained by employing the larger two size ranges and that obtained by treating the size ranges individually. The individual results for the larger two particle size ranges follow closely the result obtained by combining the two size ranges, and thus, there is insignificant disparity between model and experiment when the form of $D_e(x)$ for the larger two size ranges is employed in the model. On the other hand, the value of effective diffusivity at a given radial depth in the product of the 53-62 μm particle is much higher than the value of effective diffusivity obtained by combining the larger two size ranges. The higher mass

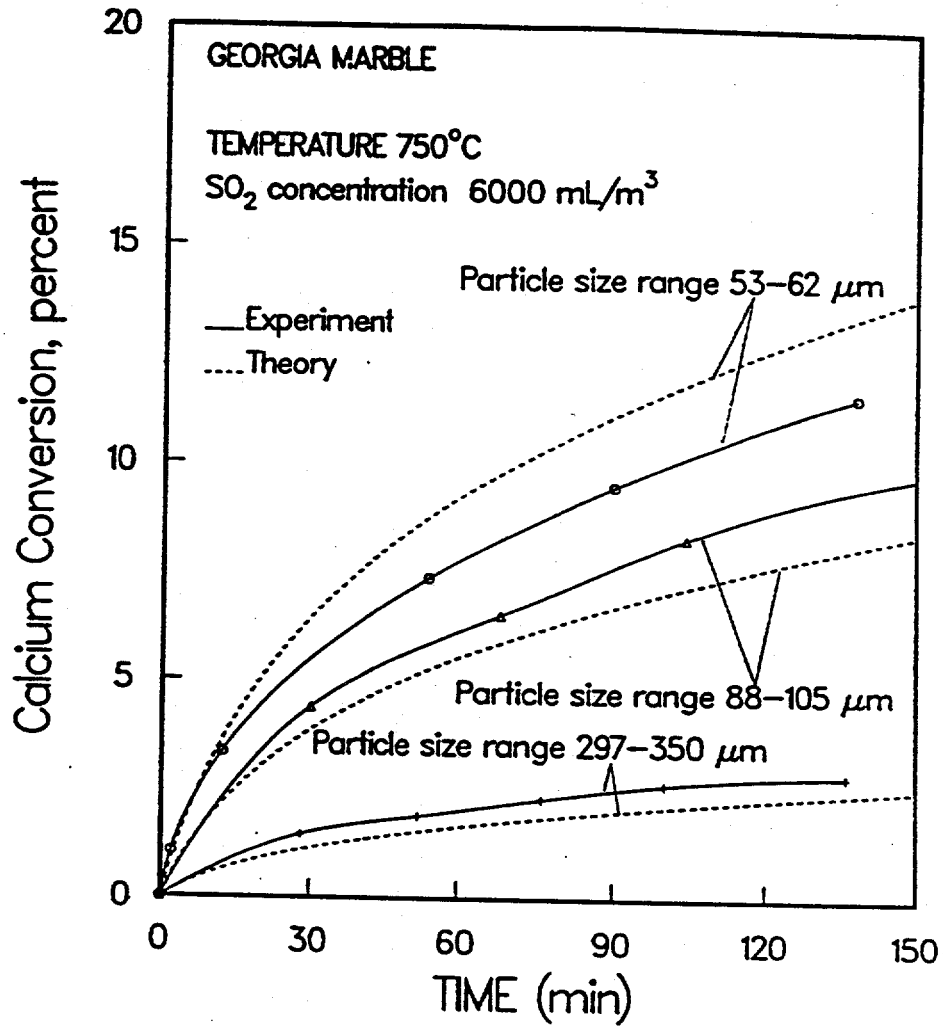

Figure 4.8: Comparison of model predictions with experimental results for Georgia marble directly sulfated at $750°C$ and 6000 mL/m^3 of SO_2 in an atmosphere of 70% $CO_2(mol\%)$.

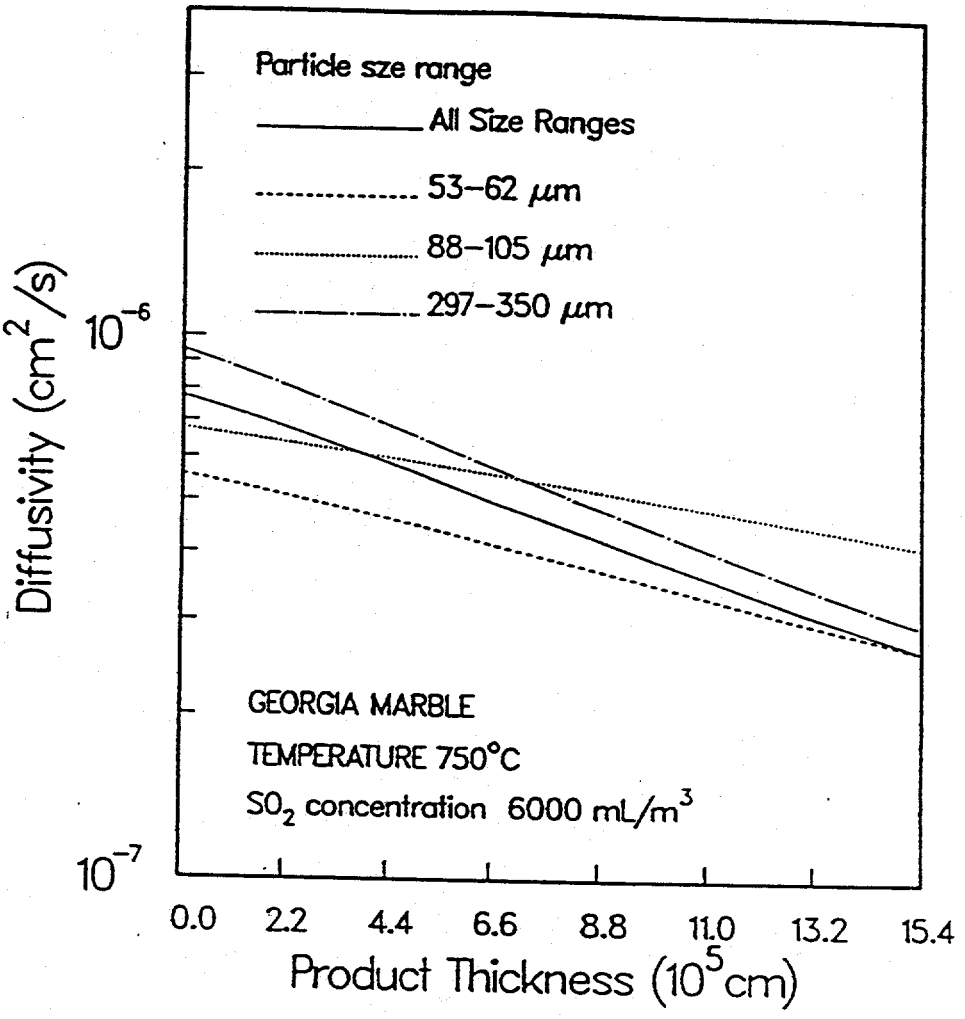

Figure 4.9: Comparison of the effective diffusivity profiles obtained for Georgia marble reacted at $750°C$ and 6000 mL/m^3 of SO_2 in an atmosphere of 70% $CO_2(mol\%)$ between employing all three size ranges together and treating each size range individually.

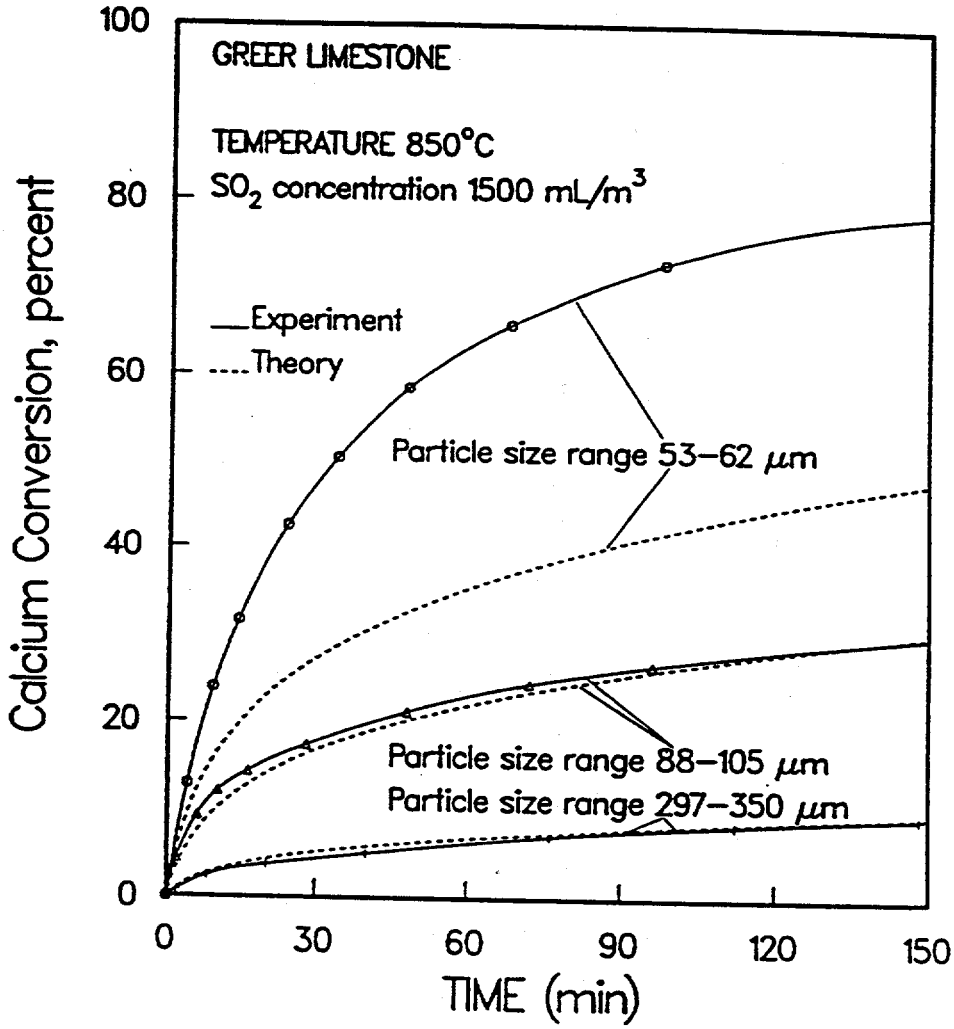

Figure 4.10: Comparison of model predictions with experimental results for Greer limestone directly sulfated at $850°C$ and 1500 mL/m^3 of SO_2 in an atmosphere of 70% $CO_2(mol\%)$.

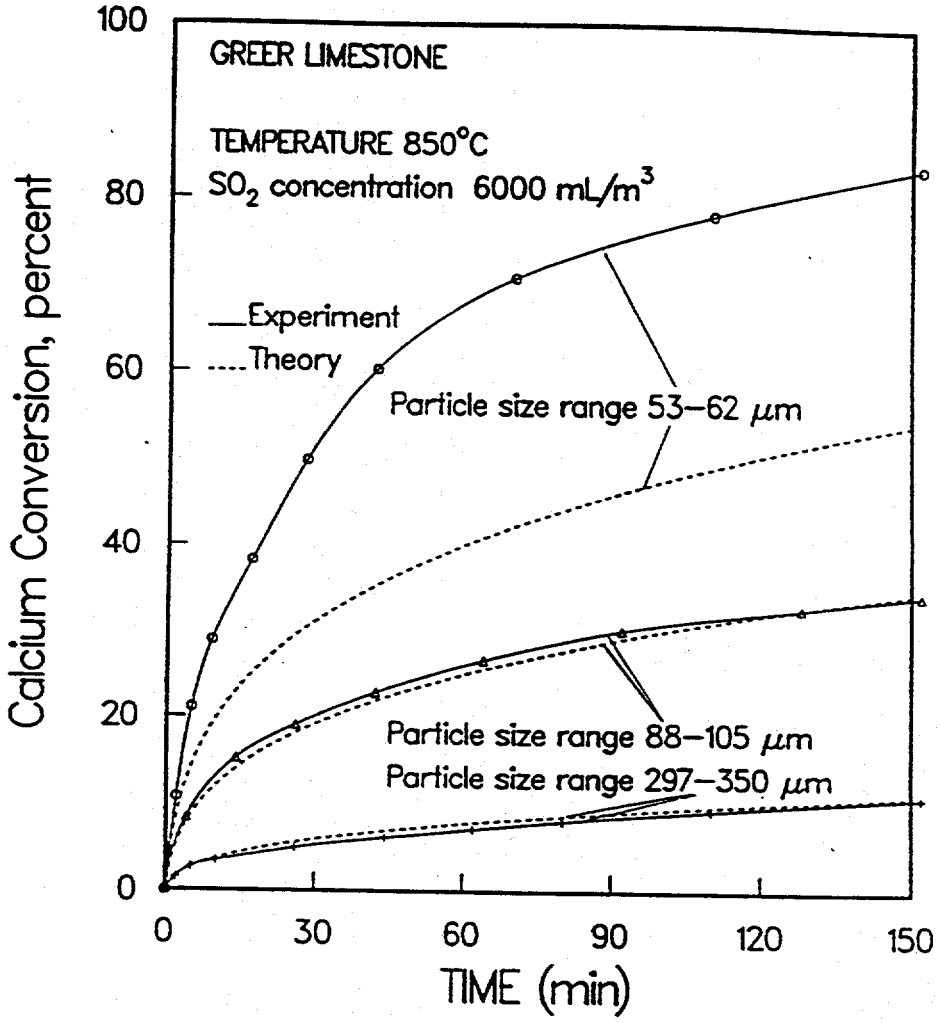

Figure 4.11: Comparison of model predictions with experimental results for Greer limestone directly sulfated at $850°C$ and 6000 mL/m^3 of SO_2 in an atmosphere of 70% $CO_2(mol\%)$.

transport resistance used in the model is the reason for having much lower conversions predicted by the model for the smallest size range in Figs. 4.10 and 4.11. Similar behavior to that seen in Figs. 4.10 and 4.11 was observed for all cases concerning Greer limestone. It should be pointed out, however, that the estimated form of $D_e(x)$ for the case of Greer limestone with all three sizes taken into account was not much different from that obtained for the 88-105 and 297-350 μm sizes only. The parameter estimation scheme tended to favor the results for the larger two sizes since they were in most cases consistent with each other. This behavior can be seen in Fig. 4.7 where, although all results were used to determine the form of $D_e(x)$, the model predictions overpredict the results for the smallest size range only.

A different way of verifying the model results is shown in Fig. 4.13 which shows the comparison between the growth of the product layer obtained from the experimental conversion-time results and that given by the model using the effective diffusivity obtained from the parameter estimation scheme. The results presented are for the three solids (88-105 μm particles) reacted at $850°C$ under 1500 mL/m^3 of SO_2 and 70% CO_2. Excellent agreement is found for all three solid samples between model predictions and experimental results.

Effect of Temperature and Concentration on Diffusivity

The experimental conversion vs. time revealed that temperature had a strong influence on the overall reaction rate not only in the earlier stages of the reaction but also at larger reaction times. Since the overall process is initially under kinetic control, the temperature of reaction was found to have a strong effect on the reaction rate constant (see Table 4.1). However, at the later stages of the reaction, the process is chiefly controlled by diffusion in the product layer, and consequently, the influence of temperature on the reaction trajectories is almost exclusively due to variations in the value of effective diffusivity with temperature. Indeed, as it can be seen in Figs. 4.5 and 4.6, a fall of nearly an order in magnitude takes place in the value of effective diffusivity at a given depth from the external surface for all reaction conditions with a decrease in temperature from 850 to $750°C$.

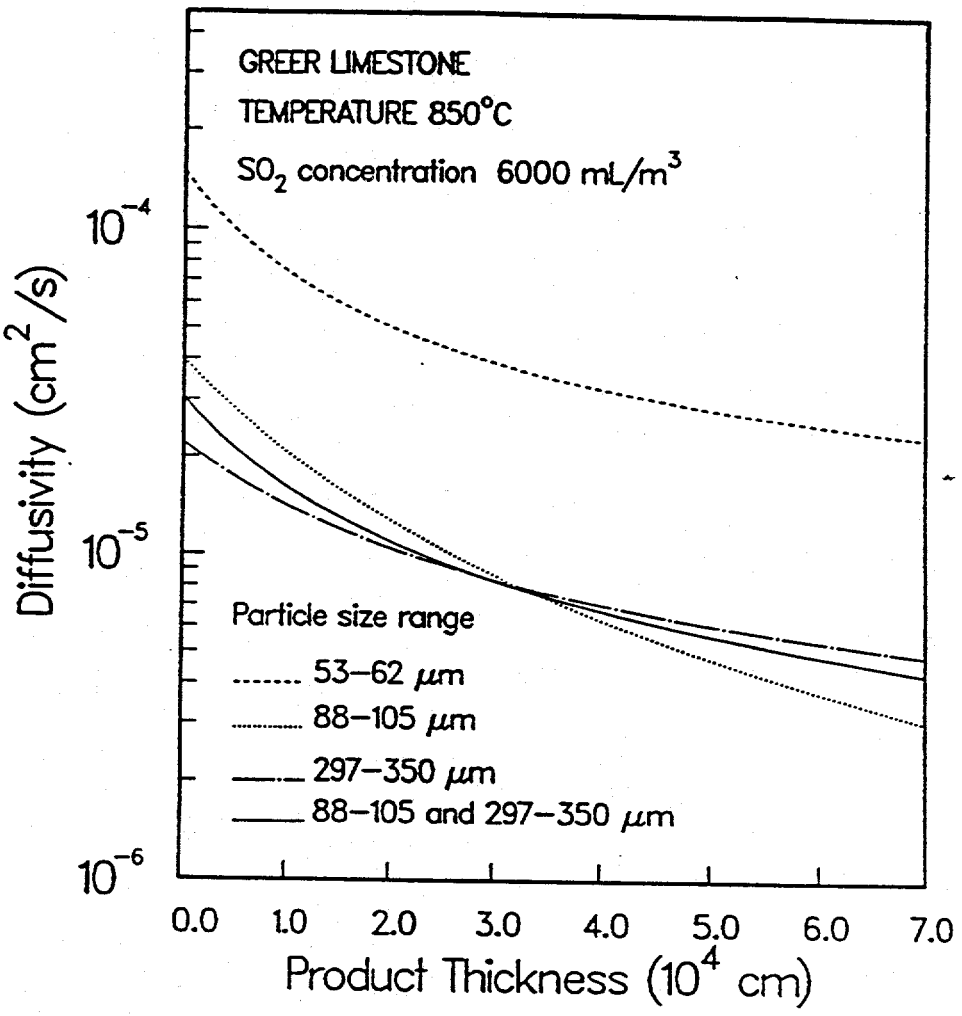

Figure 4.12: Comparison of the effective diffusivity profiles obtained for Greer limestone reacted at 850°C and 6000 mL/m^3 of SO_2 in an atmosphere of 70% $CO_2(mol\%)$ between employing the larger two size ranges together and treating each size range individually.

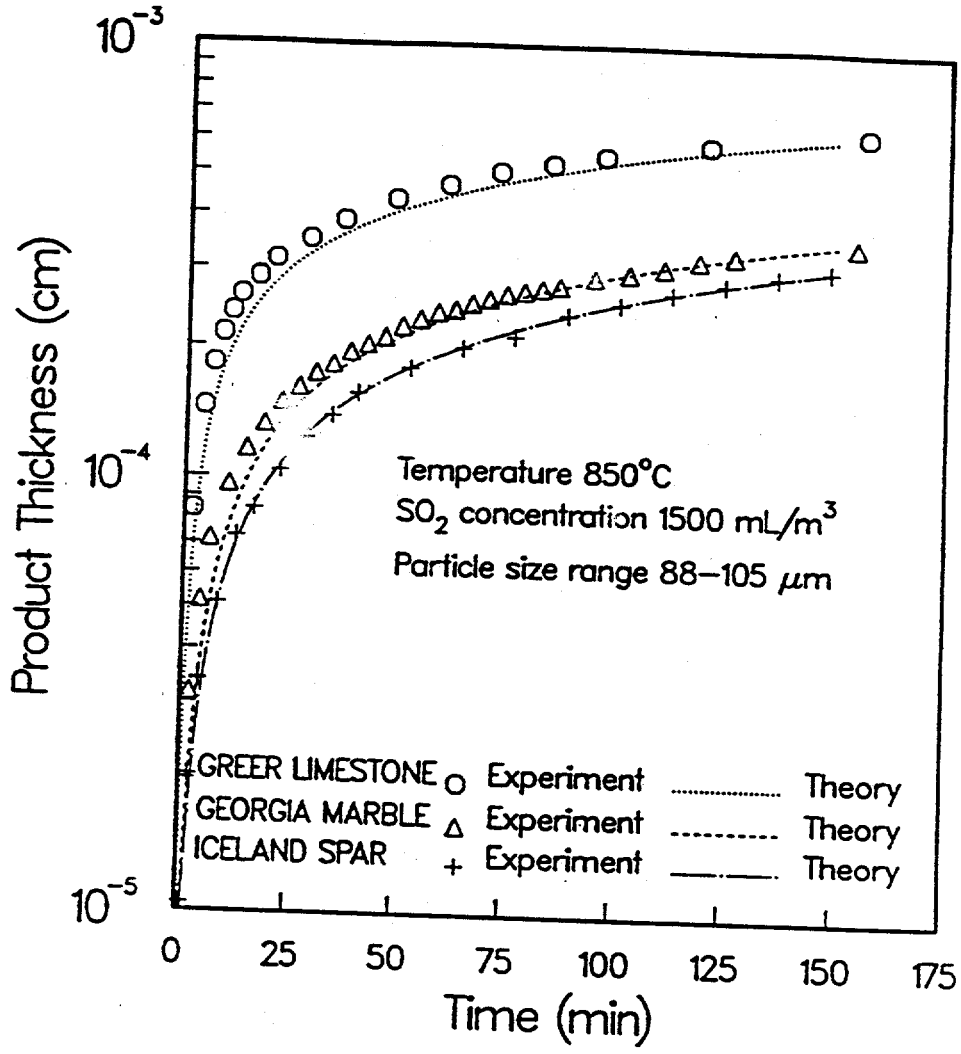

Figure 4.13: Comparison of the growth of the product layer predicted by the model and that obtained from experiments for the three samples (88-105 μm) reacted at 850°C and 1500 mL/m^3 of SO_2 in an atmosphere of 70% $CO_2(mol\%)$.

The diffusivities calculated for the solids under identical reaction conditions but at different concentrations of SO_2 in the bulk (1500 and 6000 mL/m^3) differ significantly for a given distance from the external surface (compare the results of Figs. 4.5 and 4.6). The effective diffusivity of SO_2 through the product layer at a certain depth from the surface for reaction under 6000 $mL/m^3 SO_2$ is in most cases about two to three times smaller that the value estimated at 1500 mL/m^3 of SO_2 at the same reaction temperature and for the same solid. There are two possible explanations, not necessarily mutually exclusive, for this occurrence: 1) The concentration of the gaseous reactant (SO_2) in the bulk may be influencing the structure of the product layer formed during direct sulfation, with the higher concentrations leading to denser layers of solid product; 2) the effective diffusivity in the product layer may be a function of the concentration. In our opinion, the first of these two explanations is the most plausible one since the effective diffusivities that are shown in Figs. 4.5 and 4.6 are comparable to those that one would expect for Knudsen diffusion on the basis of the pore structure characterization data that we presented in the previous study, whereas the coefficient for Knudsen diffusion is independent of the concentration of the diffusing species.

If the effective diffusivity in the product layer is a function of the concentration, it is obvious that for a rigorous application of the variable diffusivity shrinking-core model, the diffusivity would have to vary with both the concentration and the distance in the product layer. It is relatively straightforward to extend the mathematical model so that it allows for a concentration and distance dependent diffusivity and to devise a parameter estimation scheme that would extract D_e as a bidistributed parameter from the experimental data. However, examination of the concentration profile in the product layer and of its evolution in time revealed that the concentration at a given depth from the external surface varied, with the exception of a relatively small time interval after the reactant reached this depth, within a relatively narrow range. Therefore, even if D_e were allowed to vary with both distance and concentration, the obtained results would not be much different, qualitatively and quantitatively, from those shown in Figs. 4.5 and 4.6. Fig. 4.14 shows the concentration profile at 0.5, 1.0, and 2.0 μm from the external surface of the particles, as it is given by the mathematical model, for Greer limestone (53-62 μm) reacted at 750°C at the two

concentrations of 1500 and 6000 mL/m^3 of SO_2. In agreement with the general remarks made above, it is seen that after the reactant reaches a certain depth within the particles, the concentration there rises very fast reaching a 'plateau' value within a very small, on a relative basis, interval of time for both values of bulk concentration.

The product layer diffusivity was assumed to follow an Arrhenius-type dependence on temperature, and the activation energy was estimated as a function of distance from the external surface of the particles for the various cases of Fig. 4.5. The obtained results are shown in Fig. 4.15. Results are shown only for the range of product layer thickness covered experimentally at 750^oC where the lower rates of reaction were observed. It is seen from Fig. 4.15 that at a given depth, Iceland spar has the highest activation energy and Greer limestone the smallest. Therefore, temperature plays a stronger role in influencing the diffusion of SO_2 and, hence, the reaction rate for Iceland spar than for Georgia marble, with Greer limestone being the least affected of the three solids. From experimental data for the sulfation of the calcines of the same solid in the same temperature range, the activation energy for the product layer diffusivities for the $CaO - SO_2$ reaction was found to be 83, 188, and 125 kJ/mol for Greer limestone, Georgia marble, and Iceland spar, respectively (Sotirchos and Zarkanitis, 1992). Comparison of these values with the results of Fig. 4.15 shows that the effect of temperature on the product layer diffusivity during direct sulfation is qualitatively similar to that for the sulfation of the calcines for the Greer limestone and the Georgia marble solids, but it is much stronger in the case of Iceland spar. (Similar values of activation energy of product layer diffusivity were reported by several investigators for other calcined limestones: e.g., 142 kJ/mol by Hartman and Trnka (1980) and 146 kJ/mol by Marsh and Ulrichson (1985)).

It is seen in Fig. 4.15 that for Georgia marble and Iceland spar, there occurs an increase in activation energy with increasing distance from the external surface of the particles. Greer limestone, on the other hand, manifests decreasing activation energy towards the reaction interface. As we mentioned during discussion of the concentration effects on the effective diffusivity values, the mechanism of mass transport in the product layer is most probably Knudsen diffusion. Therefore, the temperature effects on the effective diffusivity seen in Fig. 4.15 in terms of the activation energy should be viewed as indicative

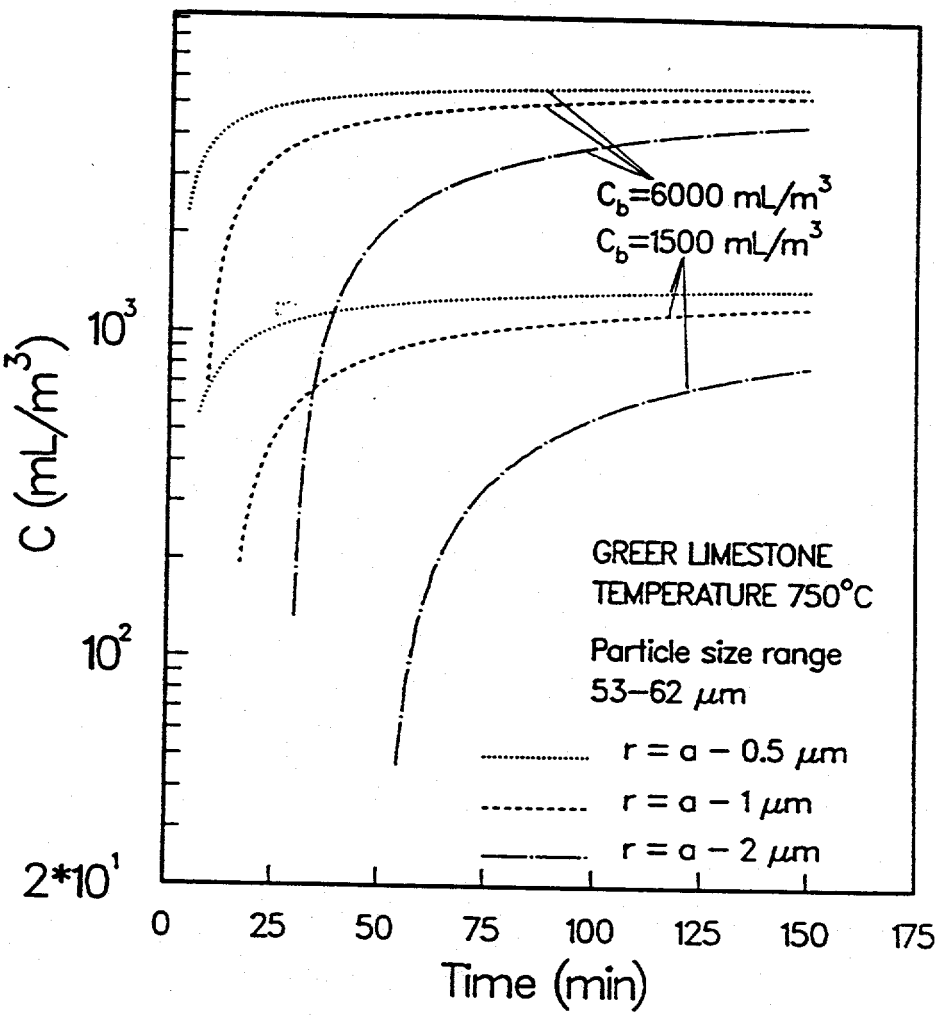

Figure 4.14: Concentration profiles obtained at fixed depths from the external surface of Greer limestone (53-62 μm) particles reacting under different bulk concentrations of SO_2 (1500 and 6000 mL/m^3) at 750^oC in an atmosphere of 70% $CO_2(mol\%)$.

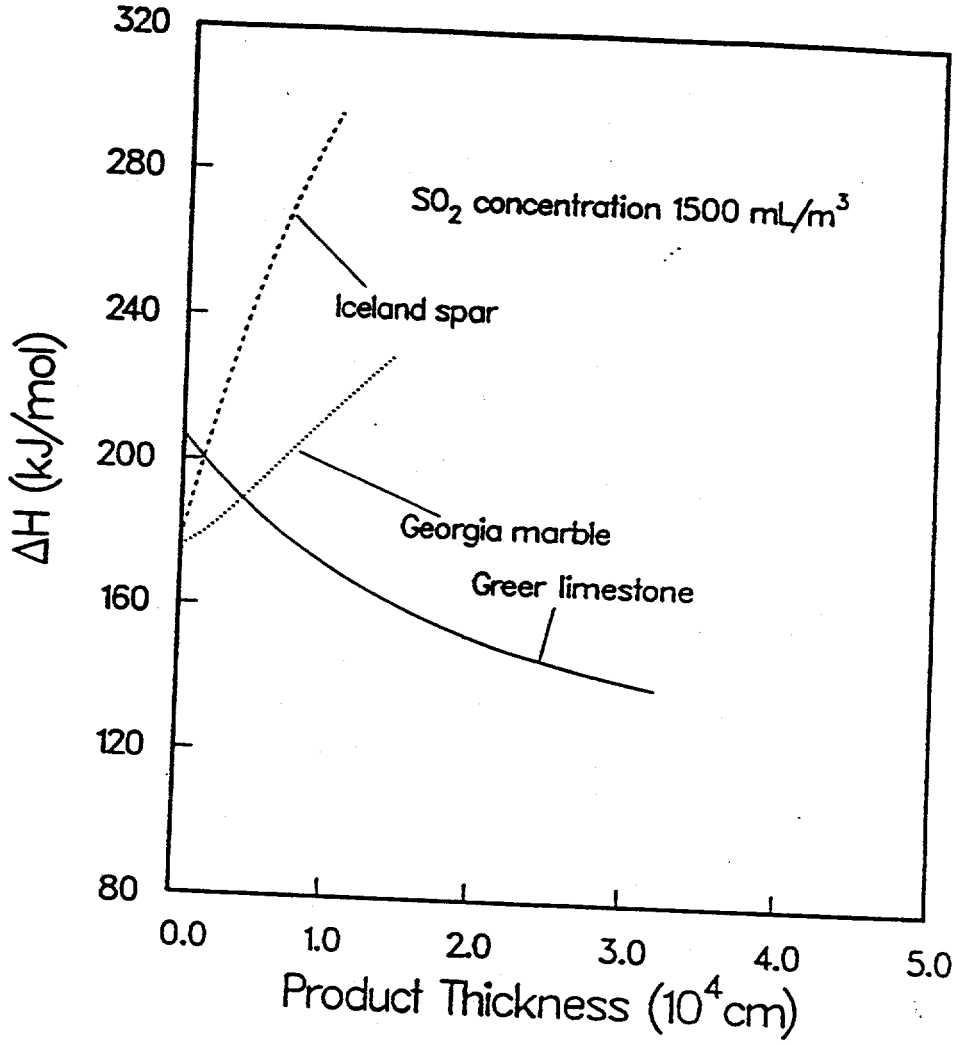

Figure 4.15: Variation of activation energy of product layer diffusivity with product thickness for the three samples reacting under a bulk concentration of SO_2 of 1500 mL/m^3 in an atmosphere of 70% $CO_2(mol\%)$.

not of the effect of temperature on the diffusion process but rather of the effects of temperature on the structure of the product layer. Examination of sulfated (directly) limestone samples by scanning electron microscopy by Hajaligol et al. (1988) suggested that the structure of the product layer became coarser and more open with increasing temperature, in agreement with the results of Figs. 4.5 and 4.6. Hajaligol et al. postulated that since an increase in the temperature increases the rate of reaction, it is the higher rate of CO_2 evolution at higher temperature that is responsible for the development of a more open structure. However, this explanation does not account for other gaseous species involved in the reaction since, as Eq. (4.2) that describes the overall reaction during direct limestone sulfation shows, there is net gas flow toward the unreacted core and not away from it – there is a loss of 1/2 mole of gas per each mole of SO_2 consumed.

In order to be able to obtain a better explanation for the effect of temperature and concentration on the structure of the product layer and, therefore, on the resistance for diffusion of SO_2 through it, one must consider the processes involved in the formation of the $CaSO_4$ layer during direct sulfation. Since the solid product occupies more space than the solid reactant, the solid product formed at the reaction interface must always push against a progressively thicker shell to accommodate itself at the interface. This scenario was used to explain the decreasing diffusivity with increasing distance from the external surface, but it can also be used to explain the effect of concentration at a given temperature and of temperature at a given concentration. A higher concentration leads to a much higher rate of reaction and, therefore, of production of $CaSO_4$ at the interface. The higher rate of $CaSO_4$ formation in turn leads to more compact layers of solid product at a given depth since it gives less time to the grains that comprise the product shell to rearrange themselves to accommodate the added solid volume at the interface. Higher rates of formation of $CaSO_4$ are also encountered at higher temperatures, but temperature is also expected to increase the 'mobility' of the grains in the product layer, thereby making it easier for them to move to accommodate the newly formed solid.

4.5. Summary and Concluding Remarks

A detailed analysis of the process of mass transport within the product shell formed

during the limestone-SO_2 reaction was presented in this study. Experimental results obtained in an earlier investigation (Krishnan and Sotirchos, 1993) for the direct sulfation of three stones of high ($> 95\%$) calcium carbonate content (Greer limestone, Georgia marble, and Iceland spar) were used in the analysis. Characterization of the pore structure of the partially reacted solid in our previous study by N_2 sorption experiments revealed a shrinking-core behavior for the limestone-SO_2 reaction, but analysis of the data with a constant diffusivity shrinking-core model failed to bring theory and experiment into agreement. It was observed that a model incorporating an increasing mass transport resistance in the product shell with time or, equivalently, conversion was needed to make the model predictions agree with the experimental results. Further analysis of the experimental data, performed in the present study, indicated uniform growth rate of the product layer for different particle size ranges, for small values of product layer thickness, at a given set of reaction conditions. Moreover, the calculated concentration of SO_2 at the reaction core had similar values for the different particle size ranges at a given reaction time. These two observations taken together indicated that the average mass transport resistance through the product shell was a function of the thickness of the shell only (without accounting for particle curvature effects).

On the basis of the above results, the direct sulfation of limestone was modelled by a shrinking unreacted core with a diffusion coefficient varying locally with the distance from the external surface of the particles. The functional dependence of the effective diffusivity on the distance in the product layer was determined by fitting the model predictions to the experimental data for three particle sizes for each solid and each set of reaction conditions (temperature and concentration). The parameter estimation scheme gave rise to an ill-posed problem – it was equivalent to the inversion of a Fredholm equation of the first kind – and a procedure based on singular value decomposition was formulated to circumvent this difficulty. Very good agreement between experimental results and model predictions was generally observed when the estimated functional form of effective diffusivity was introduced in the variable diffusivity shrinking-core model. The only exception was seen for the 53-62 μm size particles of Greer limestone at all reaction conditions, which appeared to exhibit much lower resistance for diffusion than the other two other two size ranges (88-

105 and 297-350 μm) of the same solid.

The value of effective diffusivity in the product layer for the limestone-SO_2 reaction fell by an order in magnitude for some cases and by two to three times for all others from the external surface to the maximum depth seen in the experiments. Despite this significant drop, the value of effective diffusivity at the maximum depth was at least two to three orders of magnitude higher than the value of product layer diffusivity for the $CaO - SO_2$ reaction. It is thus believed that the formation of a more open product layer is the main reason for having significant reaction rates in the limestone-SO_2 reaction despite having an essentially nonporous reactant. The effective diffusivity at a certain depth was always the highest for Greer limestone, with Iceland spar displaying the lowest value. Not surprisingly, the overall reaction rates for the three solids followed the same order. It is believed that the differences in the value of effective diffusivity for the three solids are due to the influence of the natural porosity and petrographic texture of the limestones on the structure of the product shell.

The effective diffusivity was found to be a strong function of the temperature and of the concentration of SO_2 in the bulk of the gas phase. Specifically, it increased with increasing temperature but decreased with increasing concentration. The results were in agreement with the observed sensitivity of the experimental conversion vs. time results on temperature and concentration in our earlier investigation. Since the estimated effective diffusivities were comparable to those expected for Knudsen diffusion from the pore structure data, we believe that the main reason for the strong influence of concentration and temperature on the effective diffusivity is their effects on the structure of the product layer.

4.6. Notation

a	outer radius of the particle, cm
a_0	initial radius of the particle, cm
$\mathbf{A}$	N-dimensional vector of coefficients in the expansion of $F_2(l)$
A_i	coefficients of polynomial describing the functional form of effective diffusivity in the product layer

a_c	radius of the unreacted core, cm
$\mathbf{B}$	matrix of dimension $M \times N$ (see Eq. 4.19)
c	concentration of SO_2 in the product layer, mol/mL
c_b	concentration of SO_2 in the bulk, mol/mL
c_c	concentration of SO_2 at the reaction interface, mol/mL
c_s	concentration of SO_2 at the surface of the particle, mol/mL
d	thickness of the product layer $(a - a_c)$, cm
$D_e(x)$	effective diffusivity (local) of SO_2 in the product layer, cm^2/s
D_m	molecular diffusivity of SO_2-gas mixture, cm^2/s
$F_1(t,x)$	equal to $1/(a-x)^2$ by definition
$F_2(x)$	equal to $1/D_e(x)$ by definition
$\mathbf{g}$	M-dimensional vector consisting of the right-hand side of Eq. (4.13)
$g(t)$	equal to $(c_b - c_c)/{a_c}^2 k_s {c_c}^n$ by definition
k_g	external mass transfer coefficient, cm/s
k_s	intrinsic reaction rate constant, $mol^{0.6}/cm^{0.8} \cdot s$
M	number of data points at which Eq. (4.18) is applied
N	number of terms in the linear expansion of $F_2(l)$
n	order of reaction with respect to SO_2
r	radial distance along the product layer, cm
R_s	reaction rate per unit surface area, $mol/s/cm^2$
s	shape factor – 0: slab; 1: cylinder; 2: sphere
Sh	Sherwood number defined as $2k_g a/D_m$
t	real time, s
v_s	molar volume of unreacted core, mL/mol
x	distance in the product layer from the external surface, cm
X	conversion of the reacting solid
Z	volume of dense reacted solid phase per unit volume of dense unreacted solid phase

Greek

α	value of diffusivity at external surface of particle, $x = 0$ in Fig. 4.1, cm^2/s

β parameter describing variation of diffusivity along product depth in Fig. 4.1, cm^{-1}

ϵ_0 porosity of the unreacted soild

$\epsilon(r,t)$ porosity of the product shell at position r and time t

4.7. Literature References

Akima, H., "A New Method of Interpolation and Smooth Curve Fitting Based on Local Procedures," J. ACM, **17**, 589-602 (1970).

Allison, H., "Inverse Unstable Problems and Some of Their Applications," Math. Sci., **4**, 9-30 (1979).

Brown, L.F.; Travis, B.J., "Using Diffusion Measurements to Determine Pore-Size Distributions in Porous Materials," Chem. Eng. Sci., **38**, 843-847 (1983).

Golub, G.H.; Van loan, C.F., *Matrix Computations*, Johns Hopkins University Press, Baltimore (1983).

Hajaligol, M. R.; Longwell, J.P.; Sarofim, A.F., "Analysis and Modeling of the Direct Sulfation of $CaCO_3$," Ind. Eng. Chem. Res., **27**, 2203-2210 (1988).

Hartman, M.; Trnka, O., "Influence of Temperature on the Reactivity of Limestone Particles with Sulfur Dioxide," Chem. Eng. Sci., **35**, 1189-1194 (1980).

Krishnan, S.V; Sotirchos, S.V.; "Sulfation of High Purity Limestones under Simulated PFBC Conditions," Can. J. Chem. Eng., **71**, 244-245 (1993).

Levenspiel, O., *Chemical Reaction Engineering*, John Wiley & Sons, New York (1972).

Marsh, D.W.; Ulrichson, D.L., "Rate and Diffusional Study of the Reaction of Calcium Oxide with Sulfur Dioxide," Chem. Eng. Sci., **40**, 423-433 (1985).

Perry R.H.; Green, D.W; Maloney, J.O, *Perry's Chemical Engineers' Handbook*, 6th ed., McGraw Hill, Singapore (1984).

Press W.H., Flannery, B.P.; Teukolsky, S.A.; Vetterling, W.T., *Numerical Recipes*, Cambridge University Press, New York (1986).

Snow, M.J.H.; Longwell, J.P.; Sarofim, A.F., "Direct Sulfation of Calcium Carbonate," Ind. Eng. Chem. Res., **27**, 268-273 (1988).

Sotirchos, S.V.; Zarkanitis, S, "Inaccessible Pore Volume Formation during Limestone Sulfation," AIChE J., **38**, 1536-1549 (1992).

Szekely, J., Evans, J.E.; Sohn, H.Y, *Gas-Solid Reactions*, Academic Press, London (1976).

Tikhonov, A.N.; Arsenin, V.Y, *Solutions of Ill-Posed Problems*, John Wiley & Sons, (1977).

Tullin, C., Ljungstrom, E., "Reaction between Calcium Carbonate and Sulfur Dioxide," Energy & Fuels, **3**, 284-287 (1989).

5. EFFECTIVE DIFFUSIVITY CHANGES DURING CALCINATION, CARBONATION RECALCINATION, AND SULFATION OF LIMESTONES

5.1. Introduction

Sulfation of limestones is an important gas-solid reaction used for controlling sulfur dioxide emissions from fluidized-bed coal combustors. The limestone precursors used for reducing emissions undergo several changes in their structure depending on the operating conditions of the combustor. In atmospheric fluidized-bed combustors (AFBC), limestone (primarily $CaCO_3$) decomposes almost instantaneously (reaction (5.1)) to yield its calcined form (primarily CaO):

$$CaCO_3 \rightleftharpoons CaO + CO_2 \tag{5.1}$$

The calcine then reacts with SO_2 leading to desulfurization of the flue gas (reaction (5.2)):

$$CaO + SO_2 + \frac{1}{2}O_2 \rightleftharpoons CaSO_4 \tag{5.2}$$

A different situation occurs in a pressurized fluidized-bed combustor (PFBC) where on account of the high partial pressures of CO_2, decomposition of $CaCO_3$ (reaction (5.1)) is inhibited, and direct reaction of $CaCO_3$ with SO_2 takes place instead. Since the temperature and CO_2 partial pressure are not uniform in a PFBC unit, decomposition of $CaCO_3$ (reaction (5.1)) may occur in certain regions of the reactor, while the decomposed limestone may in turn react with SO_2 like in the AFBC units (reaction (5.2)) or undergo recarbonation in regions of high CO_2 concentration or low temperature according to the reaction (reverse of reaction (5.1)):

$$CaO + CO_2 \rightleftharpoons CaCO_3 \tag{5.3}$$

The above reactions are typical examples of noncatalytic gas-solid reactions, involving a porous structure which evolves both temporally and spatially. Limestone precursors are essentially nonporous with very small surface areas. The decomposition reaction (reaction (5.1)) leads to formation of well developed pore structure, with high values of porosity and internal surface area. The sulfation of the calcine (reaction (5.2)) is a very complex reaction characterized by pore closure and formation of inaccessible pore space, both being

a consequence of the fact that $CaSO_4$ (the primary solid product) occupies considerable more space than CaO (the primary solid reactant). The ratio of the volume occupied by the solid product to that of the solid reactant, according to the stoichiometry of the reaction, is approximately 2.7 (using data from Perry et al. (1984)). The additional solid volume formed during sulfation reduces the pore space of the calcine, eventually leading to pore closure. If the reaction occurs under internal diffusion control, sulfation mainly occurs at the periphery of the porous particles, causing pore blockage at the outer surface while there is much open pore space left in the interior. However, even under kinetic control, it is possible small pores that act as feeder pores to clusters of large pores to get plugged, leading to formation of locally inaccessible pore space (Sotirchos and Zarkanitis (19920, (1993)). This situation may also be encountered in reaction (5.33) though not to the same extent as in the sulfation of calcines.

Pore closure and formation of inaccessible pore space cause incomplete utilization of the calcine to levels well below what is stoichiometrically possible. For improved sulfur capture and combustor operation, reaction conditions must be optimized to maximize the utilization of the sorbent. Limestone precursors in the size range of 50-500 μm are typically used for the purpose of desulfurization in fluidized-bed combustors. Sulfation of particles of this size usually occurs in the regime where the diffusion resistance of the reactants through the pore space is one of the important controlling parameters of the reaction (Sotirchos and Zarkanitis (1992)). Therefore, modeling of the sulfation and of the other sorbent reactions for combustor design with the aim of enhancing sorbent efficiency almost always requires knowledge of the intraparticle mass transport resistance in the solid.

Theoretical estimates of effective diffusivities of gases through porous medium have been known to significantly differ from the experimentally measured values, at times by more than an order in magnitude (Haynes (1988)), necessitating the development of reliable experimental techniques to obtain information on the intraparticle mass transport process. Experimental values of effective diffusivity ofCO_2 through porous CaO have been obtained byvarious approaches. Hills (1968) studied the mass transportof CO_2 through the porous CaO formed during the thermal decomposition of calcium carbonate (reaction (5.1)) in a thermobalance. Assuming a sharp interface at the reaction front, the diffusivity

of CO_2 through the calcined layer was obtained at various temperatures by measuring the transient weight change. However, despite the simplicity of the calcination reaction, there are conflicting views in the literature on its controlling mechanism (Narsimhan (1961); Hills (1968); Borgwardt (1985)). Therefore, the results obtained by Hills (1968) strongly depend on the validity of the model proposed for the calcinationstep. Campbell et al. (1970) measured the diffusion coefficient of CO_2 through hollow lime spheres prepared from spherical compacts of calcium carbonate with the porosity of the original compact ranging up to 0.66. Diffusion coefficients were measured directly in both the original compact and its calcined form in a manner similar to that of the Wicke-Kallenbach experiment (Wicke and Kallenbach, 1941). The diffusion coefficients measured by Campbell et al. cannot be used to obtain information about diffusion of gases in calcines of limestones or dolomites since it is difficult to isolate the individual mass transfer resistances, that is, through the pores of the original compact and through the pores formed during calcination.

Bardakci (1984) measured the effective diffusivity of argon through a calcined pellet in a Wicke-Kallenbach diffusion cell in the course of sulfation. The data were used to obtain the diffusivity of SO_2 through the porous layer by using the fact that under isobaric conditions the ratio of the fluxes of the two gases is equal to the inverse square root of the ratio of their molecular weights (Evans et al., 1961). The product layer diffusivity as a function of conversion was subsequently estimated from an expanding grain model based on the effective diffusivity of SO_2 through the reacting shell. Using the same experimental setup, effective diffusivities of Ar and N_2 were measured as a function of time during calcination (Bardakci and Gasner, 1984). Limestone pellets of large size were used in the study of Bardakci (1984) to measure diffusivities during the sequence of calcination and sulfation carried out in the Wicke-Kallenbach apparatus. As a result, only a relatively thin layer of the solid was reacted during sulfation, and thus, the measured transport resistance accounted for the resistances of both the reacted and unreacted sections of the pellet. To extract the value of the average effective diffusivity in the reacted section, additivity of the diffusion resistances in the reacted and unreacted sections was assumed, and the thickness of the reacted layer was determined from the average conversion of the pellet, the latter estimated with the aid of the grain model.

In view of the importance of intraparticle mass transport in the control of sulfur emissions from coal-fired power plants using limestones as the desulfurizing agent, an investigation of the diffusion resistance in calcined limestones is carried out in this study. Pulse chromatographic experiments are performed for this purpose byemploying two different types of limestones. Different calcination temperatures are used to study the effect of calcination temperature on the internal pore structure and effective diffusivity of the calcine formed.Effective diffusivities through the carbonated and recalcined forms of the calcines are also measured to investigate changes in intraparticle mass transfer resistance. One of the limestone calcines is sulfated, and the effective diffusivity is measured at several conversion levels. The pore size distributions of all the solids used in this study are determined from mercury intrusion (using a Micromeritics, Autopore II 9220 system) and gas sorption experiments (using a Quantachrome Autosorb-1 unit). Employing the pore size distribution and the measured values of effective diffusivities, information about the connectivity of the pores is obtained using the effective medium theory–smooth field approximation approach of Burganos and Sotirchos (1987).

5.2. Materials and Sample Preparation

Two types of limestone were used as precursors to carry out diffusivity measurements in calcines, carbonated calcines, and sulfated calcines. The two limestones, each with a very high $CaCO_3$ content ($> 95\%$ by weight), were distributed by Greer Limestone Co. and Georgia Marble Co., and will be for brevity denoted as GL and GM respectively. From mercury porosimetry and gas sorption experiments, the limestones were found to be essentially nonporous in their natural states. Petrographic examination of the two stones showed differences in their grain structure, and details are given by Sotirchos and Zarkanitis (1992). Particles in the size range of 20-24 mesh (710 - 850 μm) were used to measure the diffusivities reported in this study.

The relatively large amounts of solid sample needed to pack the chromatographic column were prepared in a fluidized-bed reactor. A brief description of the preparation procedure is given in the following paragraphs. Details on the experimental set up and the procedure used for the preparation of the samples are presented by Krishnan (1993).

About 35 g of calcined limestone was needed to fill the chromatographic column chosen in our study. To obtain this amount, approximately 120 g of the uncalcined limestone precursor was calcined in the fluidized-bed reactor for 1 hr in six batches (for each limestone and reaction temperature) to produce the required amount of the calcined material. The sample was brought to the calcination temperature under CO_2 to prevent its decomposition during heating, and calcination was started by switching the CO_2 stream to a N_2 stream. The same procedure was used for the calcination of carbonated calcines. To verify that complete calcination had taken place, the reacted material and the fines trapped in a cyclone located at the outlet of the fluidized-bed reactor were weighed at the end of each experiment. The reacted material was resieved to isolate the size range (710-850 μm) that we used to pack the chromatographic column.

Carbonation of the calcines was carried out by reversing the procedure used for calcination of the precursors. Specifically, N_2 was passed through the reactor until the desired reaction temperature was attained, whereupon the N_2 stream was substituted with a CO_2 stream. Carbonation for each batch of material was carried out for 1 hr. Approximately 50 g of the calcined material was carbonated in four batches for each case investigated. The carbonated material in the reactor and the fines in the cyclone were weighed to estimate the conversion level attained upon carbonation. Again, the carbonated material was resieved to isolate the 710-850 μm size range.

To study mass transport in calcines undergoing sulfation, fresh samples of Georgia marble calcine were prepared at $850°C$ in batches of approximately 7.5 g of the precursor. The calcines were subsequently sulfated in batches of approximately 5 g at the same temperature using a mixture of 1500 ppm of SO_2 in air. The extent of sulfation was determined by measuring the concentration of SO_2 in the exit stream with the aid of a chromatograph (Varian 3300) equipped with an flame photometric detector. The calcines were sulfated for periods of 5, 15, 30, and 45 min which resulted in conversion levels of approximately 1, 2, 5, and 8 %, respectively. The conversion levels were also verified by weighing the reacted samples and the fines collected in the cyclone. The sulfated samples from the reactor were resieved after every stage to obtain the 710-850 μm size range.

A summary of the physical properties of the solids (calcined, carbonated, and recal-

cined) prepared in the ways described above is given in Table 5.1. The reported skeletal densities were determined from He pycnometry experiments. The skeletal densities so obtained were found to be in close agreement with those estimated from the composition of the solids using values for the pure compounds from Perry et al. (1984). The surface areas of the solids were estimated from multipoint BET analysis of the adsorption isotherm. All calcines are found to have similar surface areas, with the Greer limestone calcined at $750°C$ exhibiting the highest and that calcined at $850°C$ the lowest. Very small surface areas were estimated for the carbonated samples (both Georgia marble and Greer limestone). Recalcination increased the surface areas of the solid samples, but the measured values were much lower than those of the one-time calcined samples. The variations seen in the surface areas are discussed in more detail later using pore size distributions of the solids and other experimental data.

Solid	State	React. Temp. ($°C$)	Conv. (%)	Porosity merc. int. (cc/cc)	Porosity N_2 sorpt. (cc/cc)	Porosity Eq. (5.4) (cc/cc)	Porosity moment (cc/cc)	Surface Area (m^2/g)	Skeletal Density (g/cc)
GL	calcined	850	100	0.51	0.48	0.54	0.52	45.09	3.29
GL	carbonated	850	74	0.07	0.02	0.14	0.14	0.66	2.78
GM	calcined	850	100	0.46	0.47	0.53	0.51	52.48	3.31
GM	carbonated	850	56	0.03	0.01	0.23	0.22	0.34	2.95
GM	recalcined	850	100	0.36	0.43	0.53	0.51	33.96	3.25
GL	calcined	750	100	0.51	0.49	0.54	0.52	56.19	3.24
GL	recalcined	750	100	0.34	0.44	0.54	0.52	27.36	3.27

Table 5.1: Data for Calcined, Carbonated, and Recalcined Limestones. GL=Greer limestone, GM=Georgia marble, and IS=Iceland spar.

The porosities reported in Table 5.1 were obtained employing three different approaches. Mercury porosimetry porosities were determined on the basis of intrusion volumes above an applied pressure of 80 psi (that is, for pores smaller than about 1 μm).

Sorption isotherm porosities were obtained for pores of radius up to 1000 Å. It is well known that these experimental techniques suffer from drawbacks. Mercury porosimetry is known to be unreliable in the region of small sized pores (radius less than 20 Å) because of mercury and sample compressibility effects. Nitrogen sorption, on the other hand, is unreliable for larger sized pores (pores greater than 1000 Å), and therefore, it furnishes only partial information about the internal void space. On account of the above limitations, these two experimental techniques did not yield the same porosity values for the solid samples (see Table 5.1). Moreover, for the reacted solids both gave results different from those predicted from volume changes accompanying the reaction. The predicted porosities were calculated using the expression

$$\xi = \frac{\epsilon_0 - \epsilon}{(Z-1)(1-\epsilon_0)} \tag{5.4}$$

where ξ is the conversion level of the solid, ϵ_0 and ϵ are the initial (theoretically determined) and final porosities of the solid, respectively, and Z is the ratio of the molar volume of the solid product to that of the solid reactant for each gas-solid reaction.

Conversion (%)	Porosity merc. int. (cc/cc)	Porosity Eq. (5.4) (cc/cc)	Porosity moment (cc/cc)	Surface Area (m^2/g)
0	0.46	0.53	0.51	52.48
1	0.44	0.52	0.49	33.20
2	0.43	0.51	0.47	30.80
5	0.40	0.49	0.46	31.2
8	0.38	0.47	0.43	27.5

Table 5.2: Data for Georgia Marble Calcines Sulfated at $850°C$.

Table 5.2 provides the surface areas and porosities of the sulfated samples of Georgia marble at the conversion levels studied. The surface areas were obtained from BET analysis of the nitrogen sorption data and the particle porosities from mercury intrusion data. Similarly

to the results seen in Table 5.1, the experimentally measured porosities do not agree with the theoretically estimated values (from Eq. (5.4)). The discrepancies in the estimated voidage of the porous solids by different methods are explained later on the basis of the pulse chromatographic response curves.

5.3. Pulse Chromatographic Experiments and Data Analysis

A chromatographic setup equipped with a high speed and high resolution data acquisition system was used for pulse chromatographic experiments. Details about the system are given by Krishnan (1993). Two different column lengths (50 and 150 cm) were used in our study. The chromatographic column was filled with the solid and a dilute pulse of He in N_2 (less than 15% He on a molar basis) was injected in the column with N_2 as the carrier gas. Chromatographic response curves were obtained at the same flow rate for both the 50 and the 150 cm columns packed in the same way and with the same solid. Six to seven sets of responses were used to cover the operating range of flow rates used in this study.

High flow rates and large size particles increase the sensitivity of the response to the particle effective diffusivity. The maximum flow rate is limited by the need to have insignificant pressure drop along the chromatographic column, whereas the particle size can be as large as the internal diameter of the column (single pellet string reactor). However, since our aim was to obtain uniformly calcined particles within a reasonable amount of time – very large particles require extremely long times for complete calcination – a size range of 710–850 μm was chosen for our experiments. The flow rate of the carrier gas, on the other hand, ranged from 70 to 110 ml/min. In general, these conditions led to chromatographic column responses that were highly sensitive with respect to the particle effective diffusivity.

The reproducibility of the tracer response is among the factors that have the strongest influence on the accuracy of the estimated effective diffusivity. Irreproducible response curves are most frequently caused by differences in column packing. To avoid this problem, the two columns (50 and 150 cm) were packed with particles of the same size range and with sample amounts that would result in identical bed voidage (about 0.44) for each case

(Krishnan, 1983). Test experiments were carried out using packed and repacked columns to verify the reproducibility of the response curves. Identical response curves were obtained in all cases for the same solid and bed length.

It is well known that end effects, such as those resulting from the dynamics of the response of the detector and the presence of dead space in the fittings and the injection valve, also contribute to the spread of the injected pulse. These effects can be minimized by proper design of the experimental setup but can never be eliminated. In addition to the above factors, the method of analysis plays a crucial role in determining the accuracy of the estimated value of effective diffusivities (Aust et al., 1987). In order to remove the uncertainty resulting from the presence of end effects and inaccuracies in the data at the tail section of the response, a time domain procedure (Krishnan, 1993) was employed for data analysis and effective diffusivity estimation. The method is based on the assumption that the end effects are at a given set of operating conditions the same in both the 50 and 150 *cm* columns and that the transfer function that represents them is arranged in series with the transfer function yielding the response of an ideal column.

It follows from this assumption that if the response of the real 50 *cm* column is convoluted with the response of an ideal 100 *cm* column, the result should be the response of the real 150 *cm* column. Therefore, our method of analysis rests in convoluting the response 50 *cm* column with the theoretically predicting response of an ideal (without end effects) 100 *cm* column and matching the result with the measured response of the 150 *cm* column. The method is illustrated in Fig. 5.1. In estimating the effective diffusivities of a certain sample, all chromatographic responses measured for it (that is for all flow rates) were employed. The parameter estimation scheme rests in the minimization of the integral square error between the theoretical (convoluted) and the experimental response curves of the 150 *cm* column, that is, in the minimization of the quantity

$$ISE = \sum_{k=1}^{M} \sum_{i=1}^{N^k} \left({c^k}_{th}(t_i) - {c^k}_{ex}(t_i) \right)^2 \tag{5.5}$$

where M is the number of flow rates at which the responses for both the 50 and 150 *cm* columns were recorded, and N^k is the number of data points for the k^{th} flow rate, and ${c^k}_{th}(t)$ and ${c^k}_{ex}(t)$ are the convoluted and the experimental 150 *cm* column responses,

respectively, for the k^{th} flow rate.

The Kubin-Kucera model (Kubin, 1965; Kucera, 1965) was used to describe the response of the ideal column. For the first two moments (first absolute and second central), it yields the expressions (Suzuki and Smith, 1975)

$$\mu_1 = \frac{L}{u}(1 + \frac{(1-\beta)}{\beta}\epsilon(1+K)) \tag{5.6}$$

$$\sigma^2 = \frac{2L}{u}[(1 + \frac{(1-\beta)}{\beta}\epsilon(1+K))^2\frac{D_b}{u^2} + \frac{(1-\beta)}{\beta}(\frac{b\epsilon^2(1+K)^2}{3k_g} + \frac{b^2\epsilon^2(1+K)^2}{15D_e})] \tag{5.7}$$

It is seen from these equations that in addition to several known quantities (the particle porosity, ϵ, the bed porosity bed, β, the bed length, L, the particle size, b, and the interstitial velocity, u), three more parameters are appear in the model in addition to the effective diffusivity; D_e: the axial dispersion coefficient, D_b, the mass transfer coefficient at the external surface of the particles, k_g, and the volumetric equilibrium adsorption constant, K. Some information on the estimation of these parameters is given in the following paragraphs.

Noise and inaccuracies in the measured response, especially at its tail, have a dramatic effect on the value of the second central moment (σ^2), but influence insignificantly the first moment (μ_1) (Krishnan, 1993). The first moment of the response curves was thus used to find the value of K. It can be shown that the first moment of an ideal 100 cm column can be determined by subtracting the value of μ_1 of the 50 cm column from that of the 150 cm column. K can then be determined from Eq. (5.6) provided that the particle porosity is known. Preliminary calculations using the response curves for the calcines of Greer limestone – for which the porosities found from pore structure characterization are comparable to that expected theoretically (see Table 5.1) – suggested insignificant adsorption on the solid. It was thus decided to proceed assuming nonadsorbing behavior for all cases ($K = 0$). This is a reasonable assumption considering that the diffusing species is He. The particle porosities that were determined for the once calcined solids were in rather good agreement with those predicted from Eq. (5.4) (see Table 5.1).

The external mass transfer coefficient plays a minor role in influencing the shape of the response curve under the experimental conditions used in this study. This was verified

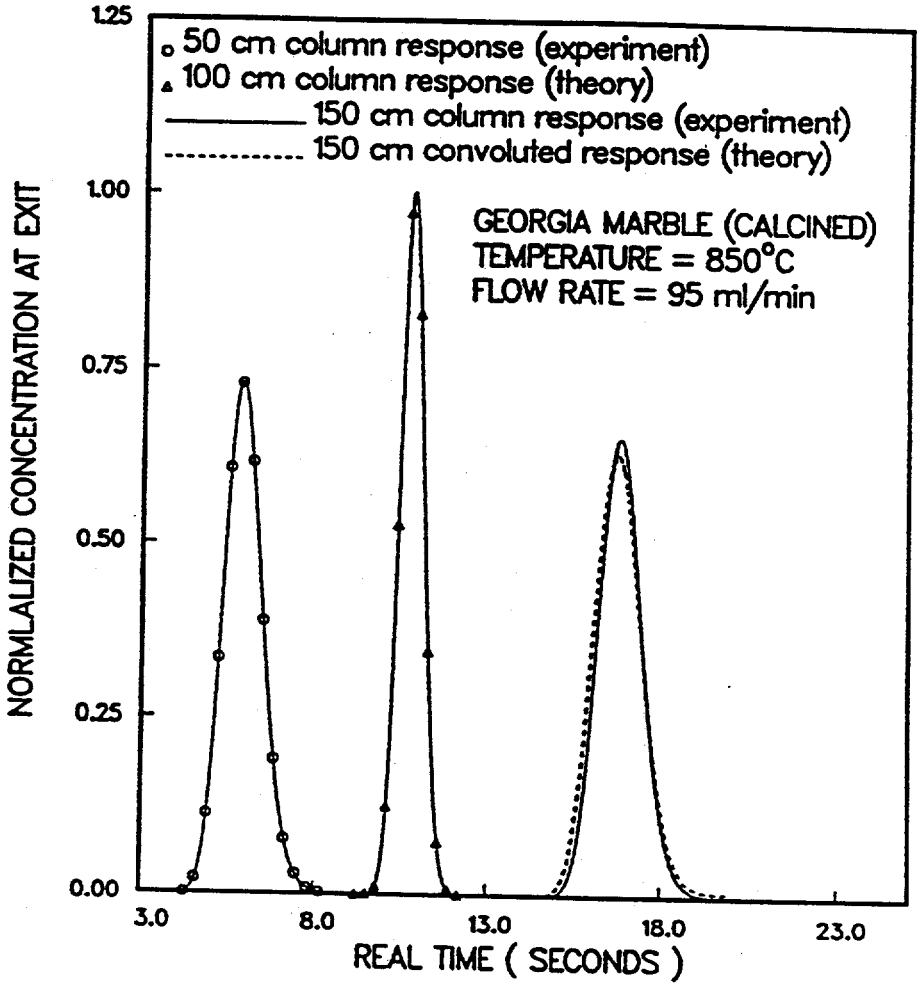

Figure 5.1: Illustration of the time domain parameter estimation procedure employed in this study showing the comparison of the 150 *cm* experimental response curve with the 150 *cm* theoretical response curve. The theoretical curve is obtained by convoluting the 50 *cm* experimental response with the simulated 100 *cm* column response.

by carrying out simulation studies in the time domain (Krishnan, 1993) using Sherwood numbers (based on particle radius) ranging from 1 (the value for a stagnant film in spherical geometry) to ∞. The response curves were thus analyzed assuming that there was no mass transfer resistance between the particles and the bulk of the gas phase.

Despite experimenting under conditions that yield high sensitivity of the chromatographic response curves with respect to the particle effective diffusivity, the axial dispersion in the column contributes a significant fraction to the total spread of the curve. For a tortuosity factor of two for the bed packing ($D_b = 0.35$ cm^2/s) and nonadsorbing molecules, the contribution of axial dispersion for the calcines to the overall spread of the curve turns out to be approximately 40% for an effective diffusivity of 10^{-2}cm^2/s at the higher flow rates. Of course, for smaller effective diffusivities – as it is probably the case for the carbonated samples – the contribution of axial dispersion to the total spread of the response is much smaller. D_b can be determined together with the effective diffusivity by minimizing the integral square error (Eq. (5.5)) with respect to both these parameters. However, since the only transport parameter that causes dispersion of the injected pulse in columns packed with nonporous solids is the axial dispersion in the bed, it was decided to determine D_b independently of D_e by using the response curves for the precursors.

Analysis of the chromatographic response curves was performed in the time domain for columns packed with Greer limestone and Georgia marble precursors. The method of analysis was again based on minimization of the quantity given by Eq. (5.4) for all flow rates used in the experiments (70-110 ml/min). Analysis of the response curves for the precursors gave a value of $D_b = 0.4$ cm^2/s for Greer limestone and 0.35 cm^2/s for Georgia marble. Excellent agreement was found to exist between theoretical predictions and experimental results (Krishnan, 1993). Based on a value of 0.69 cm^2/s for the molecular diffusion coefficient for the He-N_2 pair, calculated from the Chapman-Enskog equation (Bird et al., 1960) under the experimental conditions of our studies, the values of D_b estimated for Greer limestone and Georgia marble predict a tortuosity factor of 1.73 and 1.97, respectively, for diffusion in the space between particles.

5.4. Effective Diffusivities and Pore Structure Properties

The effective diffusivities that were estimated from the analysis of the experimental data for all the samples we employed in this study are given in Table 5.3. The relative differences that are observed among the diffusivities of the various samples are discussed in the following sections in conjunction with the mercury and gas adsorption pore size distributions and the porosity values that are extracted from the chromatographic response curves.

Fig. 5.2 shows experimental response curves obtained for the 150 cm long column packed with Greer limestone particles calcined at 750 or 850^oC and Georgia marble particles calcined at 850^oC at a flow rate of 107 ml/min. Because of their highly symmetric shape and the occurrence of their peaks at about the same time, the three response curves have first moments that are similar in value. Parameters L, u, and β have the same values for all cases of Fig. 5.2, and thus, the same porosity is determined from Eq. (5.6) for all solids (see Table 5.1). (Recall that the adsorption equilibrium constant is set equal to zero to obtain the results reported here.) The spread of the response curve decreases in the order Greer limestone calcined at 750^oC $\rightarrow$ Georgia marble calcined at 850^oC $\rightarrow$ Greer limestone calcined at 850^oC, while, as the results of Table 5.3, show the effective diffusivity increases in the same order. This result is agreement with the predictions of the equation for the second moment of the response which suggests increasing second moment with decreasing intraparticle effective diffusivity.

Fig. 5.3 shows the pore size distributions of the calcines obtained from mercury intrusion and nitrogen desorption. Pore size distributions obtained through these methods generally shift the actual pore size distribution towards smaller pore sizes (Efthimiadis and Sotirchos, 1993). Provided that all pores are filled with adsorbate before desorption starts and that nucleation effects are absent during desorption (that is, a pore empties only if it can reach the external surface of the particles through a path of empty pores), the theory predicts that mercury intrusion and gas desorption should produce the same pore size distribution curve. If there are empty pores when desorption starts – this is usually the case since most solids have some porosity residing in the above 1000 Å size range – the nitrogen desorption pore size distribution should be shifted toward larger pore

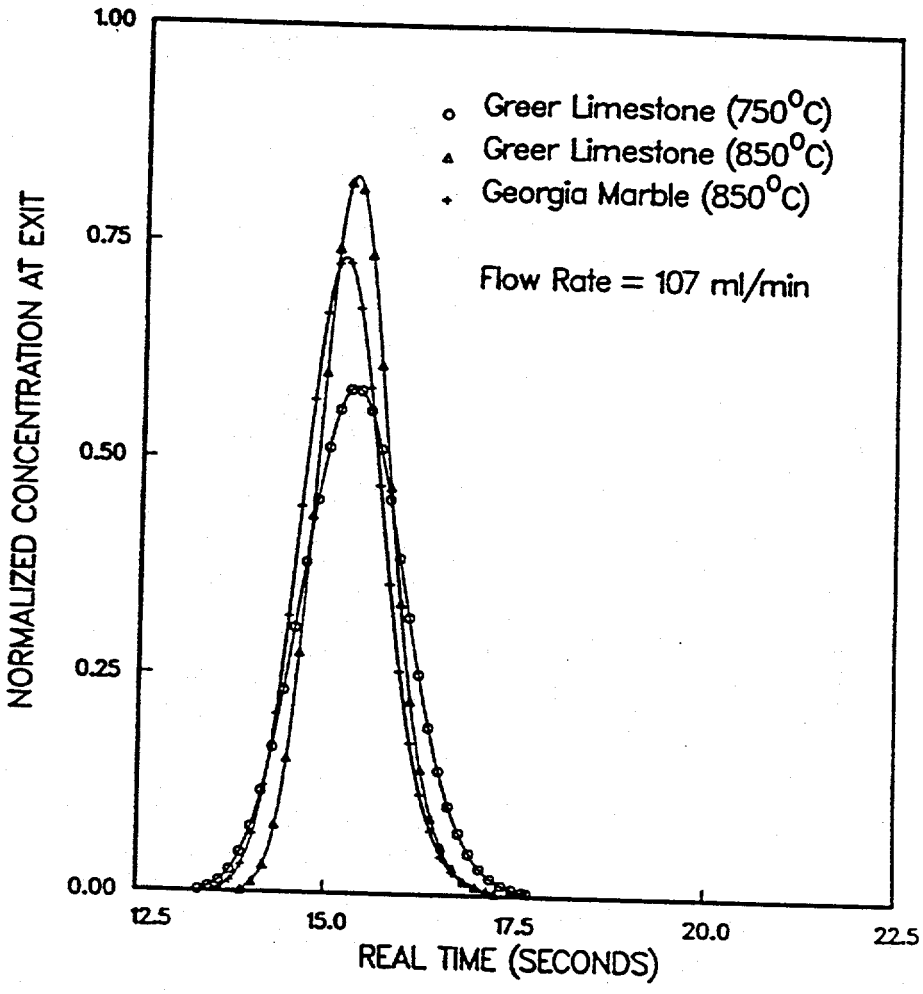

Figure 5.2: Chromatographic response curves of the 150 *cm* column packed with either Greer limestone calcined at 850°*C*, Georgia marble calcined at 850°*C*, or Greer limestone calcined at 750°*C*. The response curves were obtained at a flow rate of 107 ml/min.

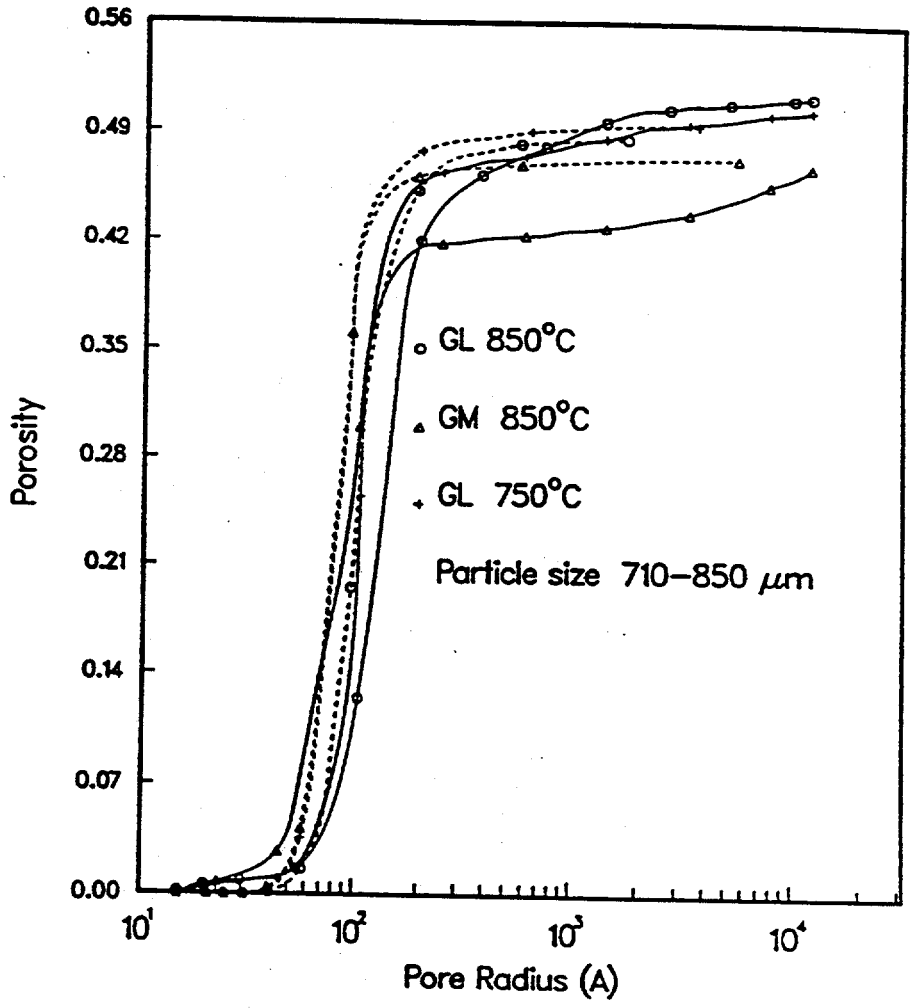

Figure 5.3: Pore size distributions of the calcines obtained from mercury intrusion (solid lines) and nitrogen desorption (dashed lines).

sizes relative to that resulting from mercury intrusion (Efthimiadis and Sotirchos, 1993). However, the opposite behavior is observed in Fig. 5.3, that is, the mercury intrusion pore size distributions are shifted towards larger pores in comparison to those obtained from nitrogen desorption. This is probably due to the destructive nature of mercury porosimetry, which can cause crushing of small pores at pressures corresponding to larger pore sizes and thus shift the measured pore size distribution toward larger pores.

Solid	State	Reaction Temp. (°C)	D_e (cm^2/s)
GL	calcined	850	1.9×10^{-2}
GL	carbonated	850	6.0×10^{-4}
GM	calcined	850	1.2×10^{-2}
GM	carbonated	850	6.4×10^{-4}
GM	recalcined	850	1.9×10^{-2}
GL	calcined	750	5.0×10^{-3}
GL	recalcined	750	7.0×10^{-3}
GM	sulfated (0 %)	850	1.2×10^{-2}
GM	sulfated (1 %)	850	9.5×10^{-3}
GM	sulfated (2 %)	850	8.0×10^{-3}
GM	sulfated (5 %)	850	7.0×10^{-3}
GM	sulfated (8 %)	850	6.5×10^{-3}

Table 5.3: Effective Diffusivities of He (in N_2) in Calcined, Carbonated, Recalcined, and Sulfated Samples. GL=Greer limestone, GM=Georgia marble, and IS=Iceland spar.

Nitrogen adsorption does not suffer from the above drawbacks, and therefore a more meaningful comparison of the pore size distributions of different solids for pores smaller than about 1000 Å can be carried out by employing the pore size distributions obtained through it. According to the results of Fig. 5.3, Greer limestone calcined at $850°C$ displays the largest most probable pore radius among the three samples, and – provided that the

pore connectivities of the three porous solids are comparable – is therefore expected to offer the least mass transport resistance, in agreement with the results obtained from the pulse chromatographic experiments (Fig. 5.2 and Table 5.3). Because of the similar pore size distributions of the other two calcines, no conclusions can be reached on their mass transport resistance from their pore size distributions. It should be noted that the pore size distributions of the three calcines that are determined from nitrogen adsorption are shifted towards larger pores, as expected because of hysteresis effects, but follow the same pattern as those obtained from nitrogen desorption (Krishnan, 1993).

The changes occurring in the intraparticle mass transport resistance during calcination and carbonation of Greer limestone at $850°C$, calcination, carbonation, and recalcination of Georgia marble at $850°C$, and calcination and recalcination and Greer limestone at $750°C$ can be qualitatively followed from the chromatographic response curves shown in Figs. 5.4, 5.5, and 5.6, respectively. The physical changes that the precursor undergoes upon reaction (that is, the development of internal pore space during calcination or the reduction of the size of existing pores during carbonation) can be the only cause of the differences seen in the response curves. The particle voidage and the intraparticle effective diffusivity are in turn (see eqs. (5) and (6)) the only parameters of the chromatographic response model that are affected by the internal structure of the particles. In all three cases, the unreacted precursors yield the response with the least spread and the smallest first moment, while the curve for the calcined sample appears in each case much later than that of the precursor.

The response of the column packed with the carbonated sample appears immediately after that of the column packed with the nonporous precursors, and this is a consequence of the fact that carbonation leads to a drastic decrease in the particle voidage (see Table 5.1). Despite the low porosity of the carbonated sample, the spread of its response is larger than that of the response of the precursor and similar to that of the response of the calcined sample. This result is indicative of a much lower value of effective diffusivity for the carbonated sample than for the calcined sample, and this is exactly what the results of Table 5.3 show. The peak of the response of the recalcined sample appears at the same time instant as that of the calcined sample (see Figs. 5.5 and 5.6), reflecting the fact that

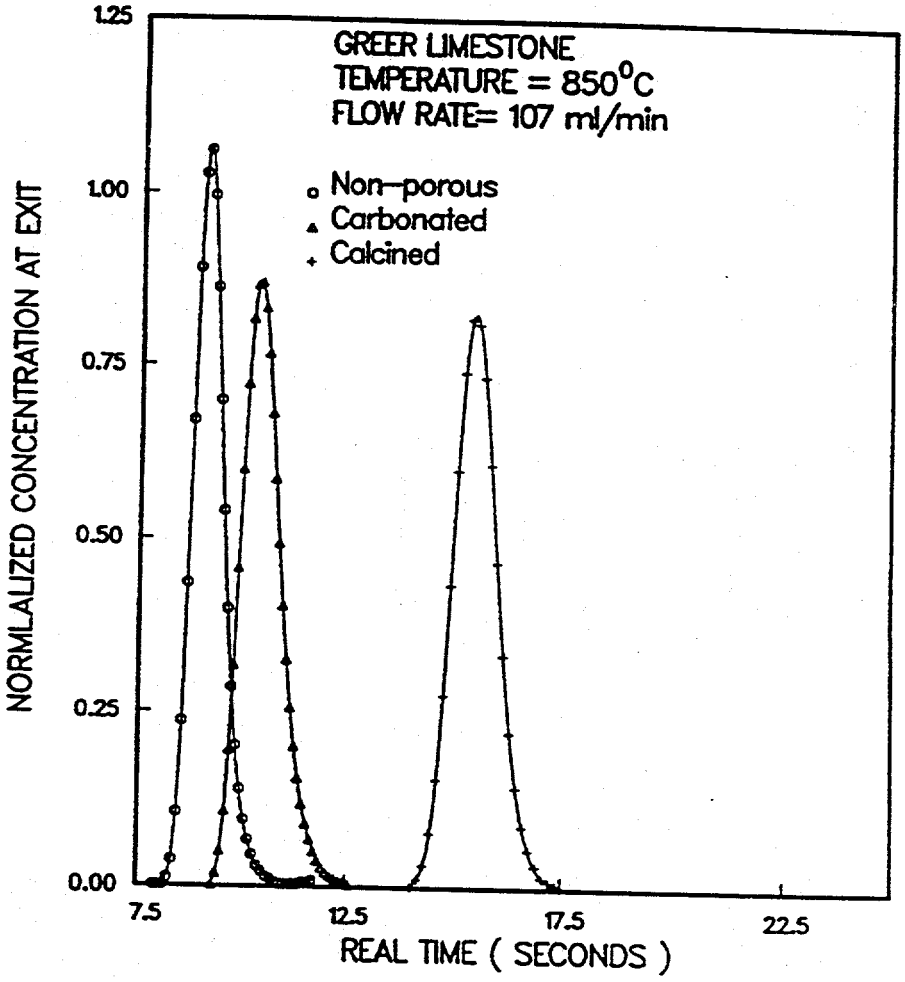

Figure 5.4: Chromatographic response curves of the 150 *cm* column for calcined and carbonated Greer limestone samples. The calcination and carbonation reactions were carried out in the fluidized-bed reactor at 850°C under pure N_2 and CO_2, respectively. The response curves shown in the figure were obtained at a flow rate of 107 ml/min.

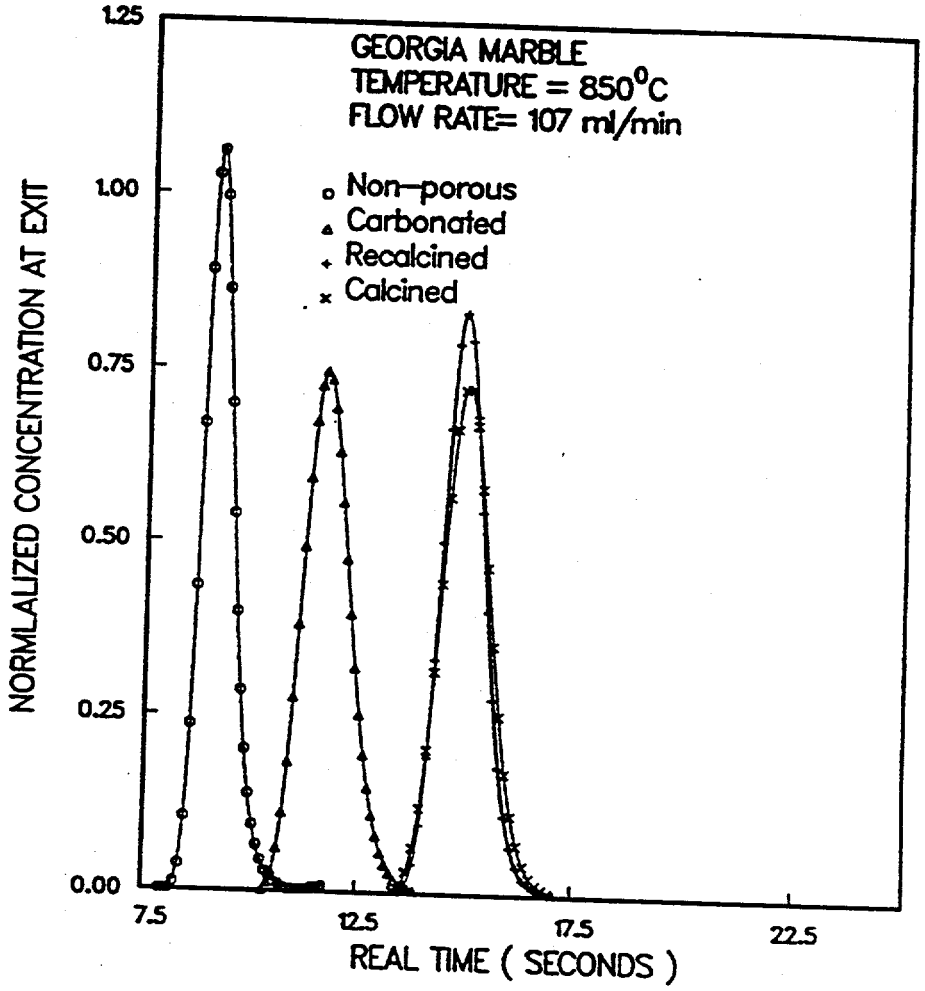

Figure 5.5: Chromatographic response curves of the 150 *cm* column for calcined, carbonated, and recalcined Georgia marble samples. The reactions were carried out in the fluidized-bed reactor at 850°C. The response curves shown in the figure were obtained at a flow rate of 107 ml/min.

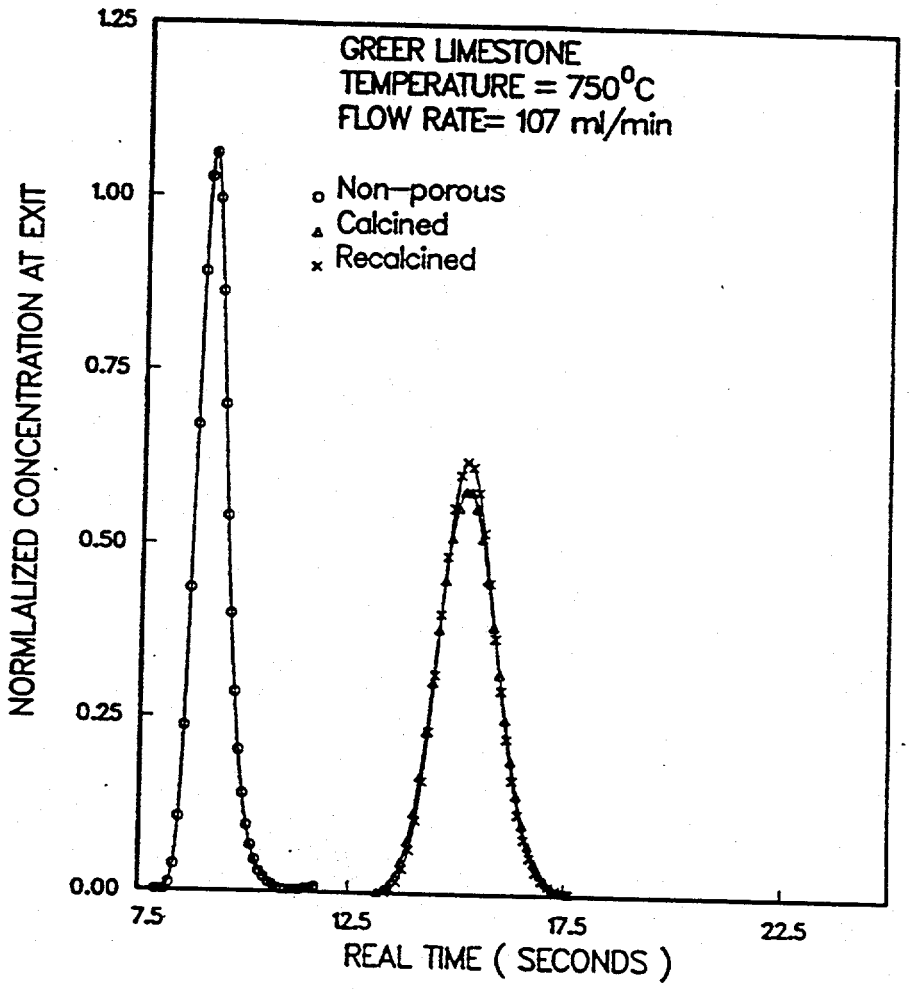

Figure 5.6: Chromatographic response curves of the 150 *cm* column for calcined and recalcined Greer limestone samples. The calcination and recalcination reactions were carried out in the fluidized-bed reactor at 750°C. The response curves shown in the figure were obtained at a flow rate of 107 ml/min.

recalcination restores the porosity to its original value (see Table 5.1). The spread of the response of the recalcined sample is smaller than that of the calcined sample, and this result is in agreement (see Table 5.3) with having a smaller diffusivity in the void space of the former.

The changes that the internal void space of the three samples undergoes during the reaction sequences considered in Figs. 5.4, 5.5, and 5.6 may be seen in Figs. 5.7, 5.8, and 5.9, respectively, which give the pore size distributions obtained from nitrogen desorption and mercury intrusion. Nitrogen desorption, which in general gives reliable information for pores with radius less than 1000 Å, shows very little particle voidage for the carbonated sample, whereas mercury porosimetry indicates much higher porosity, even for pores smaller than 1000 Å. For example, for the Greer limestone sample reacted at 850^oC, a theoretical porosity of 0.14 is predicted for the carbonated sample based on the conversion level attained (see Table 5.1). This value is identical to that predicted from the first moment but much higher than the value given in Fig. 5.7 by either of the pore structure characterization methods. BET analysis of the desorption data yields a very small surface area for the carbonated sample (Table 5.1). All these observations point to the conclusion that carbonation causes closure of most pores, and that the major part of the void space of the particles resides in pores larger than 1000 Å that are accessed from the outside through very small micropores. Mercury penetration gives much larger porosities for the carbonated sample probably because of crushing of closed pores at high pressures.

Even though the first moments of the response curves of Figs. 5.5 and 5.6 predict (see Table 5.1) that calcined and recalcined samples have the same porosity, the pore size distribution data of Fig. 5.8 and 5.9 reveal that both mercury porosimetry and nitrogen adsorptionaccount only for part of the total porosity of the recalcined samples. The inability of the mercury intrusion and nitrogen desorption methods to account for the total porosity of the recalcined solid can be due to large pores that are filled by mercury below 80 *psi* pressure or, as in the case of the carbonated solid, pores larger that1000 Å which are accessed through very small micropores. Two observations lead us to believe that the latter explanation is more probable. First, the mercury intrusion vs. pressure curves

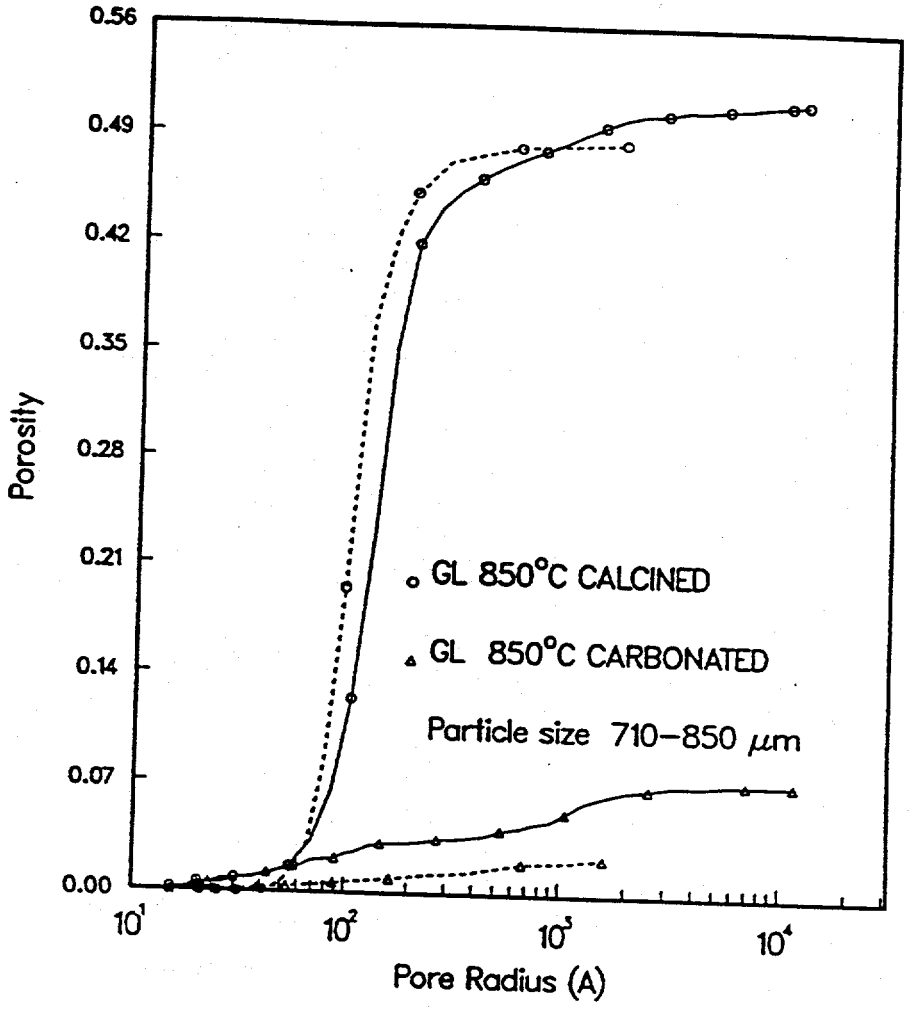

Figure 5.7: Pore size distributions of the calcined and carbonated Greer limestone samples (reacted at 850°C). The pore size distributions were obtained from mercury intrusion (solid lines) and nitrogen desorption (dashed lines).

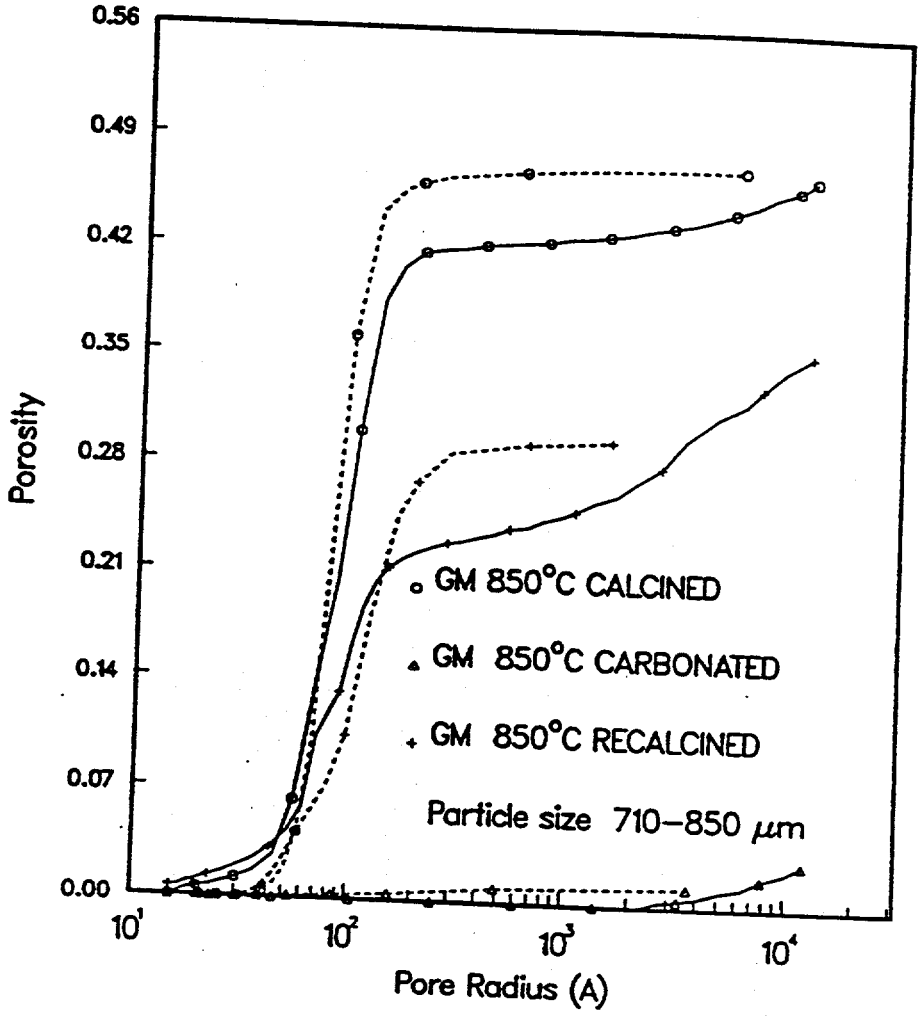

Figure 5.8: Pore size distributions of the calcined, carbonated, and recalcined Georgia marble samples ($850°C$). The pore size distributions were obtained from mercury intrusion (solid lines) and nitrogen desorption (dashed lines).

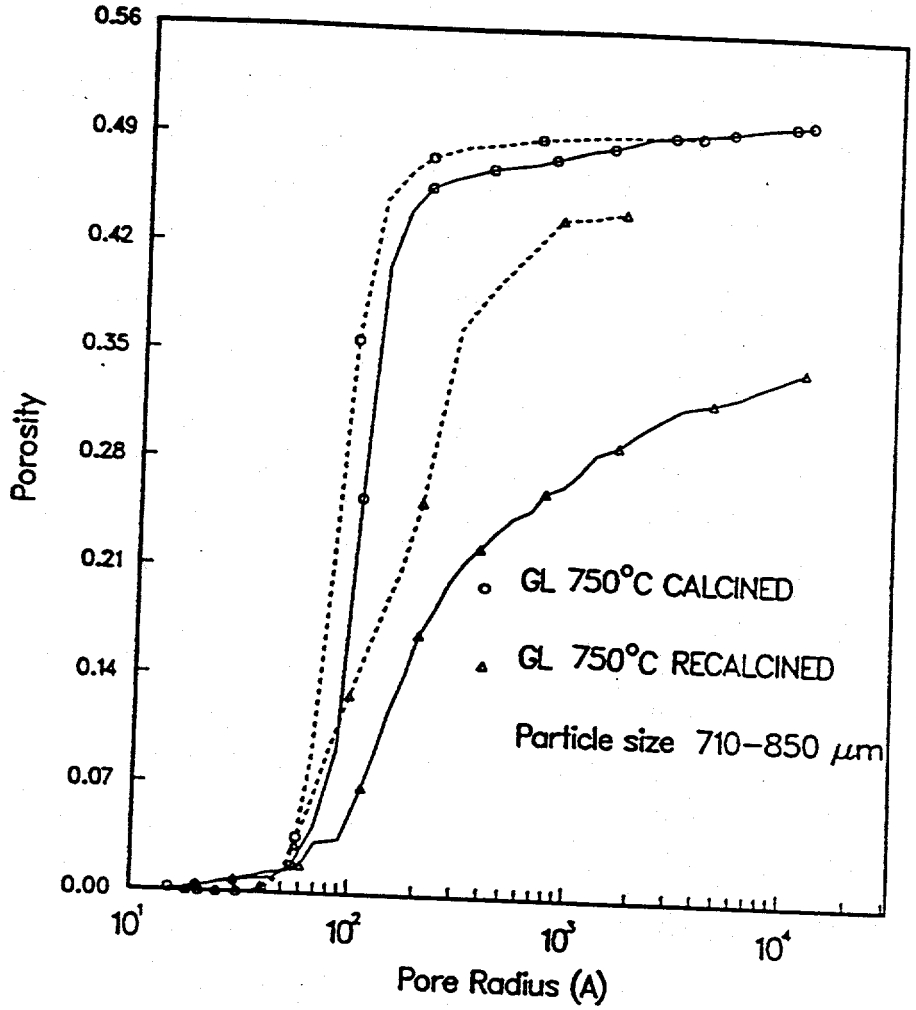

Figure 5.9: Pore size distributions of the calcined and recalcined Greer limestone samples ($750°C$). The pore size distributions were obtained from mercury intrusion (solid lines) and nitrogen desorption (dashed lines).

of the recalcined samples were not much different from those of the precursors and the calcines for intrusion pressures below 80 psi. Second, the mercury intrusion volume of the recalcined, as well as of the carbonated, sample tended to increase sharply with the applied pressure as the operating pressure limit (about 60,000 psi) of the porosimeter was approached. The existence of larger effective diffusivities in the recalcined samples was probably due to the fact that the part of their porosity that was uncovered by mercury porosimetry or gas sorption belonged to much larger pores than those seen in the calcined samples (see Figs. 5.8 and 5.9).

Pulse chromatographic response curves for partially sulfated Georgia marble calcines are shown in Fig. 5.10. These results were obtained for the Georgia marble calcines sulfated to 1, 2, 5, and 8% conversion levels. It is seen that the response curves for the sulfated calcines spread more with increasing conversion levels and their peaks appear earlier in time in the same order. The decrease in particle porosity during sulfation (see Table 5.2) is most probably the reason for the shifting of the peak of the response (see Eq. (5.6)). On the other hand, the increase in the spread of the response curves is due to increasing average diffusion resistance in the intraparticle space (see Eq. (5.7) and Table 5.3) caused by closure of the pores in the sulfated layer next to the external surface of the particles.

The experiments of Zarkanitis and Sotirchos (1989) and Sotirchos and Zarkanitis (1992) showed that the sulfation of Georgia marble calcines is a relatively fast reaction, and as a result, the maximum conversion that can be reached is a strong function of the particle size. Even particles with size in the 53-62 μm range were found to reach conversions below the value expected from the stoichiometry of the sulfation reaction for complete pore plugging with $CaSO_4$. Sotirchos and Zarkanitis (1992) showed that significant concentration gradients were present in 53-62 μm Georgia marble particles at all conversion levels, and therefore, even for particles in this size range, closure of pores at the external surface occurred while there was significant open space in the interior. For particles in the size range used in our experiments (710-850 μm), fluidized-bed and thermogravimetric analysis experiments showed that about 8% was the maximum conversion that could be achieved, and this is the reason for which bed response curves are shown only for this conversion range. The converted solid is located only in a very thin shell very close to the

external surface of the particles, and therefore, the response curves of Fig. 5.10 and the diffusivities of Table 5.3 should be viewed as being indicative only of the average transport resistance in the interior of the nonuniformly reacted particles. However, this does not mean that the reported diffusivity values are useless for model testing and validation. Given a mathematical model for the sulfation of calcined limestone particles, one can use the predicted porosity and effective diffusivity profiles in the interior of the particles in a pulse chromatographic model that allows for radial variation of the porosity and effective diffusivity and compare the predicted response curves with those found from the average effective diffusivities of Table 5.3.

Fig. 5.11 shows the pore size distributions of the sulfated samples whose chromatographic response curves are shown in Fig. 5.10. Mercury porosimetry was employed to obtain the curves shown in Fig. 5.11. The porosities of Fig. 5.11, though not in agreement with those predicted theoretically (see Table 5.2), follow the same variation pattern with the conversion as them (Fig. 5.10). Because of the nonuniformity of the structure of the reactive particles in the radial direction, the pore size distributions of Fig. 5.12 are of qualitative value only. Since the pores in the sulfated layer, which is next to the external surface of the particles, are much smaller than those in the interior, the pore size distribution of the sulfated samples from mercury intrusion data should be shifted towards smaller pore sizes had the sulfated layer maintained its integrity during mercury porosimetry. In particular, the 8% converted sample, whose conversion level corresponds to the maximum conversion that could be achieved in the experiment, should show no porosity at all outside the micropore range. The fact that the pore size distributions of the sulfated samples in Fig. 5.12 are not much different, qualitatively, from that of the unreacted solid and exhibit a larger fraction of macropores suggests, in view of the above observations, that the thin sulfated layer is destroyed by the high pressures applied during mercury porosimetry.

Fig. 5.12 is given to demonstrate that the extracted values of effective diffusivity for the various samples yield bed responses that match closely the experimental ones. The comparison is carried out between the 150 cm column experimental response (solid curve) and the curve obtained by convoluting the 50 cm column experimental response with an ideal 100 cm column (theoretically generated) response using the effective diffusivity of

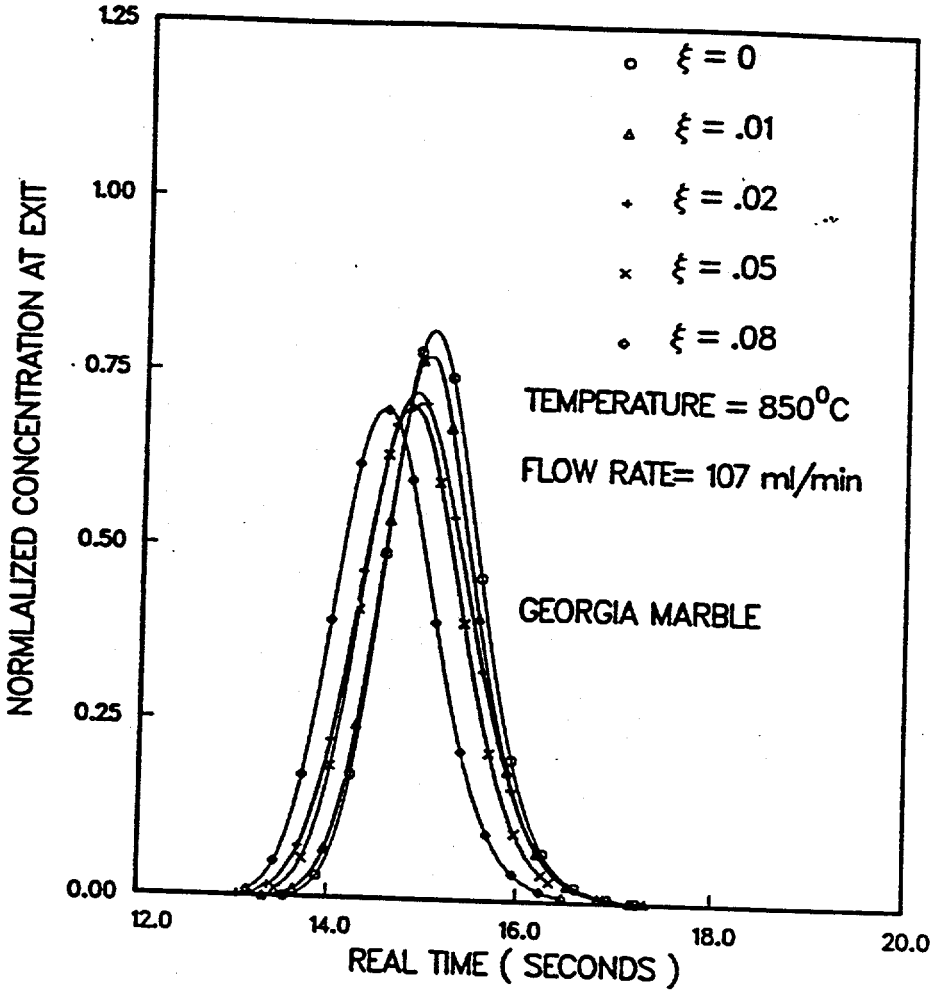

Figure 5.10: Chromatographic response curves of the 150 *cm* column for sulfated Georgia marble calcines at 0, 1, 2, 5, or 8% overall conversion levels. The sulfation of the calcine was carried out in the fluidized-bed reactor at 850°C under 1500 *ppm* of SO_2. The response curves shown in the figure were obtained at a flow rate of 107 ml/min.

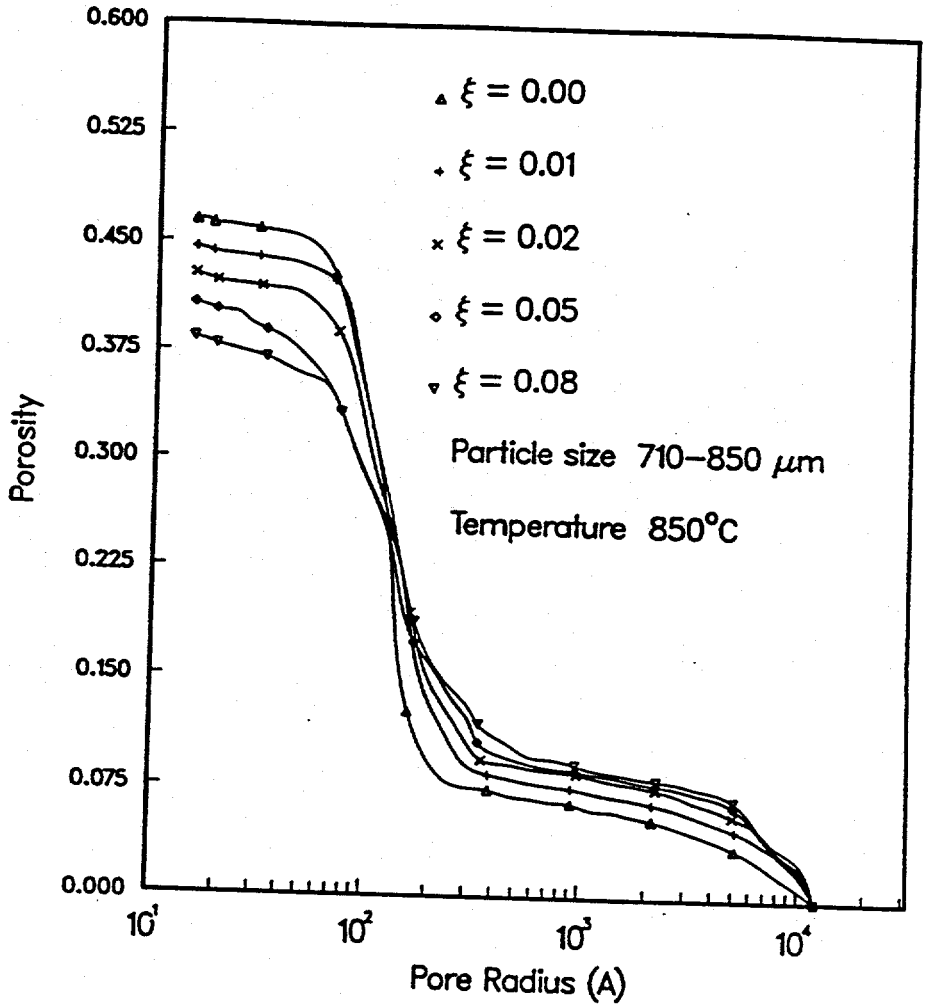

Figure 5.11: Pore size distributions of the sulfated Georgia marble calcines reacted in the fluidized-bed reactor at $850°C$ and 1500 ppm of SO_2. The curves are for calcines reacted to 0, 1, 2, 5, or 8% overall conversion levels. The pore size distributions were obtained from mercury intrusion.

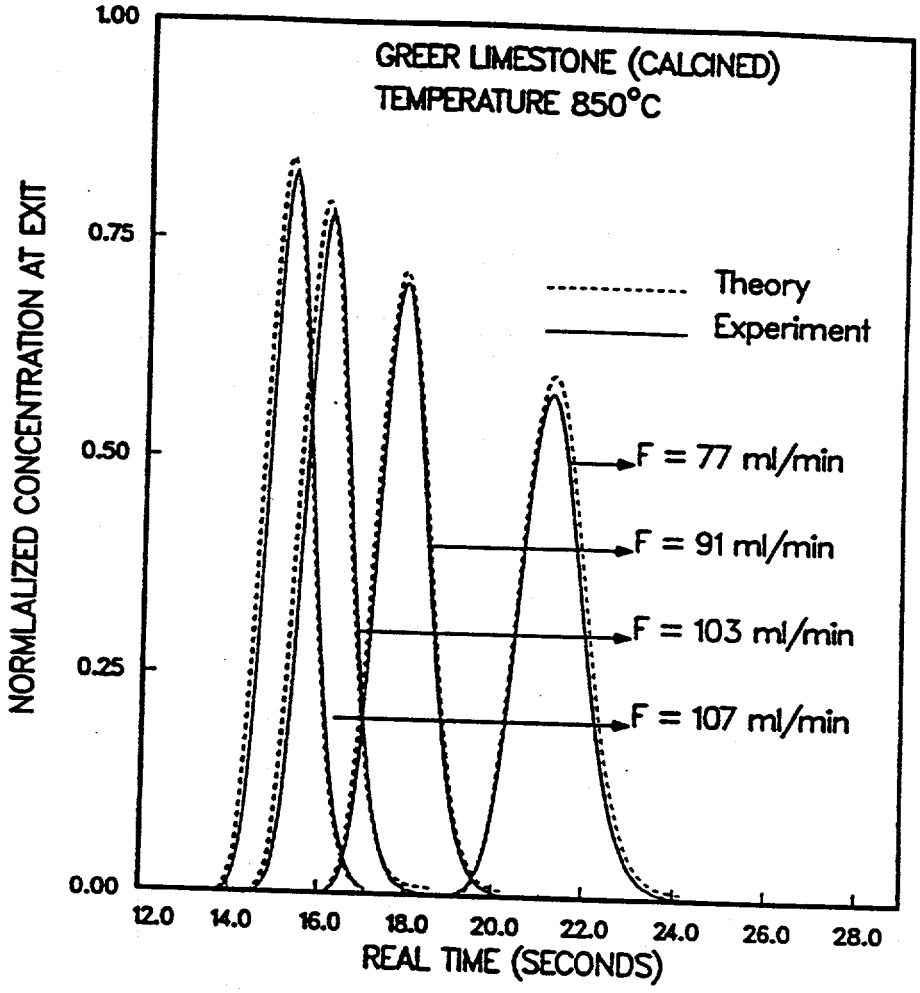

Figure 5.12: Comparison of the 150 *cm* experimental response with the 150 *cm* theoretical response for the column packed with Greer limestone calcine ($850°C$).

Table 5.4 (dashed curve). Very good agreement is seen to exist between the experimental and theoretical results for al l flow rates. Results that are qualitatively identical to those of Fig. 5.12 are obtained for all other solids (Krishnan, 1993).

5.5. Measured vs. Theoretically Predicted Diffusivities

The magnitudes of the effective diffusivities of the three calcines show a direct correlation with the conversion levels attained by these solids during sulfation or sulfidation For instance, in the study of Sotirchos and Zarkanitis (1992) Greer limestone calcined at 850^oC was found to reach much higher conversion than Greer limestone calcined at 750^oC. Similarly, Efthimiadis and Sotirchos (1992) found that the sample calcined at 750^oC was again sulfided more slowly than the sample prepared at 850^oC, although in this case complete conversion was reached for both samples on account of the lower molar volume (than $CaSO_4$) of CaS. By matching the experimental conversion vs. time results with the predictions of a mathematical model for diffusion, reaction, and structure evolution, an estimate for the connectivity of the pores was obtained in the above studies in terms of the coordination number of the pore network, z, that is, the average number of pores per node in the pore network. The effective medium theory-smooth field approximation (EMT-SFA) approach of Burganos and Sotirchos (1987) was used to calculate the effective diffusivity from the pore size distribution of the porous solid by Sotirchos and Zarkanitis (1992) and Efthimiadis and Sotirchos (1992). A brief description of this approach and of the smooth field approximation is given in the following paragraphs.

The smooth field approximation (SFA) amounts to assuming that the microscopic concentration field in each pore in the pore network coincides with the macroscopic one (Jackson, 1977). This approximation leads to an expression for the effective diffusivity in terms of the pore size distribution which is simply the average over the pore size distribution of the diffusion coefficient in a single pore, that is, the same expression as that obtained for a bundle of randomly oriented noninteracting pores (Johnson and Stewart, 1965). Specifically, for a discrete pore size distribution, like that extracted from pore structure

characterization data, we have

$$D_e{}^{SFA} = \frac{1}{3}\sum_{i=1}^{N} D(R_i)\epsilon_i \tag{5.8}$$

with N being the number of pore sizes, and ϵ_i and $D(R_i)$ the porosity and diffusion coefficient of pores of size R_i. $D(R_i)$ is computed from the reciprocal additivity (Bosanquet formula), viz.

$$\frac{1}{D(R_i)} = \frac{1}{\mathcal{D}} + \frac{1}{D_K(R_i)} \tag{5.9}$$

with $\mathcal{D}$ being the molecular diffusivity and $D_K(R_i)$ the Knudsen diffusivity in a pore of radius R_i.

The smooth field approximation violates the mass balance equations at the nodes of a network, and Eq. (5.10) turns out to be an upper bound on the actual diffusivity of the porous medium for a given pore size distribution. Burganos and Sotirchos (1987) suggested to use the effective medium theory approach (Kirkpatrick, 1973) to obtain an equivalent, with respect to the overall diffusion resistance network, of uniform pore conductance ($\pi\times$(pore radius)$^2\times$ pore diffusivity/(pore length)) and then apply the smooth field approximation to this network to determine the effective diffusivity. The result turns out to be

$$D_e{}^{EMT-SFA} = \frac{\epsilon}{3}\frac{< D(R)R^2 >_e}{< R^2 >_a} \tag{5.10}$$

where $< D(R)R^2 >_e$ is the effective medium theory average of $< D(R_i){R_i}^2 >$ with weight factor the length per unit volume of pores of size R_i, l_i and $< R^2 >_a$ is the arithmetic average of R^2 with the same weight factor. For a discrete pore size distribution, we have

$$\sum_{i=1}^{N} l_i \frac{D(R_i)R_i^2 - < D(R)R^2 >_e}{D(R_i)R_i^2 + (\frac{1}{p_c} - 1) < D(R)R^2 >_e} = 0 \tag{5.11}$$

$$< R^2 >_a = \sum_{i=1}^{N} l_i {R_i}^2 / \sum_{i=1}^{N} l_i \tag{5.12}$$

p_c is the percolation threshold of the structure, that is, the number fraction of open pores below which all pores in the network exist in the form of finite clusters and transport through the solid cannot take place (equal to $z/2$ for a network having a regular lattice

structure and $1/(z-1)$ for a Bethe lattice). For infinitely large coordination number, the percolation threshold becomes zero, and the EMT-SFA diffusivity becomes almost identical to the SFA value (Eq. (5.8)).

If pore overlapping is ignored, l_i is simply given by $\epsilon_i/\pi {R_i}^2$, while in the case of a network of randomly overlapping pore segments, it may be obtained from the equation (Sotirchos and Zarkanitis, 1993)

$$l_i = \frac{1}{\pi {R_i}^2} ln\left(\frac{1-\sum_{j=i+1}^{N}\epsilon_j}{1-\sum_{j=i}^{N}\epsilon_j}\right) \tag{5.13}$$

In writing Eq. (5.13), it is assumed that the index of the pores increases in the direction of increasing pore size.

Employing the EMT-SFA model to predict effective diffusivities during simulation of the sulfation and sulfidation processes of the calcines, Sotirchos and Zarkanitis (1992) and Efthimiadis and Sotirchos (1992) determined the coordination numbers (z) shown in Table 5.4 for the three calcines employed in this study. These z values were obtained assuming the topology of the porous network to be that of a Bethe lattice (Fisher and Essam, 1961). In the case of Greer limestone, it was found that the same z value could be used to describe both the sulfidation and sulfation behavior of the calcines, for the same pore size distribution. For the Georgia marble sample, however, Efthimiadis and Sotirchos (1992) found that the z values determined from sulfation data (by Sotirchos and Zarkanitis (1992)) were satisfactory for the sulfidation data of 53-62 and 88-105 μm particles only and that a much larger value had to be used to reproduce the sulfidation behavior of 210-250 and 297-350 μm particles ($z = 4$ vs. $z = 4000$ for the sample calcined at $850°C$). Since they had observed that large Georgia marble particles tended to explode during heating under CO_2 (probably because of decomposition of the small amount of $MgCO_3$ they contained), they attributed the above discrepancy to the existence of large pores in the interior of the larger calcine particles, formed from the cracks in the heat-treated precursors.

The effective diffusivities obtained from the EMT-SFA model employing the pore size distributions of the calcines shown earlier and the coordination numbers determined in the above studies are shown in Table 5.4. Values have been determined using the

pore size distributions obtained from all three procedures, that is, mercury intrusion, nitrogen desorption, and nitrogen adsorption. The use of a finite value for z has a much stronger effect on the effective diffusivities from mercury penetration data because of the practically unimodal and very narrow form of the nitrogen desorption or adsorption pore size distribution. (Obviously, for a solid with uniform size pores, the EMT-SFA approach produces the same estimate as the smooth field approximation irrespective of the value of z used.) Before a comparison of the predicted diffusivities with the experimental values reported in Table 5.3 is made, one should again be reminded that the pore size distributions obtained through these methods do not reflect the true morphology of the solids. This is because a pore is emptied during desorption (or filled during mercury intrusion) at the pressure corresponding to its own radius only if it is connected to the external surface through a path involving larger pores. Otherwise it gets emptied (or filled) at the pressure that corresponds to the radius of the smallest pore that must be emptied (or filled) to establish a continuous path of emptied (or filled) pores leading to the external surface. These effects are absent during nitrogen adsorption. However, nitrogen adsorption like the desorption process fails to provide reliable information for pores larger than about 1000 Å.

Very good agreement is seen between the predicted effective diffusivity for the Greer limestone calcine prepared at $850°C$ employing a coordination number of 12 and that obtained from our experimental studies (see Tables 5.3 and 5.4). All three pore size distributions yield values that are very close to the experimental effective diffusivity and to each other. The SFA effective diffusivity based on the pore size distribution obtained from mercury porosimetry overpredicts the experimentally measured value. On the other hand, the SFA effective diffusivities that are based on the pore size distributions obtained from nitrogen sorption data are very close to the experimental value. This agreement is coincidental and probably due to the fact that pores larger than 1000 Åare not included in the pore size distributions from sorption data. Despite their small contribution to the total porosity, when the the smooth field approximation is employed, these pores contribute significantly to the total flux because they are assumed to work in parallel with the smaller pores.

olid	Calc. Temp. (^oC)	Z	D_e SFA merc. int. (cm^2/sec)	D_e SFA N_2 Des. (cm^2/sec)	D_e SFA N_2 Ads. (cm^2/sec)	D_e EMT-SFA merc. int. (cm^2/sec)	D_e EMT-SFA N_2 Des. (cm^2/sec)	D_e EMT-SFA N_2 Ads. (cm^2/sec)
GL	850	12	2.98×10^{-2}	1.84×10^{-2}	1.98×10^{-2}	1.60×10^{-2}	1.45×10^{-2}	1.50×10^{-2}
G	750	6	2.41×10^{-2}	1.52×10^{-2}	2.0×10^{-2}	1.06×10^{-2}	1.13×10^{-2}	1.16×10^{-2}
GM	850	4	2.36×10^{-2}	1.35×10^{-2}	1.77×10^{-2}	7.93×10^{-3}	9.15×10^{-3}	8.87×10^{-3}
GM	850	4000	2.36×10^{-2}	1.35×10^{-2}	1.77×10^{-2}	1.45×10^{-2}	1.33×10^{-2}	1.66×10^{-2}

Table 5.4: Effective Diffusivities of He (in N_2) in the Calcines Predicted Using the EMT-SFA Model and Coordination Number Values Obtained in Previous Studies (Sotirchos and Zarkanitis (1992); Efthimiadis and Sotirchos (1992)). GL=Greer limestone, GM=Georgia marble, and IS=Iceland spar.

Reasonable estimates of the effective diffusivity are also obtained for the Greer limestone sample calcined at 750^oC from the EMT-SFA model employing any of the three pore size distributions. The predicted EMT-SFA values differ by a factor of two from the measured value of effective diffusivity (Tables 5.3 and 5.4). Differences between predicted and measured values are not uncommon, and discrepancies up to an order of magnitude have been known to occur (Haynes, 1988). However, much greater deviations occur between the SFA predicted values and the measured values.

Since, two different values of coordination number were obtained by Efthimiadis and Sotirchos (1992) for the Georgia marble calcine prepared at 850^oC, Table 5.4 reports the predicted values of effective diffusivities for both values of z and the three different pore size distributions. As for the other two solids, the SFA estimate based on the mercury intrusion data overpredicts the measured value by a wide margin (see Table 5.3 for the measured value), while the SFA effective diffusivities for the pore size distributions obtained from nitrogen sorption show very good agreement with the measured value. This again is coincidental and due to the absence of large pores from the pore size distribution obtained from sorption data. Interestingly enough, the experimentally measured value for the Georgia marble sample turns out to be between the EMT-SFA values predicted for the two coordination numbers. It should pointed out that the need to use unreasonably large

coordination numbers to describe the sulfidation of large Georgia marble particles is an indication that the pore network assumed in the EMT-SFA approach is not appropriate for these particles (Efthimiadis and Sotirchos, 1992). All pore sizes are treated in the same way in the EMT-SFA model, and therefore, if pervasive large pores are present in a porous medium – as it is probably the case for large Georgia marble particles – very large coordination numbers must be employed in order not to underestimate the contribution of the large pores in the mass transport process.

It should be noted that the mercury intrusion pore size distributions that were used in the studies of Sotirchos and Zarkanitis (1992) and Efthimiadis and Sotirchos (1992) were slightly different from those used in this study because a different arrangement (viz., a fixed-bed reactor) was employed for the preparation of the samples. Using those pore size distributions yields slightly different (actually larger) effective diffusivities both for finite (EMT-SFA) and infinite (SFA) coordination number, but the relative differences among the various diffusivities and between the EMT-SFA and SFA results are similar to seen in the results of Tables 5.3 and 5.4.

5.6. Summary and Concluding Remarks

Pulse chromatographic experiments were performed in this study to investigate evolution of the intraparticle diffusional limitations during calcination, carbonation, recalcination, and sulfation of limestones. Two types of limestones differing in their petrographic structure, one with small grains (Greer limestone) and another coarsely grained (Georgia marble), were used for this purpose. The measured chromatographic response curves were analyzed in the time domain by employing a procedure that uses the responses of two different length columns to eliminate uncertainties associated with end effects and the form of the input to the chromatographic column.

The intraparticle effective diffusivity of the once calcined samples was found to increase in the order Greer limestone calcined at $850°C$ $\rightarrow$ Georgia marble calcined at $850°C$ $\rightarrow$ Greer limestone calcined at $750°C$. The effective diffusivities of the three calcines differed by as much as a factor of 4 despite the fact that the pore size distributions of the solids were similar and gave similar values of effective diffusivity assuming a network of

randomly arranged noninteracting pores (parallel pore bundle model). The carbonated samples showed much higher resistance to intraparticle mass transport than the calcined samples. Based on several experimental observations, such as the form of pore size distributions obtained from mercury intrusion and nitrogen sorption, the low surface areas measured from BET analysis of their sorption isotherms, and the fact that the theoretical porosities of the carbonated samples were in agreement with those estimated from the first moments of the response curves but much higher than those found from mercury intrusion or N_2 sorption data, it was concluded that a significant fraction of the porosity of carbonated samples was due to large pores with feeder pores of micropore size.

The porosities estimated from first moments of the chromatographic response curves of recalcined samples indicated that recalcination restored the porosity to its original (before carbonation) value. Only part of the porosity of recalcined samples could be revealed by mercury penetration or gas adsorption experiments, and this indicated that, like in the case of the carbonated sample, some large pores were accessed through micropores only. However, the part of the pore size distribution of the recalcined samples that could be traced by mercury penetration or gas adsorption showed much larger pores than those found in one-time calcined samples, and thus, the effective diffusivities of the recalcined samples were found, for the two cases of Georgia marble reacted at $850°C$ and Greer limestone reacted at $750°C$ that we studied, to be higher than those of the unreacted calcines. Sulfation of the calcines resulted in a rapid decline in the value of the average effective diffusivity. Because of closure of the pores at the external surface of the particles, only conversions less than 8% could be achieved for the 710-850 μm particles we used in the experiments. Because of the small thickness of the sulfated layer and the strong effect of conversion on the average effective diffusivity in the particles it was concluded that the pore space of the sulfated layer presented very high resistance to the transport of SO_2.

The observed variation of effective diffusivity among the three calcines we studied (Georgia marble and Greer limestone calcined at $850°C$ and Greer limestone calcined at $750°C$) was in relative agreement with the reported behavior of the solids during sulfation and sulfidation experiments by Sotirchos and Zarkanitis (1992) and Efthimiadis and Sotirchos (1992), respectively. We used estimates that were made in the above studies for

the connectivity of the pores in the calcines, in terms of the coordination number of the pore network, to predict the effective diffusion coefficient from the mercury intrusion pore size distributions using the effective medium theory- smooth field approximation approach of Burganos and Sotirchos (1987). Fairly good, and in some cases very good, agreement was observed between the predicted and experimental values. On the other hand, the effective diffusivities that were estimated by assuming a perfectly interconnected network of pores or equivalently a network of noninteracting pores (smooth field approximation) were much larger than the experimentally measured values. This result lends further support to the conclusion reached by Sotirchos and Zarkanitis (1992) and Efthimiadis and Sotirchos (1992) in their sulfation and sulfidation, respectively, studies that the connectivity of the pores is among the most important factors that determine the performance of a limestone-derived calcine as a sorbent for SO_2 removal.

5.7. Notation

Symbols that do not appear here are defined in the text.

b	Radius of the porous particle, cm
$\mathcal{D}$	Binary diffusivity, cm^2/s
$D(R)$	Diffusivity in a pore of radius R_i, cm^2/s
D_b	Axial dispersion coefficient, cm^2/s
D_e	Effective diffusivity of the gas in the particle, cm^2/s
$D_K(R)$	Knudsen diffusivity in a pore of radius R, cm^2/s
K	Lumped adsorption equilibrium constant
k_g	External mass transfer coefficient, cm/s
l_i	Length per unit volume of pores with radius R_i, cm/cm^3
L	Length of bed, cm
N	Number of pore sizes
p_c	Number-based percolation threshold of pore network
R_i	Radius of ith group of pores ($R_i < R_{i+1}$), cm
u	Interstitial velocity, cm/s
z	Coordination number of the pore network

Greek

β	Porosity of the bed
ϵ	Porosity of the solid
ϵ_0	Initial porosity of the solid
ϵ_i	Porosity due to pores of size R_i
μ_1	First absolute moment (Eq. (5.6)), s
σ^2	Second central moment (Eq. (5.7)), s^2
ξ	Conversion of the solid

5.8. Literature References

Aust E.; Dahlke, K.; Emig, G., "Simulation and Evaluation of Chromatographic Response Curves using Various Methods," Chem. Eng. J., **35**, 179-190 (1987).

Bardakci T., "Diffusional Study of the Reaction of Sulfur Dioxide with Reactive Porous Matrices," Thermochem. Acta, **76**, 287-300 (1984).

Bardakci T.; Gasner, L.L., "Gas Transport within the Developed Pore Structure of Reactive Porous Matrices," AIChE J., **30**, 856-858 (1984).

Bird R.B., Stewart, W.E., Lightfoot, E.N., *Transport Phenomena*, John Wiley, New York (1960).

Burganos V.N.; Sotirchos, S.V., "Diffusion in Pore Networks. Effective Medium Theory and Smooth Field Approximation," AIChE J., **33**, 1678-1689 (1987).

Campbell F.R., Hills, A.W.D.; Paulin, A., "Transport Properties of Porous Lime and their Influence on the Decomposition of Porous Compacts of Calcium Carbonate," Chem. Eng. Sci., **25**, 929-942 (1970).

Evans R.B.; Watson, G.M.; Mason, E.A., "Gaseous Diffusion in Porous Media at Uniform Pressure," J. Chem. Phys., **35**, 2076-2083 (1961).

Efthimiadis E.A.; Sotirchos, S.V., "Sulfidation of Limestone-Derived Calcines," Ind. Eng. Chem. Res., **31**, 2311-2321 (1992).

Efthimiadis E.A.; Sotirchos, S.V., "Effects of Pore Structure on the Performance of Coal Gas Desulfurization Sorbents," (to appear in Chem. Eng. Sci., (1993).

Fisher M.E.; Essam, J.W., "Some Cluster Size and Percolation Problems," J. Math. Phys., **2**, 609-619 (1961).

Haynes H.W., "The Experimental Evaluation of Catalyst Effective Diffusivity," Catal. Rev. , **30**, 563-627 (1988).

Hills A.W.D., "The Mechanism of the Thermal Decomposition of Calcium Carbonate," Chem. Eng. Sci., **23**, 297-320 (1968).

Johnson M.F.L.; Stewart, W.E., "Pore Structure and Gaseous Diffusion in Solid Catalysts," J. Catal., **4**, 248-252 (1965).

Krishnan S.V., "Mass Transport in Porous Sorbents of Evolving Morphology used in Flue and Coal Gas Desulfurization," Ph.D. Thesis, University of Rochester (1993).

Kubin M., Collect. Czech. Chem. Comm., **30**, 1104 (1965).

Kucera E., "Contribution to the Theory of Chromatography. Linear Nonequilibrium Elution Chromatography," J. Chromatogr., **19**, 237-248 (1965).

Perry R.H.; Green, D.W.; Maloney, J.O., Eds., *Chemical Engineer's Handbook*, 6th ed., McGraw-Hill, New York (1984).

Sotirchos S.V., Zarkanitis, S., "Inaccessible Pore Volume Formation during Limestone Sulfation," AIChE J., **38**, 1536-1550 (1992).

Sotirchos S.V., Zarkanitis, S., "A Distributed Pore Size and Length Model for Porous Media Reacting with Diminishing Porosity," Chem. Eng. Sci., **48**, 1487-1502 (1993).

Suzuki M.; Smith, J.M., "Transport and Kinetic Parameters by Gas Chromatographic Techniques," Adv. Chromatogr., **13**, 213-263 (1975).

Wicke E.; Kallenbach, R., "Die Oberflächendiffusion von Kohlendioxyd in activen Kohlen," Kolloid Z., **97**, 135-151 (1941).

Zarkanitis S., Sotirchos, S.V., "Pore structure and Particle Size Effects on Limestone Capacity for SO_2 Removal," AIChE J., **35**, 821-830 (1989).

6. EXPERIMENTAL AND THEORETICAL INVESTIGATION OF FACTORS AFFECTING THE DIRECT LIMESTONE-H_2S REACTION

6.1. Introduction

The gasification of coal is a versatile method of coal utilization where the generated coal gas can subsequently be used to synthesize other fuels or produce energy by combustion or in fuel cells. The sulfur contained in coal reacts in the reducing atmosphere of a gasifier forming H_2S and COS. Because of their corrosive nature and potentially negative environmental impact, H_2S and COS must be removed from the coal gas before it is further processed. Coal gas desulfurization can be carried out at low ($< 120°C$) or high temperatures ($> 500°C$) (Jalan, 1983). Hot coal gas desulfurization, which uses solid sorbents, such as oxides of metals (e.g., of iron, manganese, zinc, and vanadium) and limestones, possesses several distinct technical and economic advantages over low temperature processes, which make it an attractive desulfurization technique.

Typical fixed-bed and fluidized-bed gasifiers operate around $850°C$ with a temperature at the exit between 500 and $800°C$. Entrained-flow gasifiers operate at higher temperatures, about $1200°C$. Most gasifiers operate at 200-300 psi pressures. Among the objectives of a successful desulfurization process is to carry out the removal of sulfur compounds at the temperature and pressure of the coal gas in the gasifier. This can be achieved by employing sorbents that can be used to desulfurize the coal gas within the gasifier itself.

Several reactions take place within a gasifier that employs limestones ($CaCO_3$) and dolomites ($CaCO_3 \cdot MgCO_3$) or their pre-calcined forms (CaO and $CaO \cdot MgO$) for the removal of H_2S from coal gas. The typical composition of CO_2 in an oxygen blown gasifier is 26% and for an air blown gasifier is 11% on a molar basis (Grindley, 1985). Under an operating pressure of 250 psi in the gasifier, the average partial pressure of CO_2 in the coal gas is about 1.8 and 4.3 atm for the air blown and oxygen blown gasifiers, respectively. Thermodynamic calculations for the decomposition of $CaCO_3$ to CaO show that temperatures higher than 950 °C are required for decomposition at a partial CO_2 pressure of 1.8 atm. At a CO_2 partial pressure of 4.3 atm, $CaCO_3$ decomposition can only take place at temperatures much higher than those encountered in any gasifier. The

$CaCO_3$ contained in limestones and dolomites must therefore react directly with H_2S in the gasifier to effect coal gas desulfurization according to either of the reactions:

$$CaCO_3 + H_2S \rightleftharpoons CaS + CO_2 + H_2O \qquad (R6.1a)$$

$$CaCO_3.MgO + H_2S \rightleftharpoons CaS.MgO + CO_2 + H_2O \qquad (R6.1b)$$

($MgCO_3$ contained in dolomite is shown as MgO in reaction R6.1b because the conditions prevailing in a gasifier favor its decomposition.)

There may be regions in the gasifier of higher, than the average, reaction temperature or lower partial pressures of CO_2 (than the average values) where decomposition of $CaCO_3$ to CaO may occur:

$$CaCO_3 \rightleftharpoons CaO + CO_2 \qquad (R6.2)$$

CaO formed from the decomposition of $CaCO_3$ or present in precalcined limestones and dolomites may then react with CO_2 to form $CaCO_3$ in regions of the reactor where the carbonation reaction is favored:

$$CaO + CO_2 \rightleftharpoons CaCO_3 \qquad (R6.3)$$

It can therefore be argued that in such regions reaction R6.3 might be competing for CaO with the indirect sulfidation reaction, i.e., the reaction

$$CaO + H_2S \rightleftharpoons CaS + H_2O \qquad (R6.4)$$

On the other hand, in regions that favor the decomposition of $CaCO_3$, only the latter may take place. An analogous situation occurs in pressurized fluidized-bed combustors that employ limestones for SO_2 removal, where $CaCO_3$ is believed to react directly with SO_2 (Tullin and Ljungström, (1989); Snow et al. (1988); Jansson et al. (19820; Krishnan and Sotirchos, (1993a)).

A fundamental difference between the reaction of H_2S with limestone-derived calcines (CaO) (reaction R6.4) and that with limestone ($CaCO_3$) (reaction R6.1a) is the lack of a highly developed pore structure in the reacting solid taking part in the latter. The reaction between limestone-derived calcines and H_2S proceeds through diffusion of the reactive gas

in the pore space of the calcine and the reacted solid layer at the pore walls (CaS) and its subsequent reaction with CaO at the reacted-unreacted solid interface. Similarly, the reaction of H_2S with half-calcined dolomites (reaction R6.1b) involves diffusion of the reactive gases in the pore space formed through decomposition of $MgCO_3$. However, in the case of nonporous, uncalcined limestones, H_2S initially reacts only at the external surface of the reacting particles, leading to formation of a solid product layer at their periphery. Further reaction between limestone and H_2S takes place only after the reactive gas diffuses through this product layer. Because of this difference, the information that is presently available on the sulfidation of limestone-derived calcines and of other porous oxides (e.g., see Westmoreland et al. (1977), Borgwardt et al. (1984), and Efthimiadis and Sotirchos (1992)) and sulfidation of half-calcined dolomites (e.g., see Ruth et al. (1972) and Yen et al. (1981)) from studies in thermogravimetric analysis (TGA) systems and other types of reactors is inapplicable to the direct reaction of low porosity limestones with H_2S.

Fundamental knowledge on the interplay between transport and reaction in the limestone-H_2S reaction is required for design and operation of gasifiers capable of achieving efficient removal of H_2S through limestone addition. Unfortunately, the number of fundamental studies on the direct sulfidation reaction is rather small in comparison to that for the indirect process. Moreover, most of those studies have been carried using limestones of special petrographic structure or in narrow ranges of operating conditions. As a result, it is difficult or even impossible to use the results and conclusions reported in them to predict the behavior of other limestone-H_2S systems.

Attar and Dupuis (1979) studied the reaction of $CaCO_3$ (calcite) with H_2S and found that at temperatures below $640°C$ diffusion of the gases through the product layer controls calcite consumption. However, no reliable information on the mechanism of the $CaCO_3$-H_2S reaction can be extracted from their results at higher temperatures since the occurrence reactions R6.2 and R6.4 becomes possible in their reaction environment. Borgwardt and Roache (1984) investigated the reaction of limestone particles with H_2S (reaction R6.1a) at atmospheric pressure in an environment of 70% CO_2 by volume to prevent the decomposition of $CaCO_3$ to CaO. The limestone samples were periodically removed from the reactor to determine the conversion level. Since Borgwardt and Roache

used a limestone precursor (Fredonia limestone) with 8% natural porosity, they were able to explain the behavior of the conversion-time trajectories for large particles (diameter greater than 15 μm) along the lines of the overall mechanism for the sulfidation of limestone-derived calcines (reaction R6.4). However, as a survey of the pertinent literature shows, most limestones are nearly nonporous in their natural state. For example, porosities of 1.5% and 0.7% were measured by Krishnan and Sotirchos (1993a) for Greer limestone and Georgia marble, respectively, 0.4-1% by Krishnan and Sotirchos (1993a) and Hajaligol et al. (1988) for Iceland spar, and 2-3% for Rigsby and Fredonia limestones by Hajaligol et al. (1988).

A detailed investigation of the reaction between limestones and H_2S is presented in this study. The limestones were directly sulfided in a thermogravimetric analysis (TGA) system at atmospheric pressure under 70% CO_2 (on a molar basis) to prevent the decomposition of $CaCO_3$ to CaO. The effect of reaction conditions on the limestone-H_2S reaction were examined by employing different bulk phase concentrations of H_2S (3000 and 6000 ppm) and two temperatures (650 and 750°C). The particle size effect on the conversion-time profile was investigated by employing a broad range of particle size (53-62, 88-105, and 297-350 μm). The influence of the above conditions (particle size, temperature and concentration) on the conversion-time history was examined for three limestones having high $CaCO_3$ content (> 95%) but differing in petrographic texture. A shrinking-core model was employed to obtain information, both quantitative and qualitative, on the kinetics of the reaction and the mass transport process in the sulfided layer. Finally, by using results obtained by our research group in past studies for the same limestones, a comparison of the direct sulfidation and direct sulfation of limestones (the $CaCO_3$-SO_2 reaction) and of the sulfation and sulfidation of the limestone-derived calcines (the CaO-SO_2 and the CaO-H_2S reactions, respectively) was carried out.

6.2. Materials and Experimental Procedures

Three high purity limestones, which will be referred to as Greer limestone, Georgia marble, andIceland spar, were used to study the limestone-H_2S reaction. Each has $CaCO_3$ content higher than 95% (on a mass basis), with Georgia marble having the highest $MgCO_3$

content (approximately 3% on a mass basis) of the three. The $CaCO_3$ present in the limestones was found from petrographic studies to be calcitic, with the grain size increasing in the order Greer limestone → Georgia marble → Iceland spar. The limestones supplied as fragments in the 1/4-1/2″ size range were crushed into smaller particles and screened using mechanical sieving to filter out the fine and coarse sizes and obtain three particle size ranges: 53-62, 88-105, and 297-350 μm. The porosities and surface areas of the three samples were determined from N_2 sorption data using a volumetric adsorption unit (Autosorb 1,Quantachrome, Inc.). They are listed in Table 6.1, where they are seen to increase in the order Iceland spar → Georgia marble → Greer limestone, that is, in the order of decreasing grain size.

Limestone	Particle Size (μm)	Surface Area (m^2/g)	Porosity (pores of radius < 1000Å)
GL	53 – 62	0.91	0.015
GM	53 – 62	0.31	0.007
IS	53 – 62	0.23	0.004

Table 6.1: Surface areas and porosities of Georgia marble, Greer limestone, and Iceland spar precursors. GL=Greer limestone, GM=Georgia marble, and IS=Iceland spar.

A TGA system based on a Cahn 2000 electrobalance was used to obtain conversion vs. time data. Very small amountsof solid (2-5 mg) were placed in a gold pan hang with platinum wire inside a quartz reactor. The samples were heated to the reaction temperature (650 or 750°C) in an atmosphere of 100% CO_2 flowing at 200 ml/min (standard conditions). All direct sulfidation experiments were performed in an atmosphere of 70% CO_2, and thus, the pure CO_2 stream was substituted with a 70% CO_2-30% N_2 stream to ensure the existence of noncalcining conditions for $CaCO_3$ at the conditions of our experiments. Of course, the small amounts of $MgCO_3$ present in the limestones decomposed at the temperature used to form MgO even under 100% CO_2. Once the desired reaction temperature was attained, a stream consisting of CO_2 (70% on a molar basis) and a 1%

or 2% H_2S in N_2 (molar basis) mixture was sent through the reactor, and the transient weight change was recorded.

The large quantities of reacted samples needed for pore structure characterization through N_2 sorption were prepared in a fixed-bed reactor. Approximately 0.5-0.75 g of limestone were directly sulfided under a total flow of 2000 ml/min (standard conditions) at $750°C$ and 6000 *ppm* H_2S. The procedures followed to start desulfurization in the fixed-bed reactor were the same as in the thermogravimetric experiments. The conversions of the solids were determined from the concentration of H_2S at the exit, measured using a chromatograph (Varian 3300) equipped with a flame photometric detector, as well as from the observed weight change.

6.3. Reactivity results

CO_2 and H_2S can react under the experimental conditions employed in our study and form COS according to the overall reaction

$$CO_2 + H_2S \rightleftharpoons COS + H_2O \qquad (R6.5)$$

Borgwardt and Roache (1984) reported a 12% conversion of H_2S in their experimental system (10% of H_2S to COS and 2% to S) at a reaction temperature of $700°C$. Thermodynamic calculations for the reactive gas mixture used in our experiments revealed that significant conversion of H_2S to other species could take place at equilibrium. The variation of the thermodynamic equilibrium concentrations of the various species with the reaction temperature is given in Fig. 6.1. These results were computed using the STANJAN code (Reynolds, 1986) with thermodynamic data from the JANAF Tables (Chase et al., 1985). Fig. 6.1 shows that nearly 85% of H_2S is converted to other sulfur-containing species at equilibrium at $750°C$. However, the chromatographic analysis of the exit stream of our TGA system showed a H_2S depletion of less than 9% at $750°C$. Since the reaction mixture of H_2S-CO_2-N_2 encounters the limestone sample at residence times much smaller than those at the reactor's exit, considerably lower depletion levels were measured for gas samples collected by sampling at the vicinity of the pan (less than 3% at $750°C$). In view of these results, we concluded that the concentration of H_2S in the bulk of the gas phase

around the sample could safely be assumed to be the same as the inlet concentration.

Conversion vs. time profiles for the three solids directly sulfided under 3000 *ppm* of H_2S and at a reaction temperature of $750°C$ are shown in Figs. 6.2-6.4. The conversion-time trajectories of these figures reveal strong effects of particle size on the direct sulfidation of all limestones, which suggest that the reactive gas encounters significant resistance in its transport through the intraparticle space. Similar effect of particle size on the overall reaction profile was seen for the three solids sulfided at 650 °C under 3000 *ppm* of H_2S.

Typical effects of temperature on the conversion-time profile for the direct sulfidation of the limestones is shown in Fig. 6.5 for Georgia marble reacted under 3000 *ppm* of H_2S. The reaction trajectory is seen to be very sensitive to the reaction temperature throughout the duration of the experiment. The conversion levels for Georgia marble attained at the two temperatures after two hours of direct sulfidation differ by about a factor of two for all particle size ranges. Much smaller differences are obtained at smaller reaction times, suggesting that the intrinsic kinetics of the reaction, the controlling step during the early stages of the reaction, is less influenced by the reaction temperature than the diffusion of H_2S through the product layer, the controlling step at larger reaction times. Similar effects of temperature on the conversion vs. time curves were observed for the other limestones. The influence of reaction temperature on the conversion-time profile was weaker in the sulfidation of calcines derived from the same limestones (Efthimiadis and Sotirchos, 1992). This observation suggests that the mechanisms of the direct and indirect reaction of limestones with H_2S are different.

Studies were conducted at two concentrations of 3000 and 6000 *ppm* of H_2S in the bulk phase to investigate the effect of concentration on the conversion-time history of the limestones. Fig. 6.6 shows the comparison between the conversion-time curves for Georgia marble directly sulfided at $750°C$ under the two concentrations over a 1 hr period for the smallest size range (53-62 μm). Strong dependence of conversion level attained by the reacting solid on the bulk phase concentration of H_2S is seen throughout this period. A better understanding of the effect of concentration on the limestone-H_2S reaction can be obtained by comparing the conversion vs. time curve for the reaction carried out under 3000 *ppm* of H_2S (solid curve) and the normalized curve (dotted curve) obtained by scaling

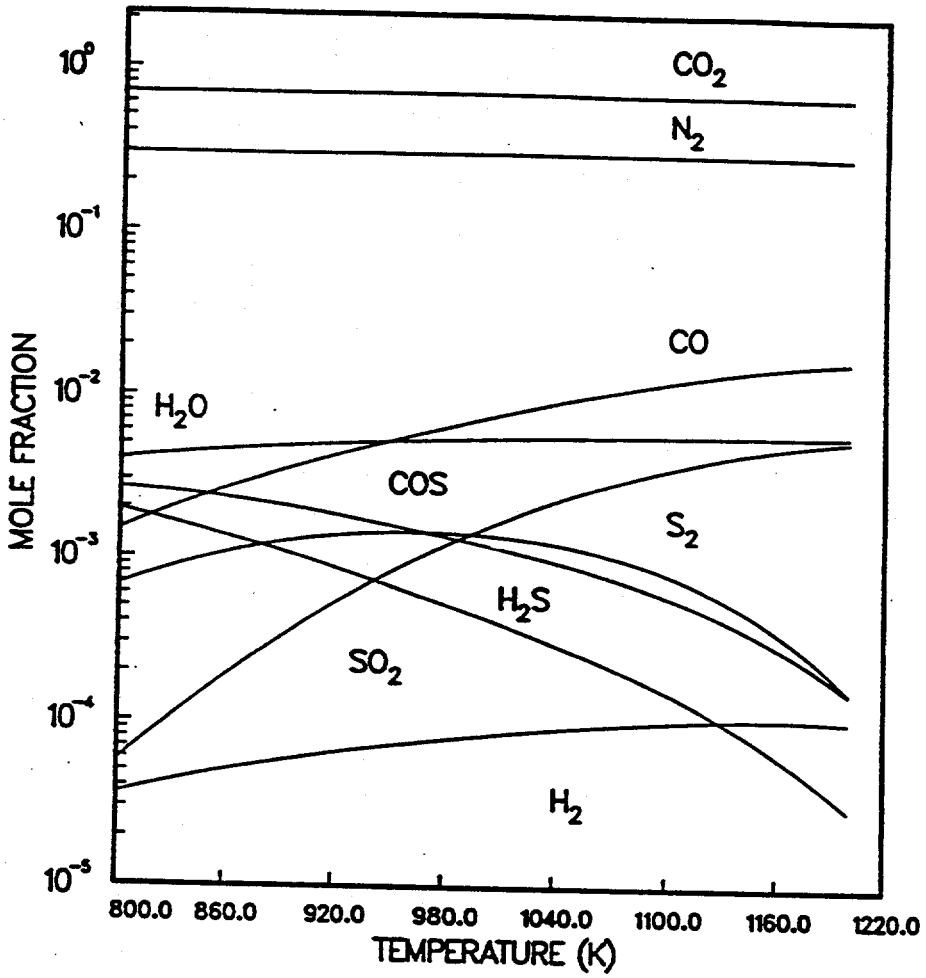

Figure 6.1: Theoretical equilibrium concentrations of species formed from a mixture of 70% CO_2, 0.6% H_2S, and 29.4% N_2 (molar basis) as a function of temperature.

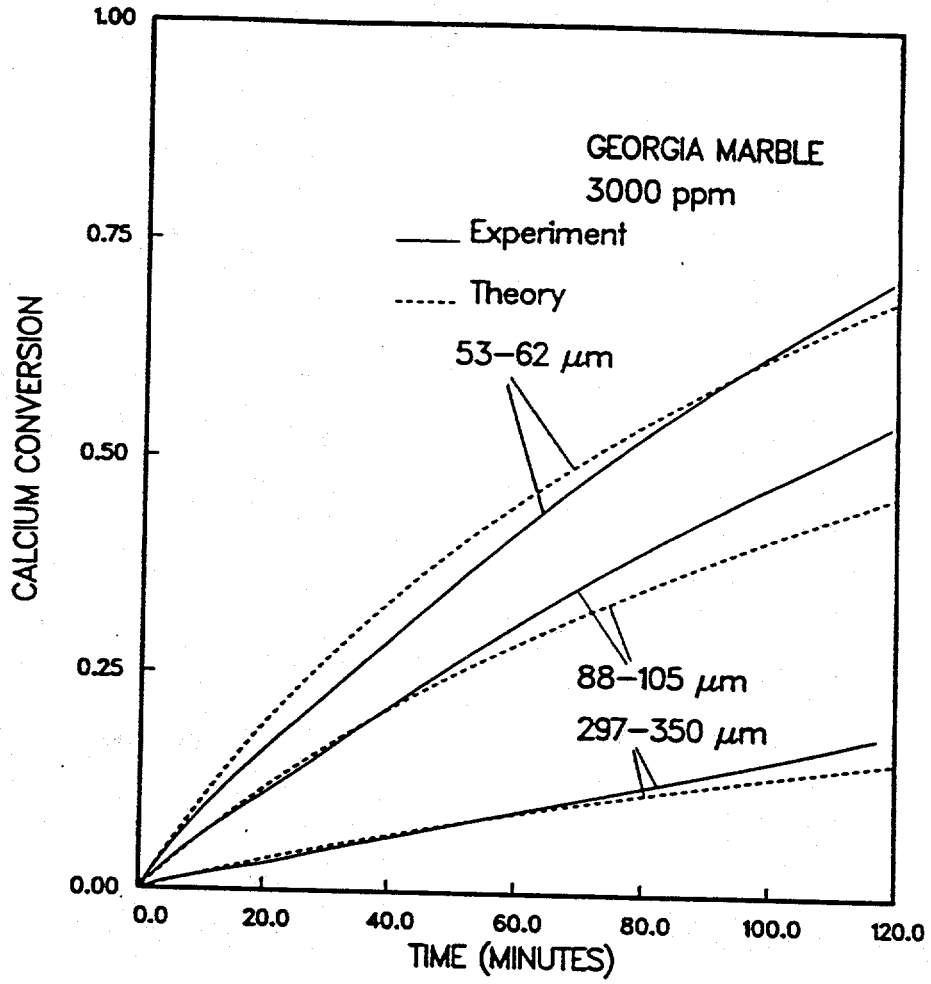

Figure 6.2: Experimental (—) and theoretical (- - - -) conversion vs. time profiles for Georgia marble sulfided at $750°C$ and 3000 ppm H_2S under an atmosphere of 70% CO_2 (molar basis) and N_2.

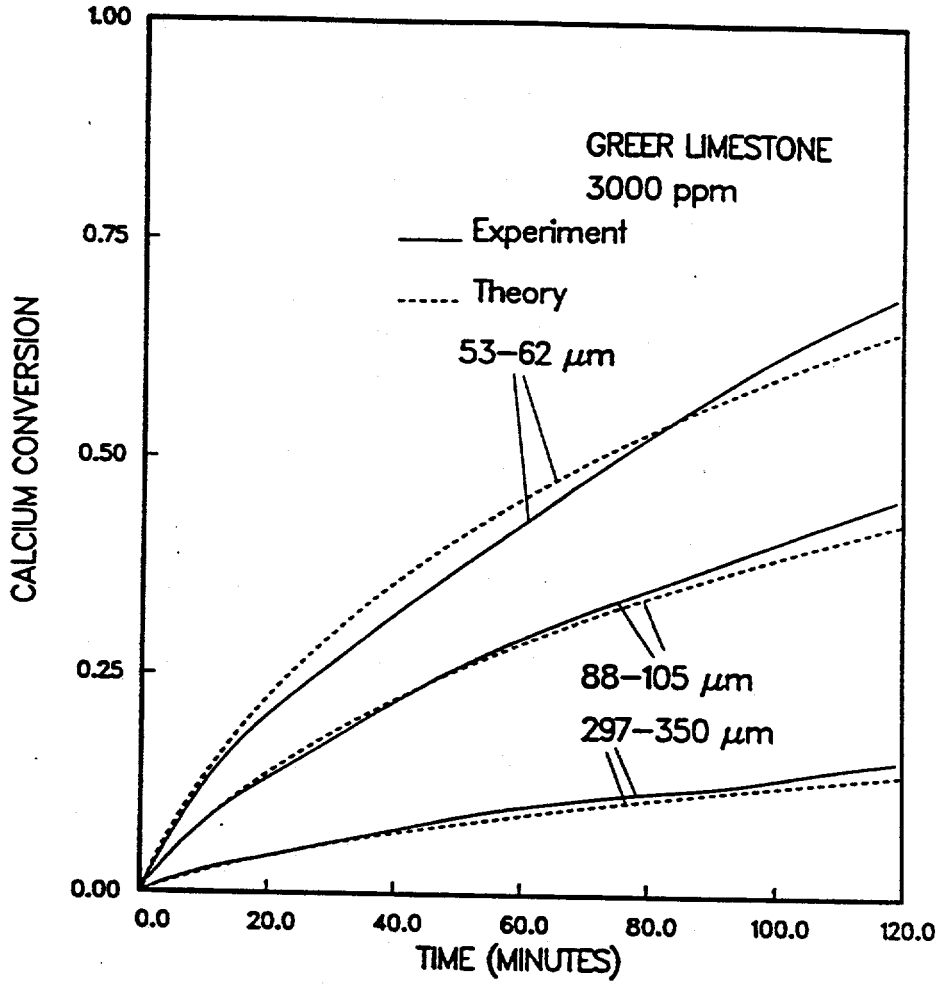

Figure 6.3: Experimental (—) and theoretical (- - - -) conversion vs. time profiles for Greer limestone sulfided at $750°C$ and 3000 *ppm* H_2S under an atmosphere of 70% CO_2 (molar basis) and N_2.

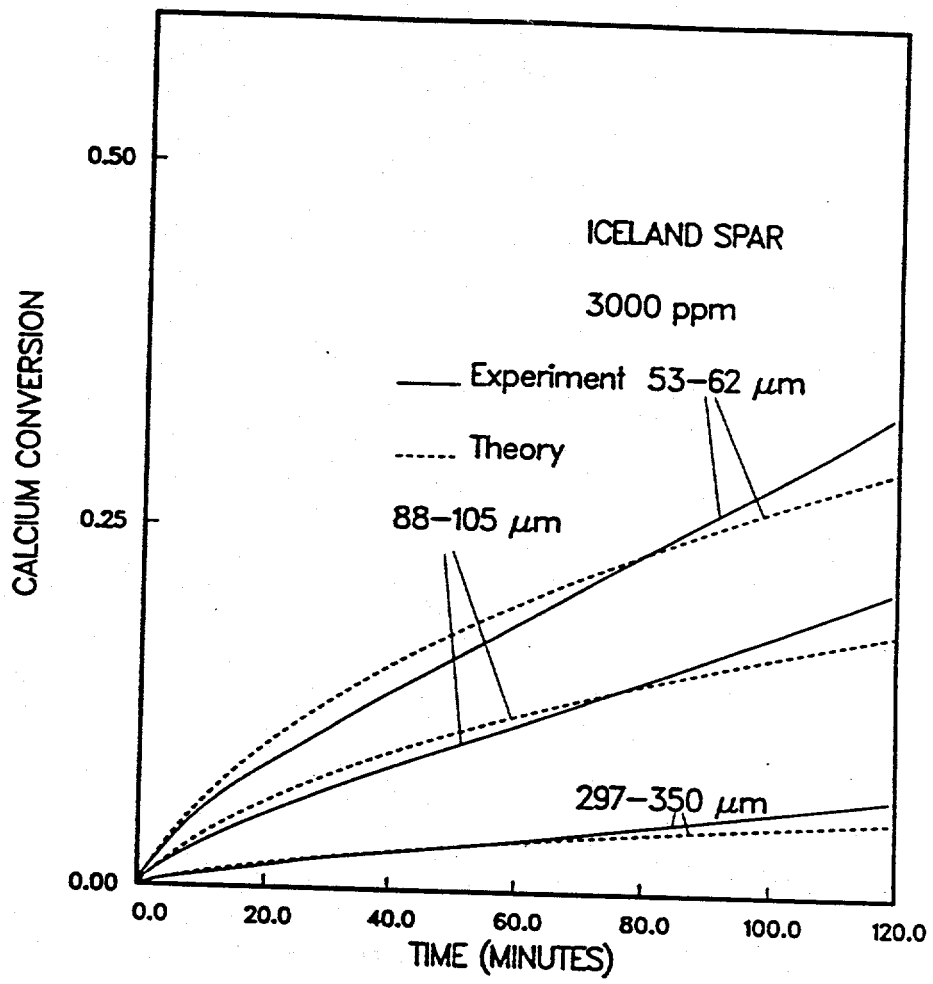

Figure 6.4: Experimental (—) and theoretical (- - - -) conversion vs. time profiles for Iceland spar sulfided at $750°C$ and 3000 *ppm* H_2S under an atmosphere of 70% CO_2 (molar basis) and N_2.

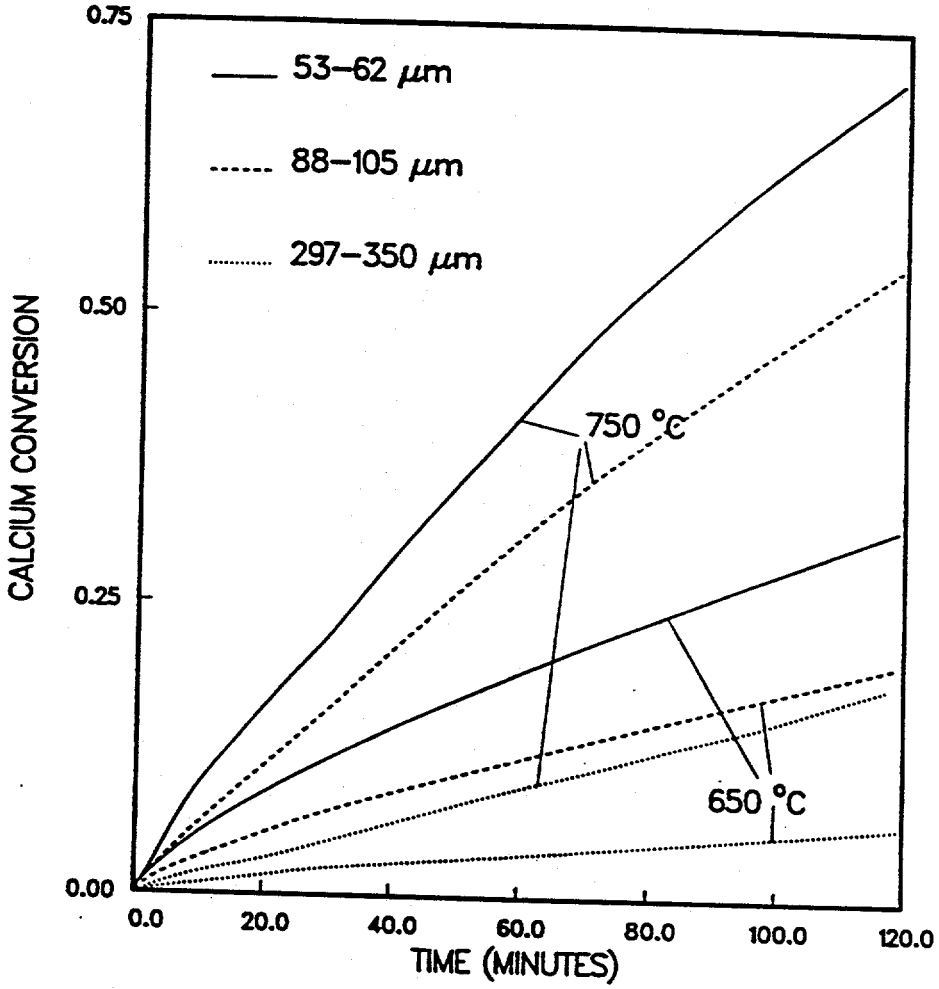

Figure 6.5: Effect of temperature on the conversion-time curves for the direct sulfidation of Georgia marble with 3000 *ppm* H_2S.

the time axis by a factor of 2 (that is, the ratio of the two concentrations) for the reaction carried out under 6000 ppm of H_2S (dashed curve). Nearly overlapping conversion-time profiles are seen from the comparison of the solid line with the dotted line over the whole reaction. This indicates that the overall diffusion-reaction mechanism of the limestone-H_2S reaction is affected linearly by changes in the concentration of the reactive gas. A similar observation was made by Yen et al. (1981) for the initial reaction rates of half-calcined dolomites with H_2S. However, the concentration of SO_2 in the bulk phase had highly nonlinear effects on the diffusion-reaction mechanism for the direct sulfation of the limestones used in our present study (Krishnan and Sotirchos, 1993a).

6.4. Estimation of kinetic parameters

The intrinsic reaction rate, R_s, was assumed to be related to the concentration at the reaction interface, c, by the equation

$$R_s = k_s c^n \tag{6.1}$$

The initial reaction rate data were used to determine the values of the reaction rate constant, k_s, and order of reaction, n. Because of the low porosity of the precursors – pore structure data will be presented and discussed later – very strong intraparticle diffusional limitations exist in the intraparticle pore space. We therefore assumed that the reaction initially occurs on the external surface of the particles only and that subsequently the process proceeds in a shrinking core fashion. The initial (time zero) reaction rate, $\bar{R}_{obs}$, is thus given by

$$\bar{R}_{obs} = 4\pi {a_0}^2 k_s {c_s}^n \tag{6.2}$$

with a_0 being the initial size of the particle and c_s the concentration of H_2S at the external surface of the particles.

A mass balance on H_2S gives

$$\bar{R}_{obs} = 4\pi a^2 k_g (c_b - c_s) \tag{6.3}$$

k_g is the external mass transfer coefficient, c_b the concentration of H_2S in the bulk phase, and a the overall size of the reacting particle. Eq. (6.3), which is valid at any time and

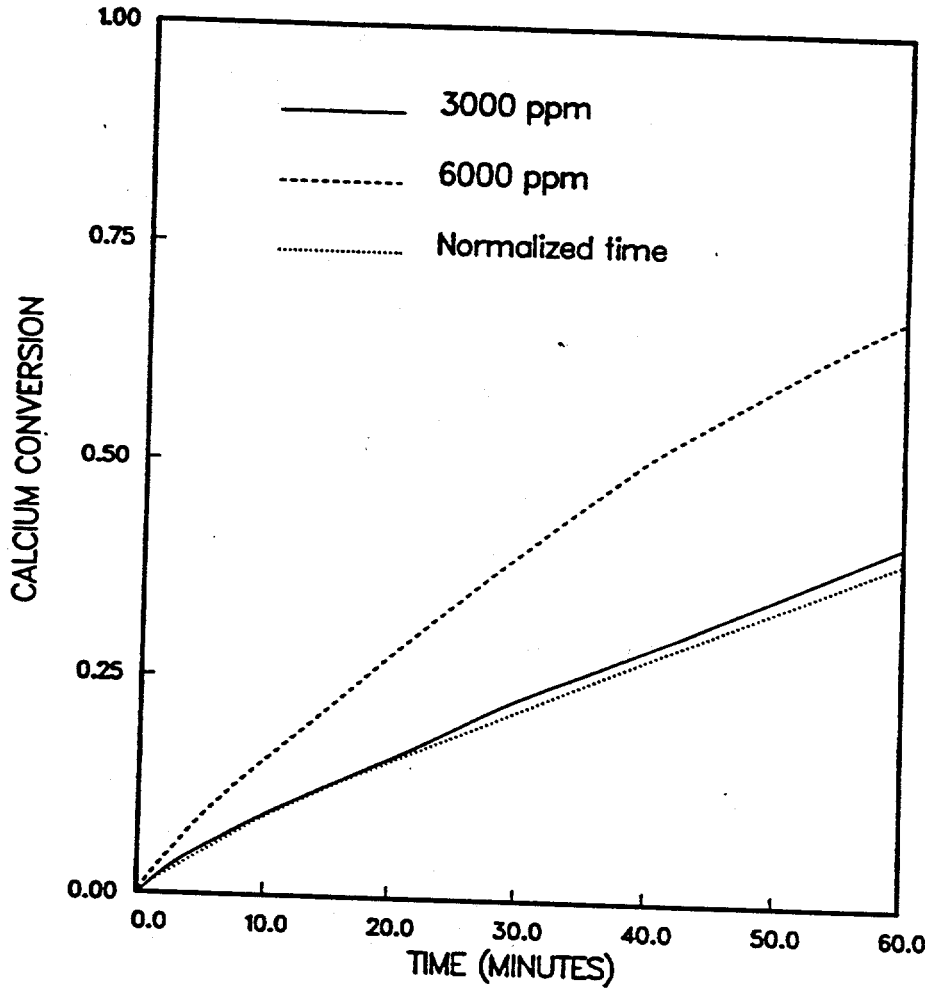

Figure 6.6: Comparison of the conversion vs. time results for Georgia marble (53-62 μm particles) for two concentrations at $750°C$. The normalized curve (dotted line) is the conversion-time curve of the 6000 *ppm* case scaled in time by a factor of 2, the ratio of the two concentrations.

not only initially, can be used to find the value of H_2S concentration at the surface of the particle, needed to determine the kinetic parameters from Eq. (6.2). k_g can be found from the Sherwood number, $Sh = k_g a/D$, where D is the bulk diffusion coefficient of H_2S in the H_2S-gas mixture. Employing a value of $Sh = 1$, the value for a stagnant atmosphere around the solid particles, it was found that, even for the largest reaction rates that we measured, the concentration of H_2S at the surface was practically equal to the concentration of H_2S in the bulk phase, viz., $c_s = c_b$.

Limestone	Temp. (^oC)	k_s (cm/s)	E ($kcal/mol$)
GL	750	0.2101	4.304
	650	0.1673	4.304
GM	750	0.1359	5.214
	650	0.1031	5.214
IS	750	0.1019	3.285
	650	0.0856	3.285

Table 6.2: Intrinsic reaction rate constants and activation energies for the direct sulfidation of the limestones. GL=Greer limestone, GM=Georgia marble, and IS=Iceland spar.

In agreement with the results of Fig. 6.6, the initial reaction rates were found to be proportional to the bulk concentration of H_2S for all combinations of limestone, temperature, and particle size, and thus, the order of reaction was estimated to be 1 for all solids. With the value of n known, Eq. (6.2) was used to find k_s for each particle size, temperature, and concentration combinations, and the average of all values determined at a given temperature was adopted as the corresponding intrinsic rate constant at this temperature. The obtained results are reported in Table 6.2, where it is seen that the magnitude of intrinsic kinetic rate decreases in the order Greer limestone $\rightarrow$ Georgia marble $\rightarrow$ Iceland spar. Table 6.2 also lists the activation energies that were computed from the intrinsic reaction rate constants by assuming Arrhenius-type dependence on temperature.

Temperature appears to affect similarly the intrinsic kinetics of all three stones, but its influence is rather weak. Much higher activation energies, of the order of 30 kcal/mole, were obtained for the direct reaction of the same stones with SO_2 (Krishnan and Sotirchos, 1993a). On the other hand, studies on the sulfidation of their calcines gave an activation energy for k_s of the order of 6 kcal/mole (Efthimiadis and Sotirchos, 1992).

6.5. Effects and structure of product layer

Fig. 6.7 compares the conversion-time profiles of the three limestones for direct sulfidation at 750^oC and under 3000 ppm of H_2S for the two smaller size ranges used in this study. The initial overall reactivities of the three stones vary in the same way as their intrinsic reactivities (see Table 6.2) for both particle sizes because the process is controlled at its initial stages by the intrinsic sulfidation kinetics. As the conversion increases and the product layer becomes thicker, the resistance for diffusion of H_2S through the latter becomes higher, and the transport of H_2S may eventually become the controlling step of the overall process. In the light of this observation, the results of Fig. 6.7 suggest that diffusion through the product layer plays a crucial role in determining the conversion vs. time trajectories of the samples. The relative differences between the conversion levels reached by the Iceland spar samples and those for the other two samples increase with increasing conversion, indicating higher resistance for diffusion through the Iceland spar product layer. Despite their smaller intrinsic reactivity, the Georgia marble particles reach higher conversion than their Greer limestone counterparts after some reaction time increases with decreasing particle size. This behavior indicates that the the product layer formed during the direct sulfidation of Georgia marble presents less resistance to H_2S transport than that of Greer limestone.

The last result was corroborated by the pore size distributions that were obtained from nitrogen sorption for fully sulfided samples of Greer limestone and Georgia marble (Fig. 6.8). The samples were sulfided at 750^oC under 6000 ppm of H_2S. Although the pore size distribution of the sulfided Greer limestone is shifted towards larger pores when compared with that of Georgia marble, the overall pore volume it represents is definitely smaller (0.027 cc/g for Georgia marble vs. 0.02 cc/g for Greer limestone). It appears like the

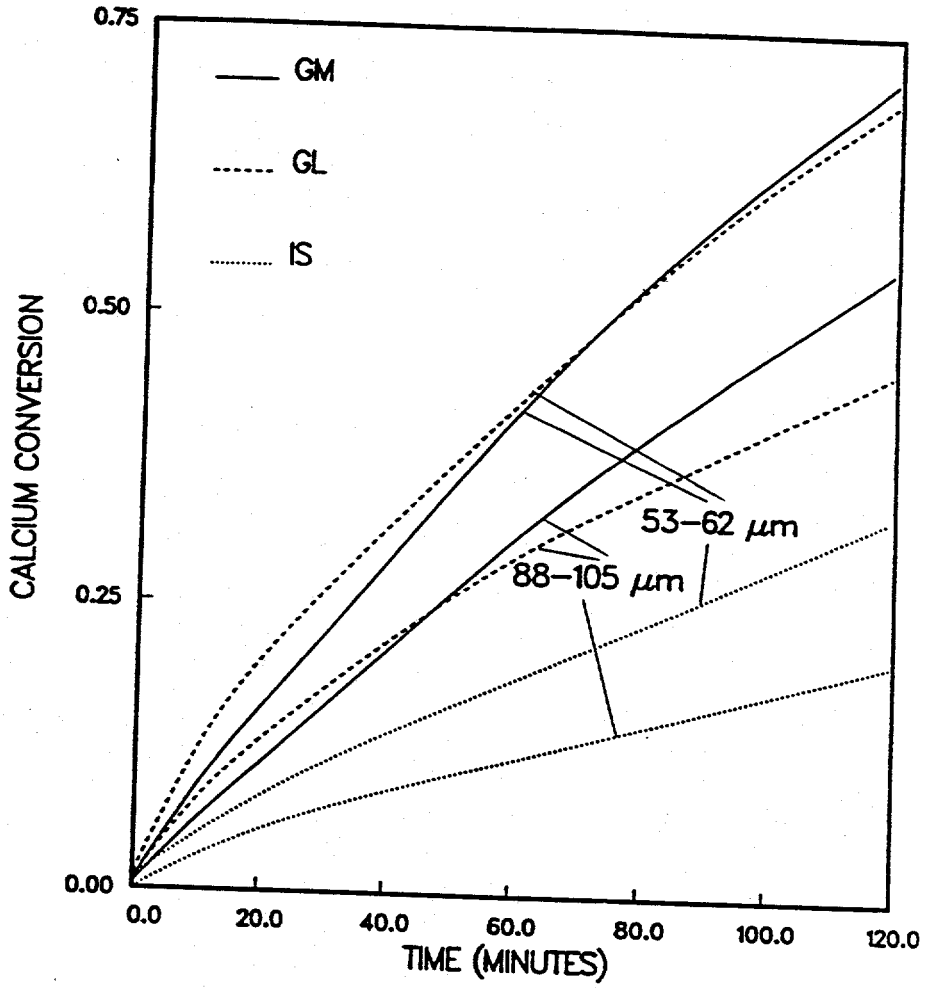

Figure 6.7: Comparison of the conversion vs. time results during direct sulfidation at $750°C$ of the three limestones under 3000 ppm H_2S for two particle size ranges.

higher porosity of the fully sulfided Georgia marble sample (approximately 7% compared to 5% for the fully sulfided Greer limestone sample), and hence its more open structure, leads to lower resistance for mass transport of H_2S in its product layer, enabling it to perform better than Greer limestone at high conversions. The observed increase with decreasing particle size in the time needed for the Georgia marble conversion to surpass that of Greer limestone agrees with this explanation. In addition to N_2 sorption, mercury intrusion porosimetry using a Micromeritics Autopore II 9220 unit was employed to characterize the sulfided samples. Intrusion of mercury was seen to occur mainly in the pore size range covered by the N_2 sorption experiments. Because of the very small intrusion volumes, the pore size distributions that could be extracted from the mercury intrusion data were thought not to be as reliable as those determined from adsorption measurements.

A comparison of the direct sulfidation and direct sulfation reactions of the limestones used in our study also reveals variations in the mass transport rates of the reactive gases caused by differences in the structure of the product layer. Fig. 6.9 compares conversion evolution curves for direct sulfidation with direct sulfation results (Krishnan and Sotirchos, 1993a) for Georgia marble at $750°C$ and 1500 ppm of gaseous reactant (H_2S or SO_2). Results analogous to those of Fig. 6.9 were obtained for all size ranges and solids, that is, in all cases the direct sulfidation process proceeded at a much faster rate than direct sulfation. The smaller overall rate of the limestone-SO_2 reaction at small reaction times is a reflection of its lower intrinsic rate. On the other hand, the tendency of the relative difference between the sulfidation and sulfation conversions to increase with the reaction time is an indication of stronger diffusional limitations in the sulfated layer. The higher intraparticle mass transport rate for the limestone-H_2S reaction could be caused by both the more open structure of the sulfid layer and its smaller thickness for the same conversion level.

Some comparative results on the structure of the product shell are shown in Fig. 6.10 which shows pore size distributions, obtained from N_2 sorption data, for different treatments of Greer limestone. The heat treated sample was prepared under 70% CO_2 and 30% N_2. Its pore size distribution is used as reference in the discussion of the results since the samples were exposed to the same high temperature environment before the start of the reaction. The effects of heat treatment under a noncalcining environment on the pore

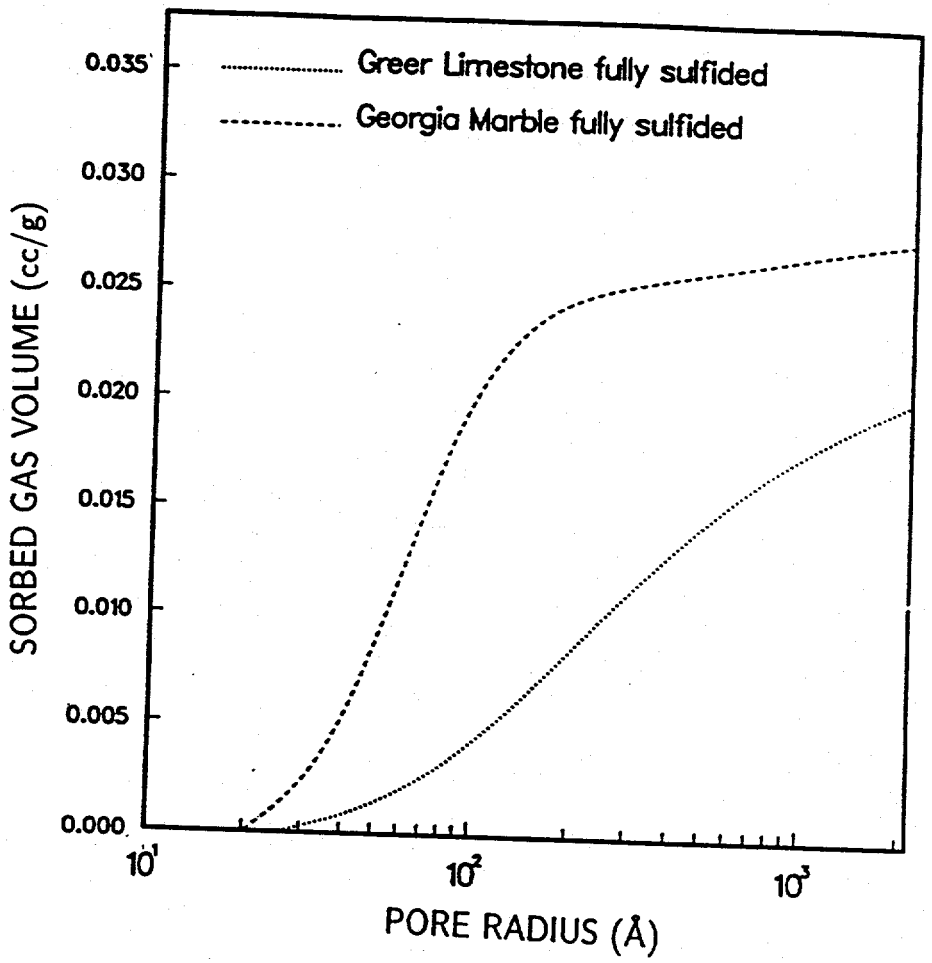

Figure 6.8: Comparison of the pore size distributions, determined from N_2 sorption data, of fully sulfided Greer limestone and Georgia marble samples at $750°C$ and 6000 ppm H_2S.

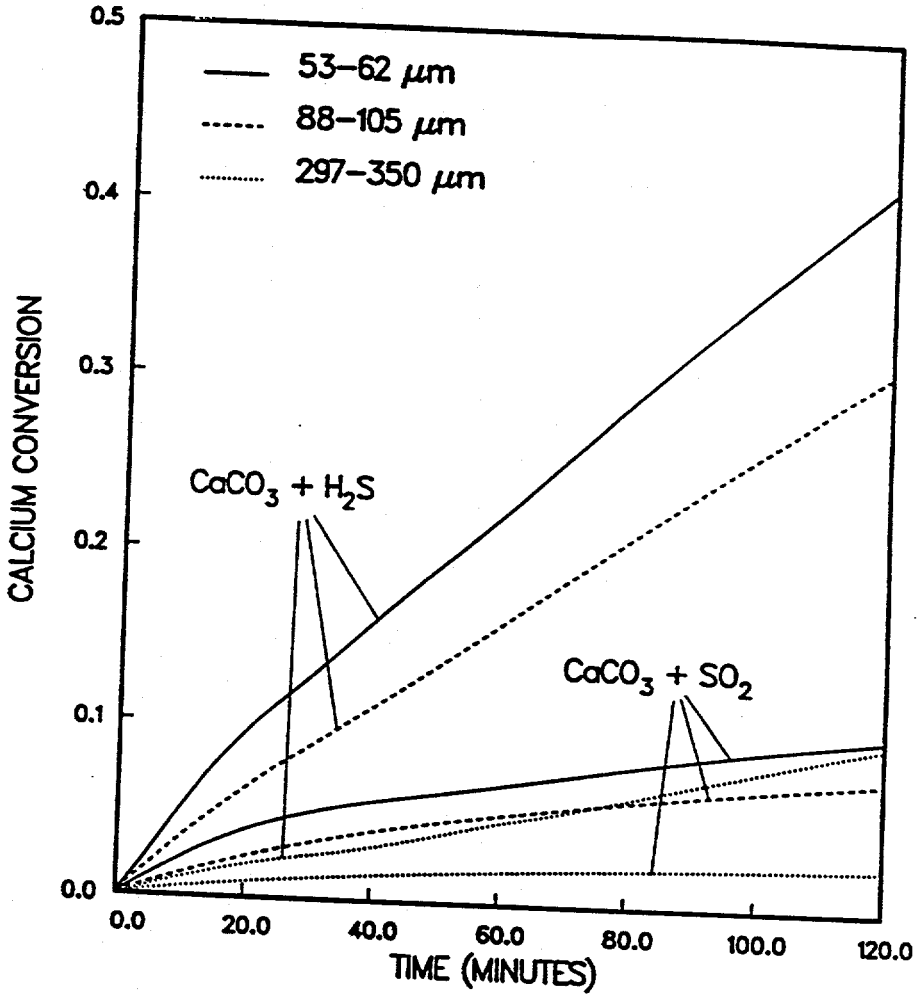

Figure 6.9: Comparison of conversion vs. time results for direct sulfidation of Georgia marble at $750°C$ and 1500 $ppm\ H_2S$ with those obtained for direct sulfation (Krishnan and Sotirchos (1993a)).

size distributions of the precursor stones have been discussed in detail by Krishnan and Sotirchos (1993a). The results of Fig. 6.10 show that the pore size distributions of the precursor, heat-treated sample, and 80% sulfated sample represent very low porosity and are not very different. The directly sulfided sample is much more porous than the heat-treated solid and the sulfated sample, and therefore, its product layer must offer less resistance to mass transport than the sulfated layer.

The measured porosity for the sulfided solid is well below the value that would result if the overall particle size remained unchanged. The solid product (CaS) occupies less space than a stoichiometrically equivalent amount of solid reactant ($CaCO_3$). Specifically, the ratio of the molar volume of product to that of reactant is about 0.7, and thus, the sulfided layer should be approximately 30% porous if there were no particle shrinkage (most probably the result of sintering of CaS) during sulfidation. A different situation is encountered in the case of sulfation where the solid product ($CaSO_4$) is bulkier than the reactant (the ratio of the molar volume of the solid product to that of the solid reactant is about 1.24), and thus, an increase in the overall particle size must occur even if a nonporous product layer is formed during sulfation. Because of this difference, the product layer thickness is larger for the same conversion level in the case of the sulfation reaction, and this along with smaller porosity of the product layer leads to a much higher overall resistance for diffusion from the external surface of the particles to the unreacted core. To all these one should also add the fact that a larger molecule (SO_2) is involved in the sulfation reaction.

We mentioned earlier that several reactions involving limestones may occur in a gasifier. The CaO-H_2S reaction and the $CaCO_3$-H_2S reaction are the primary routes of desulfurization in coal gasifiers. In contrast to the direct sulfidation where, as we have seen in Figs. 6.8 and 6.10, the solid is initially nonporous and develops limited porosity in the course of the reaction, the CaO-H_2S reaction involves a solid with a well developed porous structure and, hence, high internal surface area. The existence of high surface area in the calcined solid enables its sulfidation to proceed with a much higher rate than the limestone-H_2S reaction. Some comparative results are shown in Fig. 6.11 for Georgia marble reacted at 750^oC under 3000 ppm of H_2S. Whereas all CaO present in the calcines

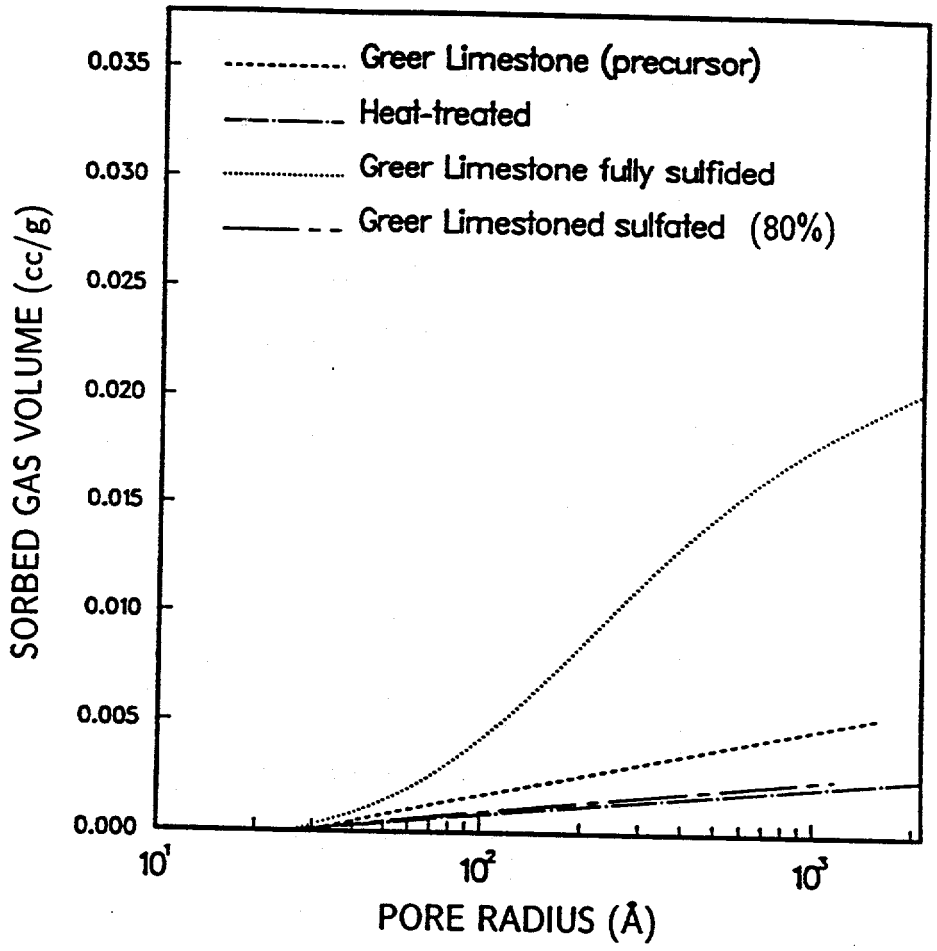

Figure 6.10: Pore size distributions of partially sulfated (directly) and fully sulfided (directly) Greer limestone. Direct sulfidation was carried under 6000 *ppm* of H_2S at 750°C. Direct sulfation was carried under 6000 *ppm* of SO_2 at 850°C.

is converted to CaS for all particle sizes, only part of $CaCO_3$ is sulfided within the time interval shown in the figure. These results lend further support to the conclusion that the mechanisms of desulfurization under calcining and noncalcining conditions differ radically and that the fundamental knowledge that exists in the literature on the CaO-H_2S reaction can only be of limited help in understanding the mechanism of the limestone-H_2S reaction.

6.6. Product layer diffusivities and discussion

Because of the low porosity of the precursor stones, the limestone-H_2S reaction starts with H_2S reacting with $CaCO_3$ mainly at the periphery of the particles to form CaS, the solid product. Further sulfidation can take place only by diffusion of H_2S through the product layer and reaction with $CaCO_3$ at the interface between reacted and unreacted solid. If the particles react in a shrinking core fashion, the product layer exists in the form of a shell next to their external surface. A mathematical model describing the shrinking core behavior observed during direct sulfation of limestones was developed by Krishnan and Sotirchos (1993b). A diffusion coefficient varying with the distance from the external surface of the particles and nonlinear kinetics were employed in that model, but preliminary computations for limestone sulfidation showed that satisfactory agreement between model and experiment could be obtained for constant diffusion coefficient in the product layer. Equations for a shrinking core model with constant diffusivity in the product layer are given in several sources of the literature (e.g., Szekely et al. (1976) and Levenspiel (1972)). For linear kinetics and spherical particles, the relation between time and conversion is given by

$$\tau = 1 - \rho + \frac{\phi^2}{2}(1-\rho^2) + \frac{\phi^2}{(1-Z')}\left(\frac{1}{2} - \frac{1}{Sh_e}\right)\left((Z' + (1-Z')\rho^3)^{2/3} - 1\right) \qquad (6.4)$$

where

$$\tau = tv_s' k_s c_b / a_0; \quad Sh_e = k_g a_0 / D_e \qquad (6.5a, b)$$

$$\phi^2 = k_s a_0 / D_e; \quad \rho = a_c / a_0 \qquad (6.6a, b)$$

and the overall conversion X is given by

$$X = 1 - \rho^3 \qquad (6.7)$$

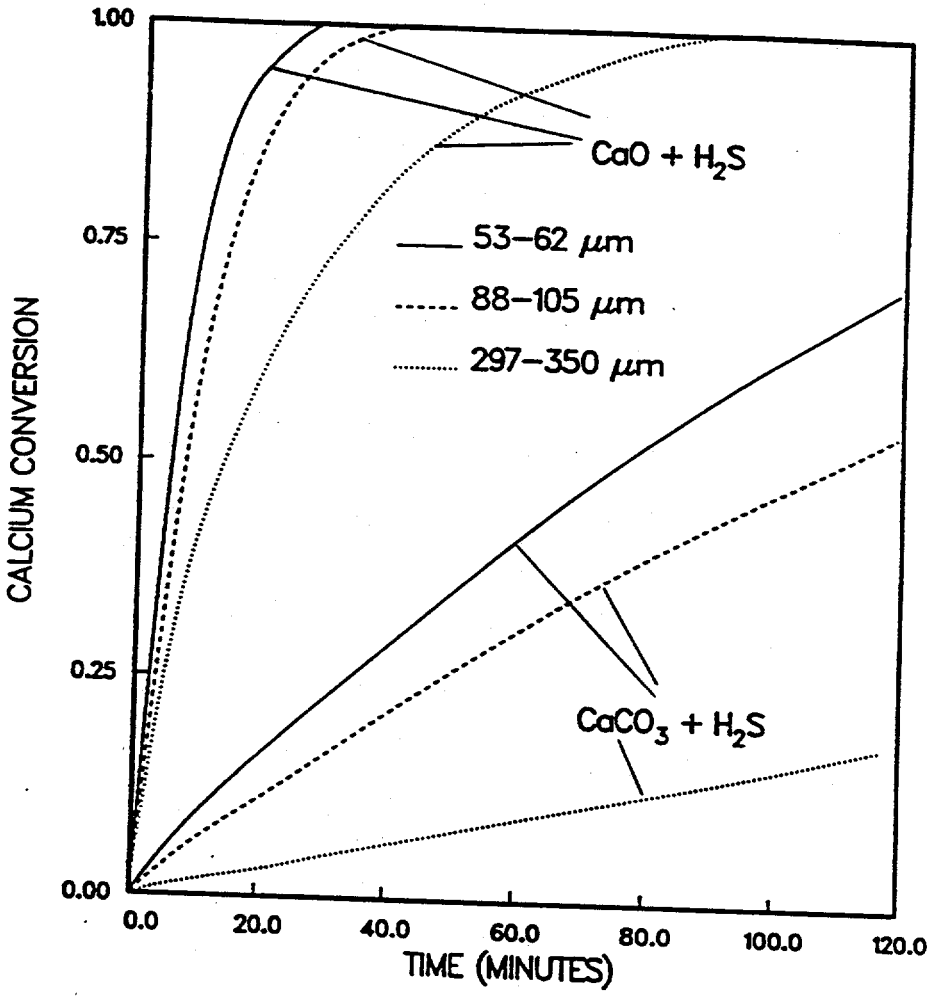

Figure 6.11: Comparison of the conversion vs. time curves for the CaO-H_2S (Efthimiadis and Sotirchos (1992)) and the $CaCO_3$-H_2S (this study) reactions. In both cases, the data are for 3000 *ppm* H_2S and 750 ^oC. The calcines were prepared at the same temperature under 100% N_2.

D_e is the effective diffusivity of H_2S through the product layer, v_s' is the volume of the unreacted solid (including the pore space) per mole of solid reactant, a_0 and a_c are the initial radius and the unreacted core radius of the particles, respectively, and Z' is the stoichiometric volume ratio of the solid product-solid reactant pair, that is, the volume of reacted solid per unit volume of stoichiometrically equivalent amount of unreacted solid.

v_s' can be estimated from the initial composition and porosity of each limestone, whereas the estimation of Z' also requires the porosity of the reacted layer. We have the equations:

$$v_s' = \frac{v_{CaCO_3}}{(1-\epsilon_s)\psi_{CaCO_3}} \tag{6.8}$$

$$Z' = \frac{(1-\epsilon_s)}{(1-\epsilon_p)}(1+(Z-1)\psi_{CaCO_3}) \tag{6.9}$$

v_{CaCO_3} is the molar volume of $CaCO_3$, Z is the ratio of the molar volume of CaS to that of $CaCO_3$, ψ_{CaCO_3} is the volume fraction of $CaCO_3$ in the solid phase of the limestone precursor, and ϵ_s and ϵ_p are the porosities of the unreacted and completed reacted solid, respectively. For high $CaCO_3$ content and low unreacted and reacted solid porosities, Eqs. (6.8) and (6.9) suggest that v_s' and Z' can be approximated by v_{CaCO_3} and Z, respectively.

The following observation may be used to check the assumption that the direct sulfidation of limestones proceeds in a shrinking core fashion. Different size particles develop product shells of different thickness at the same conversion level. It can be shown that for slab geometry particles, the variation of the product layer thickness with time is independent of particle size if the effective diffusivity in the product layer depends on the distance from the external surface of the particles only. This is also true for other particle geometries at relatively low conversion levels, that is, before the effect of the curvature of the particles becomes significant. The variation of the product layer thickness with time for Georgia marble reacted at $750°C$ under 3000 *ppm* of H_2S is displayed in Fig. 6.12. The curves shown in the figure have been obtained from the experimental conversion vs. time results with the product layer thickness computed from the expression $d = a_0[(Z' + (1-Z')(1-X))^{1/3} - (1-X)^{1/3}]$. Nearly identical variation of the product layer thickness with time is seen for all particle size ranges in Fig. 6.12, indicating that

the hypothesis of a shrinking core behavior for the reaction of Georgia marble with H_2S is correct. Similar behavior was observed for the product thickness vs. time curves of all cases investigated in this study.

The only parameter that remains to be determined from the experimental results is the effective diffusivity of the reactive gas (H_2S) through the product layer surrounding the core of unreacted limestone. We estimated the effective diffusivity by matching the model predictions (Eq. (6.12)) with the experimental conversion-time curves through a least squares error minimization procedure. In estimating D_e at a certain temperature, all conversion vs. time results available at this temperature (i.e., for all particles and concentrations) were employed. Table 6.3 lists the effective diffusivity values we estimated. The highest value of effective diffusivity was obtained for Georgia marble reacted at $750°C$, twice the value determined for Greer limestone reacted at the same temperature. This result agrees with the behavior seen in Fig. 6.7, where the overall reactivity of Georgia marble is initially lower than that of Greer limestone but surpasses it as the conversion increases, the product layer becomes thicker, and diffusion in the product layer becomes the controlling step. At $650°C$, Greer limestone reached slightly higher conversion than Georgia marble at all times, and this fact is reflected in having comparable diffusivity values for the two solids. The value of D_e for Iceland spar is at both temperatures much smaller than the values for Greer limestone and Georgia marble, indicating that its lower overall reactivity (see Fig. 6.7) is due not only to its lower intrinsic reactivity but also to the higher resistance of its product layer to H_2S transport.

In our study of the direct sulfation of limestones (Krishnan and Sotirchos, 1993), we found that the overall sulfation reactivity and the effective diffusivity in the product layer decreased in the order Greer limestone → Georgia marble → Iceland spar, that is, in the order of increasing grain size in the precursor and decreasing porosity (see Table 6.1). On the basis of this observation, it was postulated that the petrographic structure of a limestone plays a very important role in determining its product layer structure and, hence, its overall sulfation reactivity. Similar conclusions were reached from the study of the sulfation of the calcines of the same solids (Sotirchos and Zarkanitis, 1992). The overall reactivity also increased in the same order during sulfidation of calcined particles in the

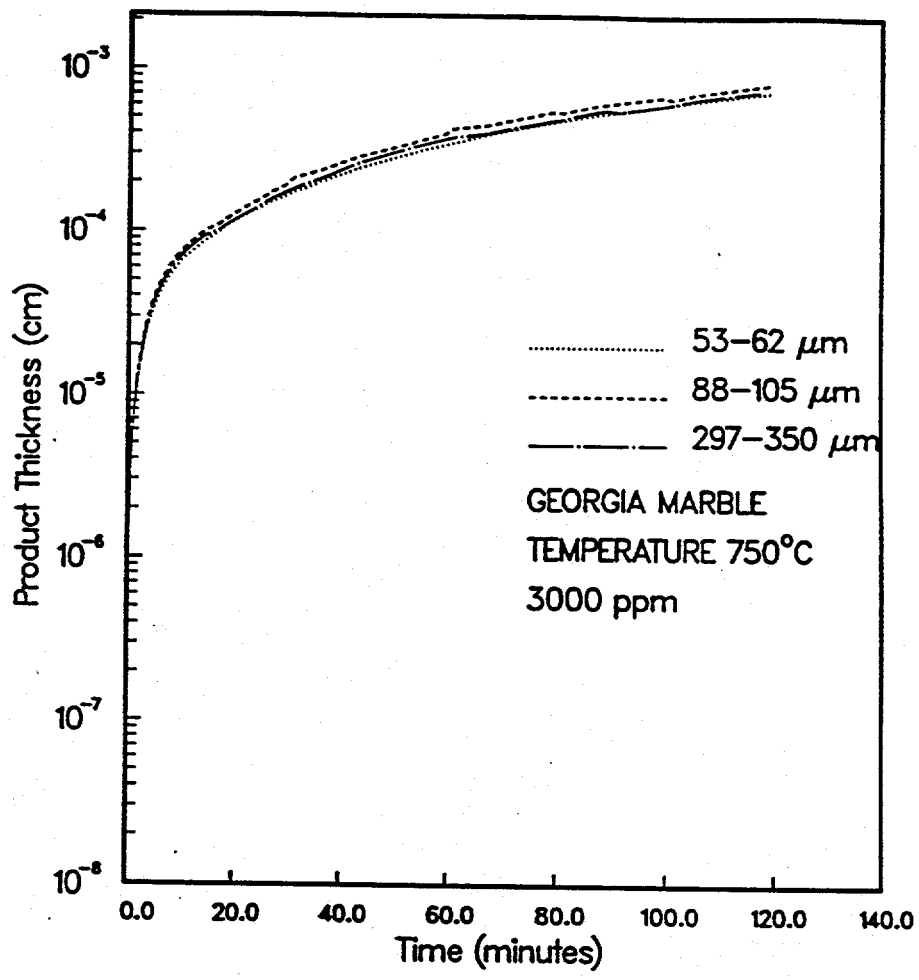

Figure 6.12: Product layer thickness vs. time for the three particle size ranges of Georgia marble assuming shrinking core behavior.

53-62 and 88-105 μm size ranges (Efthimiadis and Sotirchos, 1992), but larger particles exhibited the behavior seen here for direct sulfidation at large reaction times, that is, the Georgia marble sample reacted faster than the other two.

Limestone	Temp. (^oC)	D_e (cm^2/s)	σ^2/a_0 (cm^{-1})
GL	750	5.26×10^{-5}	665.72
	650	46.67×10^{-6}	4180.41
GM	750	1.11×10^{-4}	204.05
	650	6.25×10^{-6}	2749.33
IS	750	7.14×10^{-6}	2378.62
	650	1.82×10^{-6}	7838.83

Table 6.3: Effective diffusivities for H_2S through the product layer and values of σ^2/a_0 for the different types of limestones at 750^oC and 650^oC. GL=Greer limestone, GM=Georgia marble, and IS=Iceland spar.

Effective diffusion coefficients, for diffusion in the pore space of the calcines, larger than those used for sulfation of the same sorbents (Zarkanitis and Sotirchos, 1992) had to be employed by Efthimiadis and Sotirchos in order to be able to reproduce the indirect sulfidation data using a pore-based mathematical model. Since Georgia marble particles tend to explode during heating under CO_2 at high rates – because of the decomposition of the $MgCO_3$ contained in them – Efthimiadis and Sotirchos postulated that the apparently aberrant behavior of large Georgia marble particles was due to the development of cracks in their interior during heating which decreased the resistance for mass transport in their pore space. The formation of these cracks did not have such a dramatic effect on the sulfation behavior of the particles because sulfation leads to complete pore plugging and, as a result, even these large pores are eventually filled with solid product. This explanation may also be applicable to the observed differences between direct sulfation (Krishnan and Sotirchos, 1993b) and direct sulfidation (present study) in the variation of reactivity and effective diffusivity in the product layer among the three samples. As we mentioned earlier,

the direct sulfation involves formation of a bulkier, than the reactant, solid product, which causes plugging of any initially present pores, while sulfidation is accompanied by reduction of volume which, if particle shrinkage did not occur, would yield a porous sulfided product having about 30% porosity.

Figs. 6.2-6.4 compare the predictions of the shrinking core model, for the effective diffusivities of Table 6.3, with the experimental conversion vs. time curves for reaction at 750^oC and 3000 *ppm* of H_2S. Very good agreement between theory and experiments is seen to exist for all three limestones, and similar behavior was observed for reaction at 650^oC. The predictions of the model were also tested by comparing the theoretical and experimental product layer thickness vs. time curves. Such a comparison is made in Fig. 6.13 for the smallest size range (53-62 μm) for the three limestones reacted at 750^oC and under 3000 *ppm* of H_2S. As in the case of the conversion vs. time curves, the model reproduces satisfactorily the experimental data for the whole duration of the experiment.

The results of Figs. 6.2-6.4 and 6.13 point to the conclusion that a constant effective diffusivity shrinking core model can adequately describe the direct sulfidation of limestones. However, a closer look at the experimental and theoretical conversion vs. time curves of Figs. 6.2-6.4 reveals that in all cases the mathematical model tends to overestimate the conversion at the early stages of the reaction and overpredict it after some reaction time. This behavior suggests that the overall resistance to mass transport in the product layer decreases as the reaction progresses. The decrease in the mass transport resistance is most probably caused by the formation of a more open product layer with increasing conversion, which causes the diffusion coefficient to increase away from the external surface of the particles. On the contrary, the analysis of direct sulfation data for the same limestones revealed a progressively increasing mass transport resistance (Krishnan and Sotirchos, 1993). This opposite behavior is not surprising considering that the way of formation of the product layer during direct sulfation – where the nascent product layer pushes against a progressively thicker product layer – is in contrast to that in direct sulfidation – where the product shell collapses with the progress of reaction.

From the extracted values of effective diffusivities and the intrinsic reaction rate constants obtained earlier, it is possible to determine which mechanism controls the direct

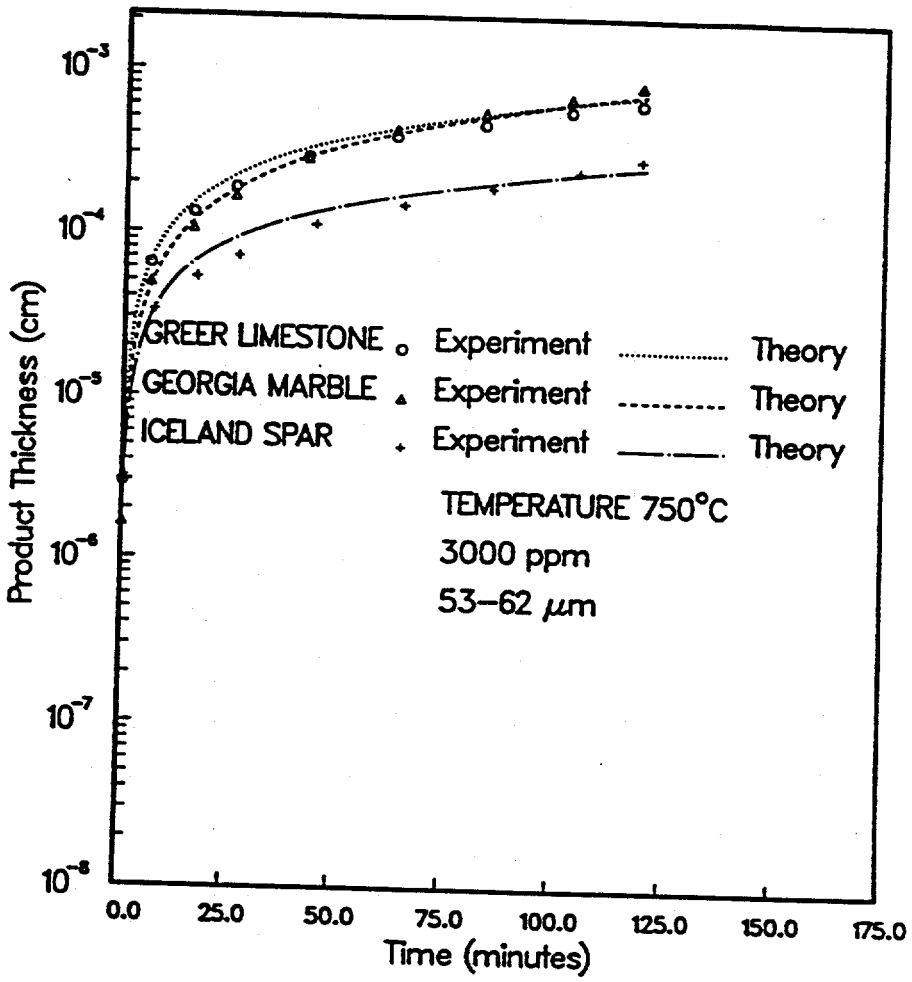

Figure 6.13: Comparison of the theoretical (continuous curves) and experimental (distinct data points) product layer thickness vs. time results for the small particles of the three solids directly sulfided at $750°C$ under 3000 *ppm* of H_2S.

sulfidation process using the ratio of the reaction time for complete conversion under mass transport control to that for reaction in the kinetically controlled regimes (Szekely et al. (1976)). For a first order reaction and negligible external diffusional limitations (i.e., $Sh_e = \infty$), it follows from Eq. (6.4) that this ratio is given by

$$\sigma^2 = \frac{1}{2}\phi^2\left(\frac{Z' - Z'^{2/3}}{Z' - 1}\right) = \frac{1}{2}\frac{k_s a_0}{D_e}\left(\frac{Z' - Z'^{2/3}}{Z' - 1}\right) \tag{6.10}$$

The overall reaction can be considered to be under total kinetic control for $\sigma^2 < 0.1$ and under total diffusional control for $\sigma^2 > 10$. Values of σ^2/a_0 for $Z' = 1$ (i.e., of $k_s/(6D_e)$) in cm^{-1} are reported in Table 6.3 for the various cases we studied. It follows from these values that at 650^oC the reaction was controlled by diffusion in the product layer in all cases except for the 53-62 μm size range of Georgia marble which yields a value of 7.9 for σ^2. On the other hand, at 750^oC the reaction was under complete diffusion control only for the larger two size ranges of Iceland spar and the 297-350 μm size range of Greer limestone. All other cases were reacted in the intermediate regime where both kinetics and diffusion in the product layer are controlling the process.

Much lower product layer diffusivities were estimated by Krishnan and Sotirchos (1993b) from the analysis of reactivity vs. time data for direct sulfation. Specifically, for Greer limestone and Iceland spar the diffusivities in the sulfated layer at the onset of the reaction – a variable product layer diffusivity was used for direct sulfation – are lower by about a factor of 5 than the sulfided layer values of Table 6.3, whereas for Georgia marble the difference is about an order of magnitude. This result and the formation of a thicker product layer during direct sulfation provide an explanation for the lower direct sulfation rates of the three solids (see Fig. 6.9 for Georgia marble). The values of effective diffusivities through the product shell developed during indirect sulfidation of the limestones (i.e., sulfidation of the calcines) are two to three orders of magnitude lower than the values of Table 6.3 (Efthimiadis and Sotirchos, 1992). Similar differences were noted (Krishnan and Sotirchos, 1993b) between the product layer diffusivities of the direct and indirect sulfation of the three samples. Nevertheless, the existence of a pore network in the interior of the calcined particles enables the reaction to take place throughout the intraparticle space, leading to higher reaction rates than in the case of direct reaction

despite the smaller product layer diffusivities. Of course, for calcine sulfation this happens before plugging of the pore space with solid product and formation of inaccessible pore space lead to stoppage of the sulfation reaction.

Arrhenius-type dependence of the product layer diffusivity on temperature was assumed, and the results of Table 6.3 were used to determine the activation energy. The highest value of 53.78 kcal/mole was obtained for Georgia marble, followed by Greer limestone with 38.61 kcal/mole and Iceland spar with 25.55 kcal/mole. These values are by almost an order of magnitude higher than the activation energies of the direct sulfidation reaction, in agreement with our earlier observation that the influence of temperature on the process becomes stronger as the conversion increases and the role of diffusion in the product layer becomes more important. Efthimiadis and Sotirchos (1992) reported much lower values for the product layer diffusivities of the CaO-H_2S reaction, namely, 13, 16, and 13 kcal/mole for Georgia marble, Greer limestone, and Iceland spar, respectively. Activation energies comparable to the values of Table 6.3 were estimated by us in our previous study of the direct sulfation of the same stones (Krishnan and Sotirchos (1993b)). This results indicates that temperature has similar influence on the product layer diffusivity during direct sulfidation and sulfation.

The large differences in the values of the product layer diffusivities at the two temperatures (650 and 750^oC) for the limestone-H_2S reaction cannot justified by the effect of temperature on the diffusion process since the diffusivity values of Table 6.3, in conjunction with the pore structure characterization data, suggest that diffusion occurs in the Knudsen diffusion regime. Therefore, the product layer structure must be strongly influenced by the temperature of the reaction. This conclusion is in agreement with observations made by Attar and Dupuis (1979) in their study of the direct sulfidation of calcites. At temperatures higher than 640^oC, they noticed a sudden rise in the rate of the $CaCO_3$-H_2S reaction accompanied by separation of the CaS crystals formed on the $CaCO_3$ surface.

6.7. Summary

The reaction between $CaCO_3$ and H_2S was studied by employing three solids of high calcium carbonate content, a microcrystalline limestone (Greer limestone), a coarsely-

grained marble (Georgia marble), and a single-crystal calcite (Iceland spar), and carrying out the reaction in the presence of CO_2 to prevent the decomposition of $CaCO_3$ to CaO. The effects of particle size, temperature, and H_2S concentration were investigated. Very strong influence of particle size and temperature on the behavior of the process was revealed by the experimental data. The concentration of the gaseous reactant was found to affect linearly both the intrinsic kinetics of the reaction and the process of diffusion in the intraparticle space. Because of the very low porosity of the three solids, the reaction was assumed to proceed in a shrinking core fashion, and the initial reaction rate data were used to estimate the intrinsic reaction rate constant. It was found that the intrinsic reaction rate constant decreased in the order Greer limestone → Georgia marble → Iceland spar at both temperatures, that is, in the same order as the intrinsic rate constant of the direct sulfation reaction (Krishnan and Sotirchos, 1993a).

The characterization of the pore structure of fully sulfided solids using mercury porosimetry and N_2 adsorption-desorption data revealed that the reacted solids possessed little porosity, much smaller than the 30% (approximately) value that would have resulted if the overall size of the particle did not change during sulfidation. A shrinking core model based on the assumption of a homogeneous product layer (and therefore of a constant effective diffusivity in the product shell) was employed to analyze the direct sulfidation data and to estimate the effective diffusion coefficient through the product layer. From the estimated values of effective diffusivity and intrinsic reaction rate constant, it was determined that in most cases studied the limestone-H_2S reaction was controlled by diffusion in the product layer, while in the rest it was under the control of both intrinsic kinetics and diffusion in the product layer. The product layer diffusivities for Greer limestone and Georgia marble were found to be comparable but higher than those determined for Iceland spar. This result agreed with the variation of the overall reaction rate among the three solids, especially at high conversion levels where the process was controlled by diffusion in the product layer.

The values of effective diffusivities through the product layer of direct sulfidation were found to be higher than those in the product layer of direct sulfation, in agreement with the higher overall reactivity of the former reaction. Also, they were much higher than

the product layer diffusivities for sulfidation of the calcines and exhibited much higher sensitivity to temperature than them. Since this strong dependence on temperature cannot be justified by the diffusion process itself – the diffusivity values in the product layer of direct sulfidation suggest that diffusion occurs in the Knudsen regime – we concluded that the structure of the product layer formed during direct sulfidation varies with the reaction temperature.

Very good agreement was obtained between theory and experiment for all cases, and it was thus concluded that a shrinking core model with a constant effective diffusivity can adequately describe the direct sulfidation process. The agreement between theory and experiment could be improved by employing a variable diffusivity shrinking core model, with decreasing mass transport resistance with progress of reaction. In contrast, an increasing mass transport resistance with progress of reaction was observed for the direct sulfation of limestones (Krishnan and Sotirchos, 1993). It is believed that the different way of formation of the product layer (outward expansion during direct sulfation vs. inward shrinkage during direct sulfidation) is the main cause for the different evolution of intraparticle mass transport resistance with the progress of reaction during these two processes.

6.8. Notation

Symbols that do not appear here are defined in the text.

a	radius of the particle, cm
a_0	initial radius of the particle, cm
a_c	radius of unreacted core, cm
c_b	concentration of H_2S in the bulk, mol/cm^3
c_s	concentration of H_2S at the surface of the particle, mol/cm^3
D_e	effective diffusivity of H_2S in the product layer, cm^2/s
k_g	external mass transfer coefficient, cm/s
k_s	intrinsic reaction rate constant, cm/s
n	order of reaction with respect to H_2S
Sh_m	effective Sherwood number defined by Eq. (6.5b)
t	time, s

v_s' volume of unreacted core per mole of $CaCO_3$, cm^3/mol

X conversion of the reacting solid

Z' volume of reacted solid phase per unit volume of unreacted solid phase (including pore volume)

Greek

ϕ^2 Thiele modulus defined by Eq. (6.6a)

ρ_c dimensionless radius of unreacted core, a_c/a_0

σ^2 shrinking core reaction modulus defined by Eq. (6.10)

τ dimensionless time defined by Eq. (6.5a)

6.9. Literature References

Attar, A.; Dupuis, F., "The Rate and the Fundamental Mechanisms of the Reaction of Hydrogen Sulfide with the Basic Minerals in Coal," Ind. Eng. Chem. Process Des. Dev., **18**, 606-618 (1979).

Borgwardt, R.H.; Roache, N.F.; Bruce, K.R., "Surface Area of Calcium Oxide and Kinetics of Calcium Sulfide Formation," Environ. Prog. **3**, 129-135 (1984).

Borgwardt, R.H.; Roache, N.F., "Reaction of H_2S and Sulfur with Limestone Particles," Ind. Eng. Chem. Process Des. Dev., **23**, 742-748 (1984).

Chase, M.W., Ed., *JANAF Thermochemical Tables. Supplement to the Journal of Physical and Chemical Reference Data* (1985).

Efthimiadis, E.A.; Sotirchos, S.V., "Sulfidation of Limestone-Derived Calcines," Ind. Eng. Chem. Res., **31**, 2311-2321 (1992).

Grindley, T.; Kim, S.S.; Gorski, E.E.; Steinfeld, G., "Aspects of the Design of a Process Development Unit for High-Temperature Coal Gas Desulfurization," Technical Report, DOE/METC-85/6025 (1985).

Hajaligol, M.R.; Longwell, J.P.; Sarofim, A.F., "Analysis and Modeling of Direct Sulfation of $CaCO_3$," Ind. Eng. Chem. Res., **27**, 2203-2210 (1988).

Jalan, V., "Studies Involving High Temperature Desulfuration/Regeneration Reactions of Metal Oxides for Fuel Cell Development," Technical Report; DOE/MC/16021-1486 (1983).

Jansson, S.A.; O'Connell, L.P.; Stantan, J.E., "Effect of Carbon Dioxide Pressure on Desulfurization in Coal Fired PFBC Systems," Proc. Int. Conf. Fluid. Bed Comb., **7**, 1095-1100 (1982).

Krishnan, S.V.; Sotirchos, S.V., "Sulfation of High Purity Limestones under Simulated PFBC Conditions," Can. J. Chem. Eng., **71**, 244-245 (1993a).

Krishnan, S.V.; Sotirchos, S.V., "A Variable Diffusivity Shrinking-Core Model and its Application to the Direct Sulfation of Limestones," Can. J. Chem. Eng., **71**, 734-745 (1993b).

Levenspiel, O., *Chemical Reaction Engineering*; John Wiley, New York (1972).

Reynolds, W.C., "The Element Potential Method for Chemical Equilibrium Analysis: Implementation in the Interactive Program STANJAN," Technical Report, Dept. of Mech. Eng., Stanford University (1986).

Ruth, L.A.; Squires, A.M.; Graff, R.A., "Desulfurization of Fuels with Half-Calcined Dolomite: First Kinetic Data," Environ. Sci. Technol., **6**, 1009-1014 (1972).

Snow, M.J.H.; Longwell, J.P.; Sarofim, A.F., "Direct Sulfation of Calcium Carbonate," Ind. Eng. Chem. Res., **27**, 268-273 (1988).

Szekely, J.; Evans, J.W.; Sohn, H.Y., *Gas-Solid Reactions*, Academic Press, New York (1976).

Tullin, C.; Ljungström, E., "Reaction between Calcium Carbonate and Sulfur Dioxide," Energy., **3**, 284-287 (1989).

Westmoreland, P.R.; Gibson, J.B.; Harrison, D.P., "Comparative Kinetics of High-Temperature Reaction between H_2 and Selected Metal Oxides," Environ. Sci. Technol., **11**, 488-491 (1977).

Yen, J.H.; Li, K.; Rogan, F.H., "Reaction Mechanism of Half-Calcined Dolomite during Sulfidation," Chem. Eng. Commun., **10**, 35-60 (1981).